Studies of Grain Boundaries in Materials Subjected to Diffusional Creep

Nørbygaard, Thomas

Publication date:
2002

Document Version
Publisher's PDF, also known as Version of record

Risø-R-1379(EN)

Studies of Grain Boundaries in Materials Subjected to Diffusional Creep

Thomas Nørbygaard

Risø National Laboratory, Roskilde
August 2002

ISBN 87-550-3147-1
ISBN 87-550-3149-8 (Internet version)
ISSN 0106-2840

Print: Pitney Bowes Management Services Denmark A/S, 2002

Abstract
Grain boundaries in crystalline Cu(2%Ni) creep specimens have been studied by use of scanning and transmission electron microscopy in order to establish the mechanism of deformation. Creep rate measurements and dependencies were found to fit reasonably well with the model for diffusional creep (Nabarro-Herring) and this impression was strengthened considerably by the microstructural finds.

Manual and automated EBSD surface scans have been performed on a specimen supplied with an inert reference grid in order to correlate individual grain boundary structure (in terms of deviation from CSL) with the activity displayed during diffusional creep testing. It was found that boundaries with low deviation from perfect Σ did not contribute macroscopically to the creep strain.

A resist deposition procedure was examined to improve the reference surface grid so as to allow determination of the grain boundary plane by use of simple stereomicroscopy directly on the surface. The etched pattern deteriorated heavily during creep testing, supposedly because of dislocation creep, due to excessive creep stress.

Grain boundaries have been studied and characterised by TEM providing an insight into the diversity of twin boundary structures. Ledges on low deviation Σ3 and Σ9 were observed repeatedly and the presence of these is proposed to relate to the inactivity of such boundaries. A handful of examples showed ledged boundaries emitting dislocations into the lattice, presumably because of stress accumulation due to restrictions on GBD movement from the ledge structure.

The present thesis has been submitted for fulfilment of the requirements set for obtaining the Ph.D. degree at Copenhagen University

Front page figure: Double transmission electron micrograph of an observed twin boundary with ledges – a relative wide twin lamella ending inside a grain.

Contents

Abbreviations and symbols

BF	Bright field (microscopy)
CBED	Convergent beam electron diffraction
CSL	Coincident site lattice (model)
DF	Dark field (microscopy)
DoF	Degrees of freedom
DSC	Displacement shift complete (lattice)
EBSD	Electron backscattering diffraction
FCC	Face centered cubic (crystal structure)
GBD	Grain boundary dislocation
GBS	Grain boundary sliding
MLI	Mean linear intercept
SAD	Selected area diffraction
SEM	Scanning electron microscope/microscopy
TEM	Transmission electron microscope/microscopy

---

a_{ij}	Misorientation matrix element
b	Burgers vector
B	Numerical constant (about 12)
B´	Numerical constant (about 50)
C	Vacancy concentration (at a boundary under stress)
C_0	Thermal equilibrium concentration of vacancies
d	Grain size
d_i	Interplanar distance
d_{ts}	True spatial grain size
D_0	Frequency factor
D_{gb}	Grain boundary self-diffusion coefficient
D_L	Lattice self-diffusion coefficient
E_f	Energy of formation for one defect
g	Diffraction vector
k	Boltzmann's constant
L	(dislocation) Line vector
L_{MLI}	Mean Linear Intercept Length
n	Integer
n_t	Total number of atomic sites
Q	Activation energy (for the stated mechanism)
T	Absolute temperature
T_m	Absolute melting temperature
u	Unit vector along the dislocation line
UVW	Misorientation axis given by
v	Angular deviation (from perfect CSL)
v_m	Maximum angular deviation (from perfect CSL)
w	Grain boundary width
θ	Misorientation angle
θ_B	Bragg angle
λ	Wavelength
σ	Stress
Σ	CSL characterisation
Ω	Atomic volume
φ_1, ϕ, φ_2	the Euler angles
χ_a ,χ_b	Angles determining grain boundary plane

Preface

The present thesis has been submitted for fulfilment of the requirements set for obtaining the Ph.D. degree at Copenhagen University. The research described within these pages have for the largest part, and when nothing else is noted in the text, been conducted at the Materials Research Department, Risø National Laboratory. Supervisors on the project have been Erik Johnson, Copenhagen University and Jørgen Bilde-Sørensen, Risø National Laboratory.

The project has in many respects been a continuation of some of the work done by Peter Thorsen, for his Ph.D. thesis of may 1998. Highlights of this work and references to articles can be found at the end section 1.3 (page 42).

In the spring of 2000 a three-month visit to the University of Purdue, Indiana resulted in a small side project on creep of nanocrystalline gold thin films. This was performed under the supervision of Alexander King, and a short examination of the work is found at the end of Chapter 2.

For valuable contributions to the work I would like to thank:

- Helmer Nilsson for advice on mechanical specimen handling, polishing procedures and light microscopy.
- Jørgen Lindbo for making great TEM specimens and help with sample preparation in general.
- Palle H. Nielsen for performing alloy casting and specimen heat treatments, well controlled and immediately upon request.
- Jan Larsen for coping with the unnecessarily complicated machinery and still manage to conduct the creep experiments in good order.
- Jørgen Stubager for fruitful co-operation in making the photoresist deposition procedure work on such awkward specimens.
- Niels Krieger Lassen who wrote the software for orientation analysis (Texmeter and Croplot) and have been very helpful in all matters concerning pattern observation and data handling.
- Alexander King for accepting me as a temporary student and making my stay at the University of Purdue a memorable experience.
- Erik Johnson for showing great interest in the work and being but a phone call away when additional help was needed.
- Jørgen Bilde-Sørensen for always being there to clear up any misunderstandings and providing the needed advice and guidance in all the phases of the work, including proof reading.

Introduction

Material science continues to celebrate many victories in these years. There is a continuous and increasing demand for new materials with improved and well-defined properties be it stronger, lighter, smaller or more reliable components. No matter what the need, the key to success is microstructural understanding of the material and how it reacts to the environmental influences (e.g. stress, temperature, corrosives) under which it has to function.

One of the very important ingredients of any polycrystalline material is the intergranular interfaces known as grain boundaries. It has been known for a century that grain size influences the overall properties of materials and this is directly connected to the amount and distribution of grain boundary present. Early models of grain boundaries considered them to be like strong amorphous cement holding the "bricks" of grain together and the atomic configurations inside boundaries were assumed to be chaotic and random. Our understanding has improved significantly since then and we know now that grain boundaries constitute a highly inhomogeneous group and come in many varieties with different degrees of atomic order. Therefore it is not unexpected either, that grain boundaries can display very different properties and have different energies. This fact has spawned the notion of designing materials so that specific (beneficial) boundaries occur in greater amounts at the expense of other less attractive boundaries in order to improve the overall properties of the material. This is not quite technically feasible yet on a large scale, although some degree of control can be exerted on surface structure and lab-materials such as thin foils and bicrystals.

Among the many ways of achieving material deformation the mechanisms known under the common term of creep are relatively obscure. This is traditionally because the technological importance of creep is reserved to high temperature industries (e.g. power generation) and is generally a rather slow deformation process. Even though the macroscopic effects (strain) thus often are limited, creep can cause heavy damage at the microstructural level leading to severely inferior material properties. This can especially be a problem in modern super-alloys where a specific microstructure is the source of powerful properties (e.g. aeroplane engines) and will ultimately limit the life expectancy of such devices. Nanocrystalline materials, which also seem to find many new uses these years, are highly vulnerable to some types of creep as well, as the diffusion distances in these materials are so small that even slow migration rates (i.e. low temperatures) can give rise to significant creep deformation rates.

The concern of this thesis is the above-mentioned microstructural feature of grain boundaries, the specific deformation mechanism of diffusional creep and in particular the scientific overlap between these two areas of interest.

1 Background

This first chapter is particularly aimed at readers with little or no prior knowledge in the particular fields of grain boundary structure, diffusional creep or electron microscopy to provide at least a basic understanding of the fundamentals needed to fully appreciate the experiments described in the second chapter.

The theory part will cover some basic concepts of crystallography and crystal defects followed by a more comprehensive examination of grain boundary structure and creep mechanisms, with focus on diffusional creep. Especially the theoretical background on diffusional creep is somewhat controversial, but to the extent it is possible I will try to keep this part close to what a majority today believes to be the naked facts about diffusional creep.

Following is a selective literature study of previous works in these areas, including a short examination of the work of Peter Thorsen, the work that I in some sense have continued and a more detailed look on the arguments of the "diffusional creep opposition".

The final part is a short description of the principles, methods and specific equipment and software used for measuring orientation of grains in TEM as well as SEM.

1.1 Grain boundaries

Grain boundaries are planar microstructural defects that are the direct cause of the immense differences between properties of single and polycrystalline materials. Understanding of boundary structure and properties are key elements in control and engineering of modern high performance materials.

Crystal structure

To properly comprehend observed microstructures it is necessary first to have a full understanding of the underlying crystal structure. All the metals used in our experiments – copper, nickel and gold – crystallize in the face centered cubic (FCC) lattice structure, why all other crystal structures will be disregarded in the following. Some selected data for these metals can be found below.

	Cu	Ni	Au
Melting temperature (T_m)	1356.5 K	1728 K	1337.58 K
Density	8.92 g/cm^3	8.90 g/cm^3	19.31 g/cm^3
Atomic volume (Ω)	11.8 Å^3	10.9 Å^3	17.0 Å^3
Burgers Vector (½<110>)	2.56 Å	2.49 Å	2.88 Å
Activation energy for lattice diffusion (Q_L)	207 kJ/mole	284 kJ/mole	174 kJ/mole
D_0 for Lattice self diffusion	0.62 cm^2/s	0.09 cm^2/s	1.9 cm^2/s
Activation energy for boundary diffusion (Q_{Gb})	104 kJ/mole	115 kJ/mole	87 kJ/mole
D_0 for GB self diffusion	0.1 cm^2/s	0.1 cm^2/s	0.07 cm^2/s

Table 1: Selected physical properties of the three metals used in the experiments. Melting temperature and density from [1], rest of the data from [2]

As is well known the FCC lattice is a close packed crystal structure. Throughout this text we use the Miller indices to indicate vectors and planes in the crystal using the standard notation:

[h k l] – a specific direction
<h k l> – a group of directions (same crystallographic type)
(u v w) – a specific plane
{u v w} – a group of planes (same crystallographic type)

Accordingly the crystal faces of the non-primitive unit cell are denoted {100} type planes and the close packed planes, which are the slip planes as well, are the {111}. As each of the four slip planes have three slip directions <110>, the FCC lattice has a total of 12 different slip systems.

The FCC lattice is (as other cubic structures) highly symmetric and contains 6 two-fold axes, 4 three-fold axes and 3 four-fold axes. As will be discussed later, this symmetry has important consequences for orientation analysis of specimens.

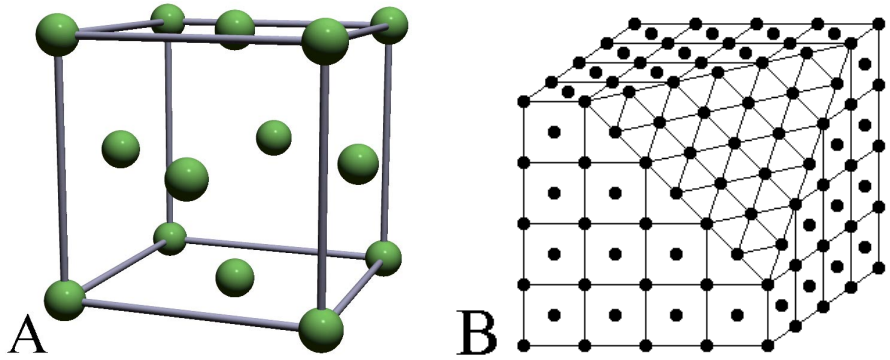

*Figure 1: A) Non-primitive FCC unit cell, B) 5*5*5 unit cell of FCC lattice with a {111} cut.*

Point defects and dislocations

No matter how seemingly perfect, all real materials however are imbued with lattice defects. Defects are typically divided into four groups: point defects such as interstitial atoms and vacancies, line defects such as dislocations, planar defects such as stacking faults and volume defects such as voids or bubbles.

Care taken during specimen preparation can help avoid a great deal of defects but not all. Point defects can be spontaneously emitted from free surfaces or grain boundaries and diffusion will given time make sure that they are incorporated into the material in thermodynamically stable concentrations. The equilibrium concentration of point defects C_{eq} is given by:

$$C_{eq} = n_t \exp\left(-\frac{E_f}{kT}\right) \qquad \text{(Eq. 1)}$$

Where n_t is the total number of atomic sites, E_f is the energy of formation for one defect and kT is the usual Boltzmann constant and absolute temperature. The concentration is thus extremely temperature dependant and for copper, where $E_f \approx 1.3$ eV for vacancies, the fraction of vacant atom sites can hence be calculated to approx. 10^{-22} at 300K and approx. 10^{-5} at 1300K – a difference of 17 orders of magnitude! For interstitial atoms the energy of formation is typically 2-4 times higher than for vacancies, making the equilibrium concentration of interstitials negligible compared with the amount of vacancies. For this reason vacancies are normally considered to be the primary material carriers in diffusional processes, while interstitials are usually ignored.

The rate of migration for vacancies, i.e. the speed with which they move about, is exponentially dependant on temperature as well, so that effectively

diffusional mechanisms can be completely stopped by lowering temperatures sufficiently.

Another type of defect that is found in all crystalline materials (except in rare cases of e.g. carefully grown nanoscale whiskers) is dislocations. Dislocations are one-dimensional defects, in the sense that the lattice is only disturbed along the dislocation line, and they come in two archetypes: the pure edge and the pure screw dislocation (Figure 2). The edge dislocation can be thought of as an extra halfplane inserted into a perfect crystal, the dislocation propagating along the edge of this plane. The screw dislocation on the other hand is of a helical nature with the dislocation line at the centre of the spiralling crystal distortion. The linear distortion that either type of dislocation represents produces a stress field in the surroundings, giving rise to internal strain in the crystal. The larger part of this dislocation strain energy can be accounted for as pure elastic strain in the lattice immediately surrounding the dislocation. The remaining, non-elastic strain energy is attributed to the centre of the dislocation, known as the dislocation core. The exact size of the core is hard to measure or even define, but the diameter is typically estimated to be of the order of 1–4 atomic distances. The strain energy per unit length is about 50% higher for edge dislocations than for screw dislocations.

In addition to the line vector **L**, which describes the direction of the dislocation line, dislocations are usually defined and identified by their Burgers vector **b**. The Burgers vector is, in some sense, a measure for the deformation a given dislocation induces upon the crystal, as will be demonstrated later. Edge and screw dislocations are readily distinguished by their Burgers vectors, which are normal or parallel to the line vector respectively, as shown in Figure 2. If the Burgers vector of a dislocation exactly joins two points in the lattice it is called a lattice translation vector and the dislocation is known as perfect.

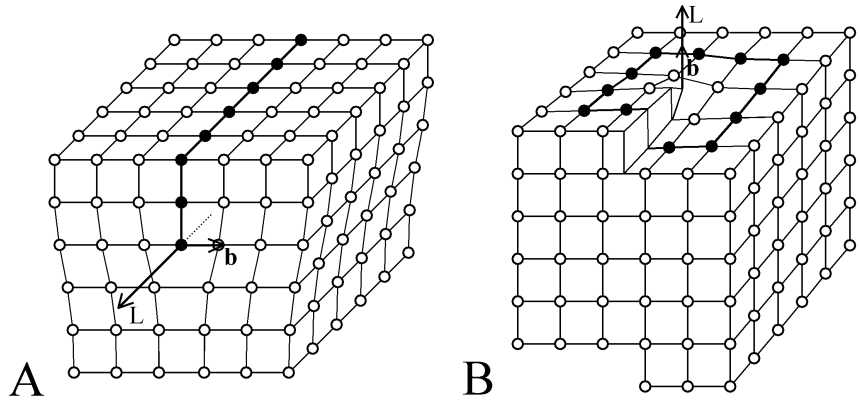

*Figure 2: Cubic lattice with A) pure edge dislocation B) pure screw dislocation. The line vector **L** and Burgers vector **b** for each dislocation is shown as well.*

In the general case dislocations are usually combinations of edge and screw. As dislocations are hardly ever completely straight lines, different parts of the dislocation will have different degrees of edge and screw character.

The nature of the dislocation defect dictates that it cannot terminate inside a perfect lattice. Instead one will find dislocations forming closed loops or dislocations branching into other dislocations before finally terminating at a free surface or at grain boundaries. For geometrical reasons branching dislocations have to meet the requirements of Burgers conservation. If we consider the dislocation with Burgers vector $\mathbf{b_1}$ which branches into two dislocations with $\mathbf{b_2}$ and $\mathbf{b_3}$ the following must be fulfilled:

$$\mathbf{b_1} = \mathbf{b_2} + \mathbf{b_3} \qquad \text{(Eq. 2)}$$

Dislocations have two basic types of movement, glide and climb. Glide, also called conservative motion, is movement in the plane containing both the line vector and Burgers vector. During each glide step a single row of atoms changes nearest neighbour and the passage of the dislocation clearly displaces the upper part of the grain with respect to the lower (see Figure 3A). Simultaneous glide of many identical dislocations under a stress is known as slip and this is the most common mechanism of plastic deformation in crystalline materials.

The second type of dislocation movement is called climb and this process is closely coupled with absorption or emission of vacancies. For an edge dislocation climb can be pictured as receding of the extra halfplane (see Figure 3B). This movement results in surplus atoms in the dislocation core, a condition that can be remedied by absorption of vacancies. If vacancies are not in abundance the climbing process cannot proceed and thus the rate of climbing becomes coupled to the rate of diffusion.

The reverse procedure, negative climb, is growth of the halfplane that correspondingly causes an emission of vacancies from the dislocation.

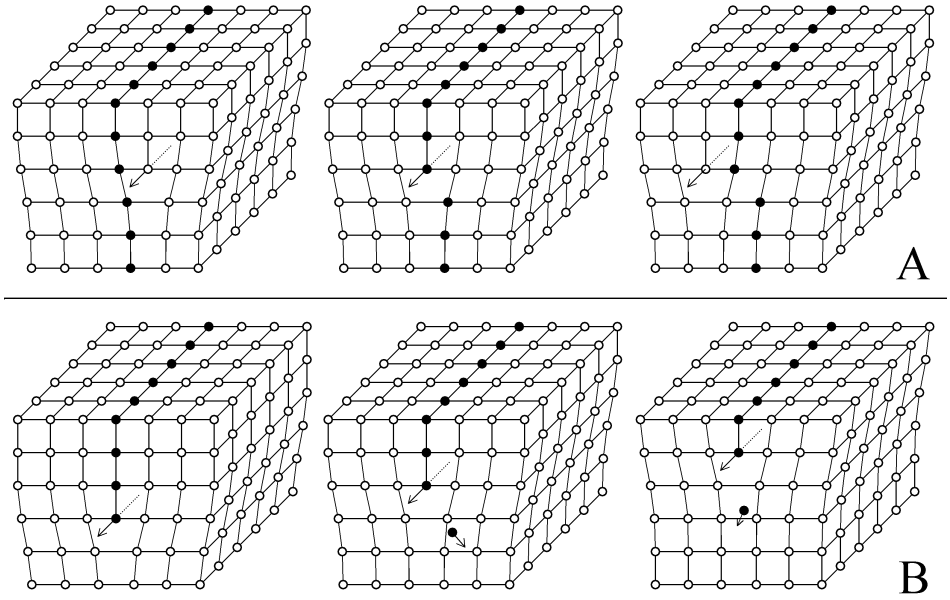

Figure 3: Glide and climb of a dislocation. A) Glide displacing the upper grain with respect to the lower part. B) Seen from left to right one has positive climb with emission of interstitial atoms.

In certain cases it will be energetically favourable for a dislocation to dissociate into two partial dislocations, known as Shockley partials. The Shockleys will be dissociated onto one of the {111} slip planes and an area with a stacking fault will separate them. Dissociated dislocations can move freely on the plane on which they are dissociated, while it can be very difficult or even impossible for them to utilise any of the other slip planes (i.e. cross-slip).

Grain boundary basics

When crystallisation is initiated in a cooling melt (or from gaseous form), it usually does so in many independent places simultaneously. As the crystals grow they will eventually occupy the entire volume and further growth will by then be restricted by the presence of neighbouring crystals. Odds are that two neighbouring crystals, or grains as they are called at this stage, will be rotated relative to each other and will thus not fit perfectly together. The boundary re-

gion between the grains will consist of atoms that are arranged with a lower degree of order than found in the interior of the grains, as they will try to accommodate the differences of the two grain faces.

It should be evident that the packing of atoms in the boundary region generally will be far from optimal (i.e. close-packed) and thus the average volume occupied by an atom in the boundary region, will be larger than the volume occupied by an atom in the lattice. This "porosity" in the boundary is known as the excess free volume, or just excess volume, and is one of the principal reasons that grain boundaries exhibit different properties than the lattice. The excess volume of a given boundary is closely related to the total energy of that boundary [3].

On average the width of grain boundaries is less than 2 atomic diameters [4] why grain boundaries in "normal" polycrystalline materials will constitute only a fraction of the total volume. As grains become very small though, the fraction of "boundary atoms" increases dramatically, e.g. from 0.03% at a grain size of 1 μm to 50% at a grain size of 2 nm [4]. This increase in the amount of boundary is largely responsible for the highly different properties obtained in nanocrystalline materials compared with ordinary polycrystalline counterparts having grains in micrometer or even millimetre size. Nanocrystalline materials can e.g. be created by rapid quenching during solidification of a melt, and generally one will find that the faster the cooling, the more individual grains will be grown, and hence a smaller average grain size will be achieved. A slower cooling rate will leave more time for grain growth and thus result in a larger average grain size. Subsequent heat treatment can alter these parameters significantly.

Grain boundaries can also be created after the initial solidification and crystallisation. Plastic deformation of crystalline materials can introduce an abundance of free dislocations into the grains giving rise to the familiar hardening effect. Further deformation will cause these free dislocations to gather in bundles, effectively splitting a single crystal into several regimes with slightly different crystallographic orientation, a grain into several sub-grains. Heat treatment of such material will cause relaxation and recovery, creating low-angle grain boundaries.

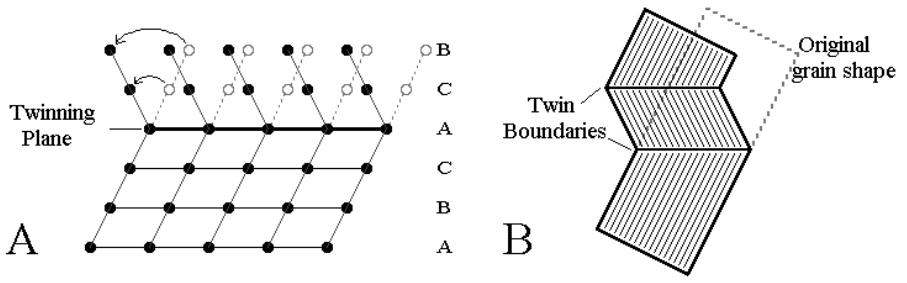

Figure 4: Formation of twin boundaries by deformation twinning. A) Mirroring of the atom positions in the twinning plane and inversion of the stacking sequence B) Deformation of a single grain by twinning.

Another important source of grain boundaries in certain materials is the deformation mechanism known as twinning. Twinning occurs predominantly under stresses at low temperatures and can be briefly described as an inversion of the stacking sequence at the twin plane, thus making the boundary a mirror-plane for the lattice (se Figure 4). The creation of a twin can for all purposes be regarded as an instantaneous event as the propagation of atom re-arrangement happens extremely fast (by slip of a partial dislocation) and no middle positions or "half twins" have ever been observed. Twins can also be created during recrystallisation or grain growth where just a small error in the stacking sequence

causes the grain to grow a twin. The two types are known as deformation and growth twins respectively, even though they can be hard to distinguish by e.g. microstructural observation.

It has been evident for a long time that the structure, and thus properties, of grain boundaries varies significantly, not only from the lattice structure but also from boundary to boundary. The different processes by which grain boundaries can be formed also lead to markedly different boundaries with varying properties and in any given material the choice of casting and machining procedures, heat treatments etc. can give rise to very different microstructures in terms of grain boundary texture.

Misorientation

Some early models were based on the notion that grain boundaries consisted of atoms forming amorphous intercrystalline cement [5]. Once this notion was discarded in favour of a crystallographic and geometrical approach, it became clear that grain boundary structure is highly dependent on how the implicated grains are oriented with respect to each other, the so-called misorientation.

For a single phase alloy (which is the only type that will be discussed in this thesis) neighbouring grains will be of identical crystal structure, and it will always be possible, by means of a single rotation about an appropriate axis, to bring the crystal axes of the first grain in perfect conjunction with the crystal axes of the second. This rotation axis is known as the misorientation axis UVW, conveniently described by the Miller indices, and the angle as the misorientation angle θ. If we mentally expand the lattices of two neighbouring grains into one another such that they become interpenetrating and partly occupy the same space, so to speak, the misorientation between the lattices is then a description of the rotation that will bring the one lattice to coincide perfectly with the other, as illustrated on Figure 5. Note that although we use three variables, to describe the misorientation axis, they only represent two independent variables.

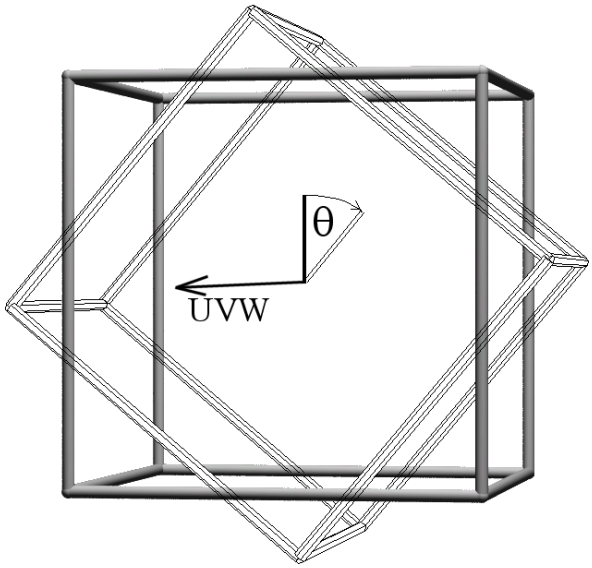

Figure 5: Two interpenetrating lattices. The misorientation axis UVW and angle θ are shown (in the present case (001) and 40°).

To talk of the misorientation as a single unique rotation is somewhat misleading, as several different descriptions will exist for each possible misorientation. Because of the high symmetry of cubic systems a lot of different rotations can actually lead the lattices to coincide, giving many possible axis/angle pairs as a description of the misorientation. Another way of looking at this multiplicity is that the crystal axes of the first grain can be chosen in several different ways (the crystal axis of the second grain will be fixed in respect to the first grain or vice versa) and consequently several different axis/angle pairs can express the exact same misorientation. What it comes down to is that 24 equivalent descriptions exist for any given misorientation. As way of example the misorientation across a twin boundary, which is usually given as a 60° rotation about the [111] axis, can equally well be described by [110]/70.5°, [211]/131.8°, [211]/180°, [311]/146.4° or one of 19 other axis/angle pairs. By convention, and to lessen the confusion, the solution usually given is the misorientation axis associated with the smallest θ value (hence [111]/60°). This particular axis/angle set, which is sometimes known as the disorientation, will be used exclusively in all of the following.

Another popular notation to express misorientation (or orientation in wider terms) makes use of the so-called Euler angles. The rotation that brings the interpenetrating lattices to coincide is broken down into 3 sequential rotations around specific axes chosen from the crystal axes of the two lattices. If the crystal axes of grain 1 and 2 are named $x_1y_1z_1$ and $x_2y_2z_2$ respectively the following 3 rotations are performed in the specified order to align the axes of grain 2 with those of grain 1:

Rotation 1:	φ_1 about z_2	
Rotation 2:	ϕ about x_2'	
Rotation 3:	φ_2 about z_1	(Eq. 3)

where x_2' denotes the x_2 axis after the first rotation. The angles φ_1, ϕ and φ_2 are thus the Euler angles describing the rotation and thus the misorientation of the two grains.

For calculation purposes, a more convenient way of describing the misorientation is in the form of a 3*3 matrix - the misorientation matrix. The misorientation matrix consist of columns, which are the direction cosines of the crystal axes of grain 1 translated to the co-ordinate system of grain 2 (the choice of which grain becomes the reference grain is arbitrary). The elements of the matrix (a_{11}……a_{33}) are related to the misorientation axis/angle and Euler angles as:

$$
\begin{aligned}
a_{11} &= U^2(1-\cos\theta)+\cos\theta && = \cos\varphi_1\cos\varphi_2 - \sin\varphi_1\sin\varphi_2\cos\phi \\
a_{12} &= UV(1-\cos\theta)-W\sin\theta && = \sin\varphi_1\cos\varphi_2 + \cos\varphi_1\sin\varphi_2\cos\phi \\
a_{13} &= UW(1-\cos\theta)+V\cos\theta && = \sin\varphi_2\sin\phi \\
a_{21} &= VU(1-\cos\theta)+W\sin\theta && = -\cos\varphi_1\sin\varphi_2 - \sin\varphi_1\cos\varphi_2\cos\phi \\
a_{22} &= V^2(1-\cos\theta)+\cos\theta && = -\sin\varphi_1\sin\varphi_1 + \cos\varphi_1\cos\varphi_2\cos\phi \\
a_{23} &= VW(1-\cos\theta)-U\sin\theta && = \cos\varphi_2\sin\phi \\
a_{31} &= WU(1-\cos\theta)-V\sin\theta && = \sin\varphi_1\sin\phi \\
a_{32} &= WV(1-\cos\theta)+U\sin\theta && = -\cos\varphi_1\sin\phi \\
a_{33} &= W^2(1-\cos\theta)+\cos\theta && = \cos\phi \qquad \text{(Eq. 4)}
\end{aligned}
$$

and vice versa as:

$$
\begin{aligned}
&\cos\theta = (a_{11}+a_{22}+a_{33}-1)/2 \\
&U = (a_{11}+1)^{1/2}\ , \quad V = (a_{22}+1)^{1/2}, \quad W = (a_{33}+1)^{1/2} \qquad \text{(Eq. 5)}
\end{aligned}
$$

Note that the matrix and Euler representation of misorientation have the same inherent problem that 24 apparently different descriptions exist for the exact same misorientation, due to the cubic symmetry. For the matrix description,

though, the relationship is obvious from the fact that the 24 degenerate misorientation matrices are permutations composed of the same elements. This can be used to our advantage, and used to find the disorientation for a given misorientation by maximising the trace of the matrix (i.e. $a_{11}+a_{22}+a_{33}$) cf. Eq 5.

The grain boundary plane

The crystal misorientation between two grains, no matter which of the above equivalent descriptions is used, is however not sufficient to fully describe grain boundary geometry. First of all, the misorientation contains no information at all about the actual boundary plane, as it is only a description of the orientational differences of the *crystal structure* of the two grains. Below is envisaged two bi-crystals with identical misorientation but different grain boundary plane, to demonstrate the point.

The grain boundary plane expresses not only the interface between the grains, but also the ”cut” of the individual grain, like the facets on a gemstone. As gemstones favour cuts along certain crystal planes, so grains can have more or less ”successful cuts”. Success in this respect is measured in low ”surface” energy of the grain facet, and in the case of grain boundaries, also in how well the neighbouring grains fit on the atomic level.

Looking at bi-crystals like those of Figure 6, the grain boundaries are readily discernible as planar. In real polycrystalline materials this is not always the case though, and looking at a real micrograph such as Figure 25 (page 54) one can find many examples of bend boundaries, in cases where equilibrium is not attained. For short distances, though, boundaries are planar to a good approximation, and often one will find that the part of a boundary dividing 2 specific grains is almost planar in it’s entire length. Thus grains assume polygonal shapes, like faceted gemstones, each face bordering to a different neighbouring grain. In two dimensions a grid of hexagons is a decent mental picture of a grain structure, and a popular geometry for modelling grains, as it happens. Under all circumstances it is therefore implicitly understood that when determining a grain boundary plane, the here from calculated geometry is only valid for a limited distance from the point of measuring.

The boundary plane is usually described by its normal vector **N** expressed in the reference system of either grain. In practice it is conveniently measured by the angles χ_a and χ_b which refers the boundary plane directly to the x,y,z coordinate system of the specimen surface (as defined on the figure below).

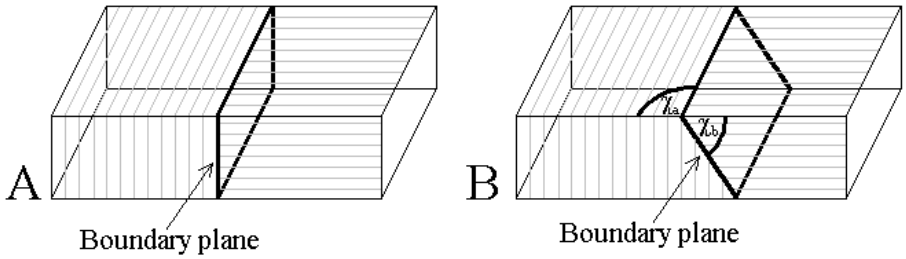

Figure 6: Two bi-crystals with identical misorientation (indicated by the lines on the grain ”surface”) but different grain boundary plane.

Degrees of Freedom

It has long since been established [6] that in general a boundary between two crystal faces have no less than *eight* degrees of freedom (DoF) in total, all of which must be determined in order to have a complete description of the boundary. Five of these have been discussed in the previous paragraphs and are known as the macroscopic degrees of freedom. They consist of two degrees of freedom covered by the misorientation axis, one by the angle and the last two by the grain boundary plane. In addition to these there are three known as the microscopic degrees of freedom.

		Degrees of Freedom
•	Misorientation axis	2
•	Misorientation angle	1
•	Grain boundary plane	2
•	Microscopic x,y,z	3
=	Total	8

The five macroscopic degrees of freedom can be described in other ways (e.g. the interface plane scheme) but for convenience and to avoid any misunderstanding this work will refer exclusively to the misorientation scheme.

The microscopic degrees of freedom can be regarded as a vector defining rigid body translations of the two grains faces relative to one another, parallel and perpendicular to the boundary plane. The microscopic degrees of freedom are determined by relaxation processes at the boundary and little influence can be exerted over them, as nature, so to speak, chooses them so as to minimise the free energy of the system for the given misorientation and boundary plane [7]. Thus they may not be varied independently of the macroscopic degrees of freedom. When non-perfect (in the DSC lattice) dislocations like e.g. Shockley partials are present in a boundary the microscopic degrees of the boundary will differ from one side of the dislocation to the other.

The microscopic DoF are not readily measurable using standard techniques but they can be evaluated by modelling of grain boundary relaxation and in this way help further the understanding of boundary behaviour. Utilising the microscopic degrees of freedom falls outside the scope of this thesis.

Types of Grain boundaries

On the basis of properties and geometry grain boundaries can be divided into either special or general boundaries. General boundaries are sometimes called random boundaries, as boundaries created with a random misorientation (e.g. by crystallisation from a melt) statistically tend to be general boundaries, with only a precious few special boundaries. In this text the term random boundaries will only be used to refer to the boundary creation process and not the actual misorientation these boundaries might have.

In practice the boundaries of a polycrystalline sample will never actually exhibit a random spread among the possible misorientations. Low-energy boundaries are favoured over high-energy boundaries during the solidification process overriding mere statistical reasons for misorientation spread. Different types of relaxation will also help reduce the ”randomness” of grain boundary misorientations in a specimen. Mechanisms such as re-crystallisation, grain growth, grain rotation etc. will all tend to diminish the fraction of high-energy boundaries in favour of more stable boundaries. The surface of samples will very often exhibit some sort of texture, induced by the mould, growth medium etc., meaning that certain grain orientations are favoured while others are inhibited. This is in turn reflected on the boundaries so that misorientations about certain common axes

can be found in high proportions. For these reasons the proportions of special boundaries in experimentally determined distributions will normally exceed the proportions predicted by mathematically random misorientation simulations [8].

General boundaries are characterised by a relative high energy and by a low degree of geometrical symmetry, for which reason the structure of such boundaries is still somewhat a blank page. It is important to stress though, that general boundaries come in many different types and is not a homogeneous group.

Special boundaries exhibit, by contrast, behaviour or have values for specific boundary parameters that are very different from the average. In particular, special boundaries have very low excess volume, which is one of the important reasons for their special behaviour and a property that is directly related to the geometry and structure. Several special properties have been described for these boundaries including selective immunity to intergranular corrosion [9,10], low boundary embrittlement [11], resistance to diffusional creep [12] to name a few. Two kinds of special boundaries are presently known namely low-angle boundaries and CSL. Low-angle boundaries are also known as sub-grain boundaries as they in some senses aren't "proper" grain boundaries – they behave and look different from high angle boundaries and they are created differently as well.

Lets consider the simplest kind of low-angle boundary – the symmetrical tilt boundary as depicted in the figure below. A slightly deformed single crystal or isolated grain (Figure 7A) relaxes, e.g. due to heating, into two regimes divided by a boundary with a low-angle misorientation across (Figure 7B). To accommodate this misorientation and preserve the perfect grain structure on both sides, an array of identical edge dislocations is found in the boundary region. Each dislocation is thus responsible for making the upper part of the bi-crystal contain one more atomic layer than the lower part, as the half-planes of the edge dislocations end inside the crystal. The more of a bend the larger the misorientation and the more dislocations will naturally be needed to accommodate e.g. "fill the gap" between the two crystals and the closer these dislocations will be spaced.

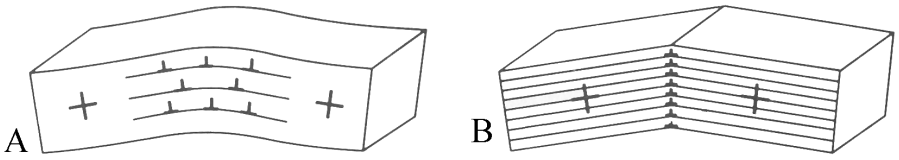

Figure 7: Schematic on the formation of a low angle boundary. A) Cold worked grain with a uniform distribution of edge dislocations. B) After heating the dislocations have rearranged to form a low-angle boundary (illustration from Hull and Bacon [13]).

In this case of a symmetrical tilt boundary, only one type of dislocation is needed to accommodate the misfit. In the general case, a low-angle boundary will need up to 3 different types of dislocation, and will thus contain three independent arrays of primary dislocations.

Above a certain angle of misorientation, the amount of dislocations needed becomes so great that the spacing between them dwindles to nothing and the cores of the dislocations begin to overlap. At this point the dislocations cease to exist individually and thus the description of the boundary as arrays of dislocations breaks down and another description is needed. Models and calculations have shown this to happen at misorientations of 10-15°. By a novel approach this transition has recently been determined experimentally to occur at 13.6° for

symmetrical <112> and <111> tilt boundaries [14]. This angle should be expected to vary somewhat depending on boundary type (dislocation content) and axis why we as a ground rule consider all boundaries above 15° of misorientation to be high angle boundaries.

CSL boundaries

Kronberg and Wilson originally introduced the concept of coincident sites in 1949 [15]. Later it was developed into the Coincident Site Lattice (CSL) model put forth in 1964 by Brandon et al. [16] and is to this day still one of the most successful attempts to describe special cases of high-angle grain boundary structure.

To grasp the idea of coincident sites it is again useful to consider two interpenetrating lattices. Because of symmetry one will find that at certain angles of misorientation a large fraction of lattice points in one lattice will be periodically overlapping lattice points in the second lattice exactly i.e. some lattice points will actually belong to both lattices simultaneously. This is shown in a two-dimensional case (or for a simple cubic structure seen along the [100] axis, if you will) on Figure 8 and while the principle is equivalent in a 3D system (tilt along a different axis) this is somewhat harder to picture. In the below example the grids are misorientated 36.8° with respect to each other (around the normal to the paper obviously), and every fifth lattice point in each lattice, marked with black, can be seen to coincide in a periodic array - a coincident site lattice. The implication of this is that a boundary placed between grains with such misorientation will contain particularly stable positions where atoms fit perfectly to both lattices. In other words one gets a rather good overall fit between the two neighbouring grain faces, resulting in a relatively stable – that is low-energy grain boundary.

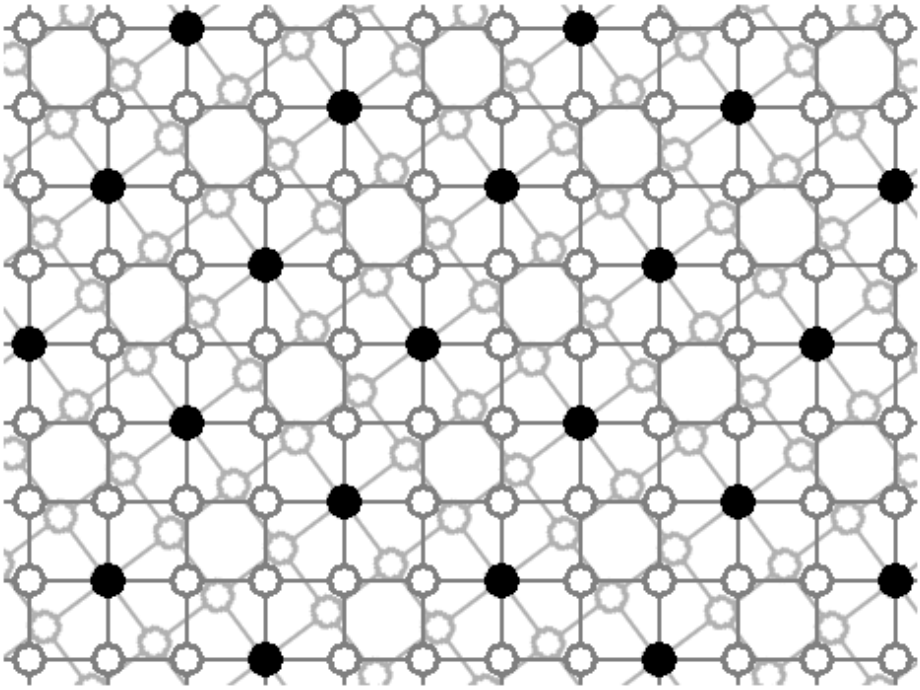

Figure 8: 2-dimensional illustration of the CSL principle. Two interpenetrating lattices are shown, the lighter turned 36.78° anti-clockwise with respect to the darker lattice. Coincident site positions are marked with black.

Boundaries satisfying such conditions of misorientation are designated with a sigma number derived as the reciprocal of the fraction of coincident sites present. Using this nomenclature on the above 2D case we would thus arrive at a designation of Σ5 (or Σ=5 as some prefer) and the most common of real CSL boundaries, the coherent twin, we would designate Σ3, as a third of this particular boundary is comprised of coincident site lattice points. Note that the CSL designation is based entirely on the misorientation, and that the position of the grain boundary plane is secondary. The orientation and inclination of the boundary plane will however determine how many coincident sites that will actually be present inside the grain boundary, and can thus also play a major role in determining how stable the boundary is.

For high values of Σ there can be more than one misorientation for which the same fraction of coincidence sites are generated (not to be confused with the 24 equivalent descriptions for *each* misorientation). Thus e.g. two misorientations exist giving a value of Σ=13, three giving Σ=31 and these are named a, b and c accordingly.

In real polycrystals the chance of a grain boundary misorientation being exactly that of a CSL is small indeed. However the special properties associated with such boundaries are also observed to occur in boundaries with misorientations which are close to but not exactly at CSL. It is found that for small angular deviations from perfect CSL, the coincident structure is preserved by arrays of dislocations known as secondary (intrinsic) grain boundary dislocations - analogous to the way the perfect lattice structure is preserved on each side of a low angle boundary by primary (intrinsic) boundary dislocations. In the same way one will find that the larger the deviation from perfect CSL the more secondary dislocations will be needed to accommodate.

Brandon [17] developed a criterion for the maximum deviation from exact CSL that was allowed while still conserving the special structure and properties. The sound argument went that as the density of coincident sites decreases with increasing Σ the maximum permissible density of boundary dislocations must also decrease with Σ, so that only coincidence boundaries with small Σ will persist over any appreciable range of orientation. Low-angle boundaries can be considered a special case of CSL with Σ=1 (every lattice point is a coincident site for very low angles) for which the maximum angular deviation is found experimentally and theoretically (core overlap) to be approx. 15°. This led to the expression for the Brandon criterion:

$$v_m = v_0 \Sigma^{-1/2} \qquad \text{(Eq. 6)}$$

with v_m as the maximum angular deviation and $v_0 = 15°$. The exponent was later modified by Palumbo and Aust on theoretical grounds and in better agreement with experiments [9, 18] to the more restrictive:

$$v_m = v_0 \Sigma^{-5/6} \qquad \text{(Eq. 7)}$$

which is now known as the Palumbo-Aust criterion. The Palumbo-Aust criterion is especially restrictive to higher sigma values compared with the Brandon criterion, so that for a Σ3 a deviation of up to 6° is acceptable within the CSL model while for a Σ25 only about 1° degree of deviation can be accepted. The Palumbo-Aust criterion will be used exclusively in the present thesis to give angular deviation v from perfect CSL, usually in the form v/v_m, which consequently will be a parameter ranging between 0 and 1.

Another part of the original criterion that has been modified is the upper limits of sigma values. Empirical investigations of grain boundaries suggest that special behaviour is only displayed for $\Sigma \leq 29$ [19, 18], why this upper limit will be used in the present work. On the table below, all these CSL are shown in geometrical detail.

Σ	θ	UVW	v_m	Planes of Mirror symmetry
3	60	111	6.00	111 211
5	36.87	100	3.92	210 310
7	38.21	111	2.96	321
9	38.94	110	2.40	221 411
11	50.48	110	2.03	311 332
13a	22.62	100	1.76	320 510
13b	27.80	111	1.76	431
15	48.19	210	1.57	521
17a	28.07	100	1.41	410 530
17b	61.93	221	1.41	322 433
19a	26.53	110	1.29	331 611
19b	46.83	111	1.29	532
21a	21.79	111	1.19	541
21b	44.40	211	1.19	421
23	40.45	311	1.10	631
25a	16.25	100	1.03	430 710
25b	51.68	331	1.03	543
27a	31.58	110	0.96	511 552
27b	35.42	210	0.96	721
29a	43.61	100	0.91	520 730
29b	46.39	221	0.91	432

Table 2: Angle and axis of misorientation, maximum deviation (Palumbo-Aust) and twinning planes for all CSL ($\Sigma \leq 29$).

Notice that only odd values of Σ arise for cubic crystal systems. Note also that in the general case the deviation from exact CSL will be on the axis as well as the angle of misorientation. This should naturally be taken into account for calculation purposes and measured misorientations should never be quoted by angles alone. The angular deviation v is properly taken between the measured misorientation axis UVW of the boundary and the axis for perfect CSL. To illustrate this point the calculated misorientation and deviation for two different experimentally measured twin boundaries are given here as:

1) [0.5867 0.5770 0.5682]/59.8°, $v/v_m = 0.08$
2) [0.5786 0.5784 0.5750]/59.6°, $v/v_m = 0.02$

Even though the first boundary has the misorientation angle closest to 60°, the axis is further from the [111] direction of a perfect $\Sigma 3$ than the second boundary, and thus ends up with the greater deviation.

Take heed that one strictly speaking should distinguish between boundaries which are special in the geometrical sense (low-angle and CSL) and boundaries which display special properties. While most boundaries that have been found to have special properties are also geometrically special, the reverse is not necessarily true. With the adoption of a stricter criterion for CSL (Palumbo-Aust) the agreement between the two types has increased significantly but it is still not a perfect match.

The O-lattice model

The O-lattice model was developed by Bollmann [20,21,22,23,24] in an attempt to find a more general kind of description for periodic occurrences between crystal lattices, than that of the CSL model.

This led to the concept of generalised coincidence or O-points, that is coincidence of points with the same internal co-ordinates in the two crystal unit cells. This could be e.g. coincidence between cell centres with internal co-ordinates ½,½,½ (which contains no atoms in a FCC lattice) rather than the CSL coincidences of 0,0,0 and 0,½,½. In addition coincidence of lines and planes (O-lines and –planes respectively) are included as well in order to help determine configurations of best fit between two crystal faces. In this respect the CSL can be regarded as a special sub-lattice of O-lattices since the CSL comprise coincidences of lattice points only. In the same way as CSL-points the O-points (-lines and –planes) represent regions of exact matching or points of 'minimum strain' implying that between the O-points there is an accumulating disregistry. Physically this disregistry is assumed to be concentrated into dislocations approximately midway between O-points and this connection allows for determination of dislocation content in crystal interfaces through the usage of the otherwise purely geometrical O-lattice construction.

One of the constructions of the O-lattice model that have proved particularly useful is the so-called Displacement Shift Complete (DSC) lattice. The DSC lattice can be geometrically defined as being the coarsest lattice, which can be constructed so that it contains both crystal lattices 1 and 2 in the coincidence orientation and position as sub-lattices. This lattice defines the possible Burgers vectors of secondary dislocations, perfect grain boundary dislocations that conserve the structure of the optimal boundary for the given misorientation. Thus the DSC can be used for determining possible Burgers vectors of secondary dislocations in a given boundary, fusing the dislocation model description with the periodicity (e.g. coincidence) description.

Another practical application of O-lattice models is for determining best fit of phase boundaries. CSL structures between crystals (or grains) of different composition and lattice parameters such as phase boundaries are extremely rare if geometrically possible at all. The much wider scope of the O-lattice model however allows for describing periodic structures in such boundaries as well and for determining lowest-energy constructions.

For our present purpose though, the CSL model is quite adequate to describe creep mechanisms and results, and the O-lattice model will therefore not be touched further upon in this text. More information can be found in the original texts or e.g. in the review by Smith and Pond [25]

Twin boundaries

The twin boundary, or the $\Sigma 3$, is as mentioned a unique type of CSL. Not only is it the CSL with the largest fraction of coincidence sites (every third) and by far the lowest energy of all high angle boundaries, it is also created by its very own mechanisms, deformation or growth twinning. Twin boundaries are thus very common in some materials, while rarer in others.

Due to the way twins are created the twin boundary is preferentially aligned along a {111} plane common to both adjacent grain lattices, forming what is known as a coherent twin boundary. Across the coherent twin boundary the regular stacking sequence of close packed {111} planes is inverted from ABCABC to ACBACB as seen in Figure 4, creating a narrow band of hexagonal close packed structure (around the twinning plane). Since the coordination between nearest and next-nearest neighbour is unchanged, though, the energy of

the boundary is extremely small, and consequently many coherent twin boundaries are virtually completely planar and relatively immobile.

Σ3 boundaries that are not parallel to a {111} plane in both adjacent grains are termed incoherent. A possible special case of incoherent Σ3 is when the boundary plane coincides exactly with a {211} plane common to both crystals. This {211} will then be a plane of mirror symmetry (as the {111} plane is in the coherent twin) and will be lying normal to the {111} plane of the coherent twin boundary. As the {211} boundary is highly symmetric, compared with other incoherent Σ3, it is sometimes referred to as "the symmetric incoherent twin boundary" and one would expect this to be of particularly low energy. Alas this is surprisingly not the case, as will be discussed later (page 41).

Often one will find that twin boundaries are not completely coherent along their entire length and that parts of the boundary will display an incoherent boundary plane. This occurs whenever a twin lamella ends within a grain or at ledges in a facetted twin boundary. Facetting is decomposition of a high-energy boundary plane into a mixture of two relative low energy boundary facets (see figure below). This will tend to occur whenever the facets are of sufficiently low free energy (per unit area) to more than compensate for the increase in interface area that occurs [26], and can be feasible for twin boundaries because of the very low energy of the {111} boundary plane.

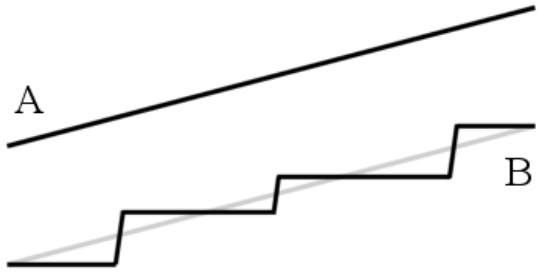

Figure 9: Facetting A) Initially flat high-energy (twin) boundary B) Facetted boundary containing two new low-energy boundary phases (facets).

The size of individual facets can vary immensely from single steps of one (111) plane height to ledges of hundreds of nm (as shown in the examples throughout section 2.4). In Figure 10 the formation of a single step is described as a consequence of mechanical twinning. Gathering of such single steps may lead to construction of actual ledges, but the laws governing the ideal size of ledges in a given boundary seems not yet entirely understood. When ledges arise as a consequence of facetting new properties are introduced to the boundary, compared to a completely flat coherent twin, e.g. the mobility of the boundary is greatly enhanced [26].

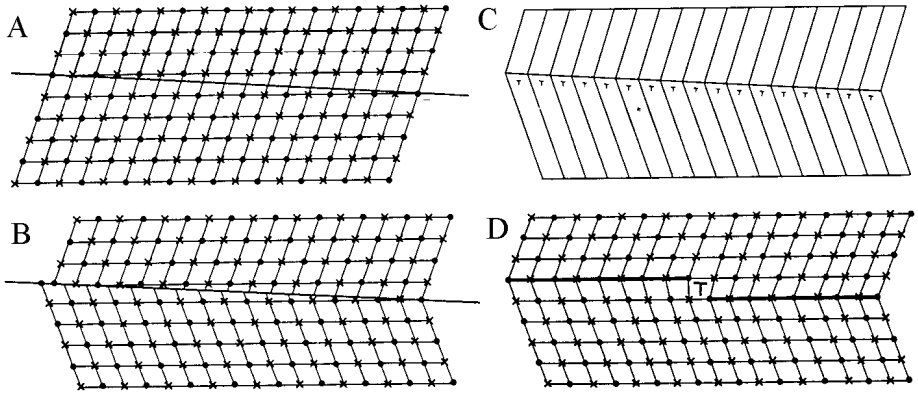

Figure 10: The formation of a step in a (111) mechanical twin boundary. A) a single FCC lattice structure as seen along the [1-10] axis B) The lower half undergoes mechanical twinning and it is seen that the two halves no longer fit. C) To fit the two parts once more stress is introduced, continuously distributed. D) Localisation of the stress into a 1/6 [11-2] dislocation associated with a step of one (111) plane height (figure from [26]).

It is noticeable, as seen on Table 2, that every CSL misorientation is geometrically disposed for one or two planes of mirror symmetry, completely equivalent to the Σ3. No other sigma boundaries than the Σ3 is known however, to be generated by a similar ”twinning” procedure and the grain boundary planes of randomly generated CSL boundaries will therefore be statistically biased to other than the high symmetry mirror plane.

Triple junctions

As two grains meet at a surface, namely a grain boundary, three grains can meet at a line, called a triple line or triple grain junction. The physics of triple junctions are governed by several geometrical and energetical considerations that can be formulated in the following simple but interesting rules [4]:

- The angle between each grain at the junction is 120° for grain boundaries that are in equilibrium and have equal energies. This balance is obviously disturbed when low energy CSL boundaries are involved.
- The misorientation matrices $\mathbf{M_1}$, $\mathbf{M_2}$, $\mathbf{M_3}$ for the three boundaries satisfy the condition:
  $$\mathbf{M_1} = \mathbf{M_2}\,\mathbf{M_3}^{-1}$$
  where the three matrices are expressed in the same reference system.
- The three boundaries share a common misorientation axis (bearing in mind that the misorientation of each boundary can be described by 24 different axes)
- The sum of the angles of misorientation for two of the boundaries equals the angle of the third boundary (for the common axis of misorientation only)
- The product or quotient of two of the Σ values equals the third (works only for CSL triple junctions obviously)

In a heavily twinned material such as ours, the natural choice of example to display the consequences of the last three rules is the triple junction of a Σ3, a Σ9 and a Σ27:

$$[110]/31.6° \; + \; [110]/38.9° \; = \; [110]/70.5°$$
$$\Sigma 27 \quad / \quad \Sigma 9 \quad = \quad \Sigma 3$$

Note that the final rule is only applicable for Σ boundaries very close to perfect CSL and that even though it obviously goes against the rule it is not uncommon to find triple junctions with only 2 CSL boundaries. As the allowable angular deviation from perfect CSL decreases with increasing Σ value, the boundary with the highest Σ value of the three will thus often be just outside the CSL description ($v/v_m>1$).

The geometrical sisterhood of Σ3, Σ9 and Σ27 means that a material, which is rich in Σ3 boundaries, such as ours, will automatically exhibit an increased amount of Σ9 and Σ27 as well. Thus if a twin grain, for some reason, creates a twin grain of it's own, this new grain can either have an orientation completely equal to the original grain or be misorientated Σ9 with respect to it. On Figure 35 (page 68) an example of a heavily twinned grain is shown displaying Σ9 and Σ27 boundaries.

As triple junctions thus are an important part of the structural network of grain boundaries, they play a crucial role in the movement of grain boundary dislocations. Secondary dislocations will start moving in the boundaries under certain circumstances (like diffusional creep) and according to modern boundary models this movement must obey certain rules that can be formulated as [27]:

- The secondary GBDs are confined to the grain boundaries. Lattice dislocations can, however be emitted from the grain boundary by suitable reactions.
- Secondary GBDs do not generally have Burgers vectors lying in the plane of the grain boundary, and their motion will therefore be controlled by climb. This motion will also generally give rise to simultaneous grain boundary sliding and grain boundary migration.
- The allowed Burgers vectors for secondary GBDs depend on the particular boundary in which they are situated. Therefore secondary GBDs cannot simply move from one boundary to another across a triple junction but must undergo reactions to produce new GBDs in the two boundaries beyond the junction. Such product dislocations will not necessarily be intrinsic but can have extrinsic character instead.

From the previous it should be clear that triple junctions present an obstacle to the movement and transference of GBDs between different grain boundaries. Therefore it is reasonable to expect dislocation pile-ups at triple junctions in conditions of heavy GBD movement. It would also be natural to expect distinct differences in how readily the transference of dislocations occurs when high-symmetry boundaries are involved.

The reactions required for secondary GBDs to enter e.g. the highly distinctive Σ3 boundary structure are likely to result in "residue" dislocations, that have no place in either of the involved triple junction boundaries. Such "residual dislocations" could be thought to prevent further dislocation transference between the boundaries or they could, given the sufficient stress, be dispersed into the grain structure.

As movement of secondary GBDs is an intricate part of diffusional creep, as we will examine later, triple boundaries play an important part of this deformation mechanism, although their role in resolving creep rates is still not quantitatively understood.

The Structural Unit model

An alternative description of grain boundary structure, which is also prevalent, is the model of structural units. The approach in this model is to focus on individual clusters of atoms in the boundary and identifying the characteristic con-

figurations in which they are arranged. These polyhedral configurations – structural units – can be shown to adopt a limited number of different shapes and any boundary can be described as a 2-dimensional array of such repeating units. Boundaries containing only a single type of structural unit are found to posses relative low energy, and if this type additionally can be classified as one of the basic (or primitive) units the boundary is called favoured.

There is found to be a large coincidence between CSL boundaries and these favoured boundaries, especially for low Σ values. While boundaries close to perfect CSL have secondary dislocations to retain the low energy configuration the 'favoured boundary' counterpart are found to contain a minority of "secondary" structural units with a periodicity identical to that of the CSL [28]. The potential to translate structural units directly to dislocations (or vice versa) finally helped establish that the geometrical and atomistic descriptions are equivalent and not independent as was initially proposed. While the structural units model give a more detailed understanding of grain boundary structure it doesn't solve the problem of defining a definitive criterion for separating boundaries with special behaviour from others. It can be argued that as some minimum of order can be found in the arrangements of structural units in even highly energetic boundaries it gets actually more problematic.

The structural units model has been developed from grain boundary energy calculations and the utilisation of the model still relies heavily on computer simulations to identify the structural units, which will be present in a given boundary. Given a certain minimum of information the structural unit model allows the prediction of both boundary structure and certain properties such as grain boundary self-diffusion but the usefulness of the model seems limited to pure tilt and pure twist boundaries with low index rotation axes [29].

1.2 Diffusional Creep

The deformation mechanism (or mechanisms rather) known as diffusional creep have for some time been under attack for not being able to deliver in observations and measurements what is predicted in the otherwise very appealing models. These attacks have been made to the extent of denying the occurrence of this type of creep in metals altogether and have forced the creep community to reconsider the available evidence and obtain new (phenomenological) facts to support the basic physical principles. To this day the fiercest sceptics remain unconvinced.

Creep

Creep is the common term used to describe slow, time-dependant plastic deformation exhibited by crystalline materials subjected to a stress, usually at elevated temperatures. Elevated temperatures is a relative term, and the ground rule is that creep becomes appreciable at temperatures for $T/T_m \geq 0.4$, were T_m is the melting point (in K). T/T_m is also known as the homologue temperature. In contrast to "conventional" plastic deformation, which is practically only dependent on stress, so the creep strain is dependent on temperature and time as well. For this reason the concern of creep is particularly important in specific applications and industries (e.g. power generation and aerospace).

Creep tests are typically carried out by loading a specimen, either in tension or compression, inside a furnace where temperature is carefully controlled (control of atmosphere is usually necessary as well to avoid oxidation or other unwanted reactions). Usually the load as well as temperature is kept constant and the ex-

tension of the sample is measured as a function of time resulting in a creep curve of the general shape seen in Figure 11.

The curve is usually divided into three areas of interest, namely the primary, the steady state and the tertiary creep stage. Primary creep occurs in the initial phase of the test and is characterised by a fast, decreasing creep rate in a limited amount of time. The steady-state (or secondary) stage takes over when the creep rate has stabilised and throughout this stage the creep rate keeps relatively constant. It is this steady-state stage that is normally of concern and this stage only that the following creep rate equations are trying to describe. It is important to note that the somewhat misleading term 'steady-state' refers to the creep rate only. Microstructurally the material degenerate throughout the entire creep test and thus the state of the material is not steady at any point. The final tertiary stage will see a continually increasing creep rate that usually spells the beginning of the end for the life of the test specimen. It is from the onset of tertiary creep that the macroscopic evidence for creep damage begins appearing e.g. voids and cracks opening up in the grain boundaries.

It is pretty dangerous to generalise too much over creep behaviour, though, as creep curves more often than not will have completely different proportions (than those shown below) between the three stages and in some creep experiments individual stages can even be seen lacking entirely.

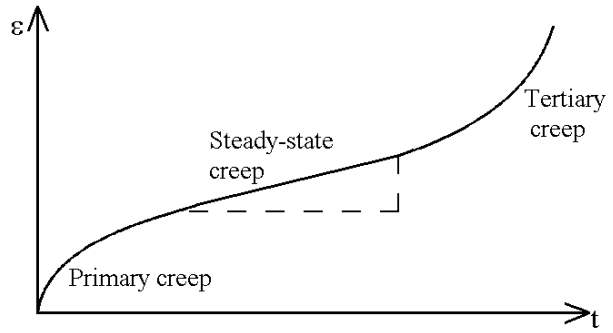

Figure 11: "Typical" creep curve (strain as a function of time).

Behind the term 'creep' several more or less independent mechanisms are hiding, each of which can be the dominating deformation mechanism for a given choice of material and creep parameters. A simple overview of these can be had from a stress/temperature diagram such as the one seen in Figure 12, which is known as a deformation mechanism map or an Ashby diagram. Each field in the diagram represents a range of stress and temperature where a single deformation mechanism is the dominating i.e. the fastest (rate-controlling) of all possible mechanisms and at the boundaries where the fields of two mechanisms meet these will contribute equally to the strain-rate.

The dotted line at the top marks the theoretical yield strength of the material given a perfect (without defects) single crystal. The field immediately below this line is the conventional, well-known plastic deformation mechanism born by the glide of dislocations. In addition we have three fields of different creep mechanisms, which we will return to in detail. Finally we have the field 'elastic regime', which is but a region where the strain rate is below what is readily measurable (arbitrarily chosen to 10^{-8} s^{-1}). Note that lowering this limit would serve to extend the fields of creep dominance.

The diagram can thus be used as a guide to help appreciate which mechanisms might be operating in a given situation and what strain rates to expect. On the other hand one has to be careful not to exaggerate the usefulness of such diagrams, as they clearly has severe limitations. First of all the diagram can hardly

be expected to be more accurate than the strain equations from which it has been constructed; equations that are describing only the steady-state creep phase and which may even be controversial or contain poorly determined constants. Secondly the shown mechanisms have different dependencies on microstructural features (grain size, precipitates, texture) which are not expressed directly in the diagram and which can alter the size of the respective areas significantly. One also has to be aware that although the creep experiment is performed in an area where one specific mechanism is rate controlling, significant contributions to the overall strain can still occur from other mechanisms. For all these shortcomings deformation mechanism maps such as these can still be quite useful for *roughly* defining the different regimes as long as the limitations are kept in mind.

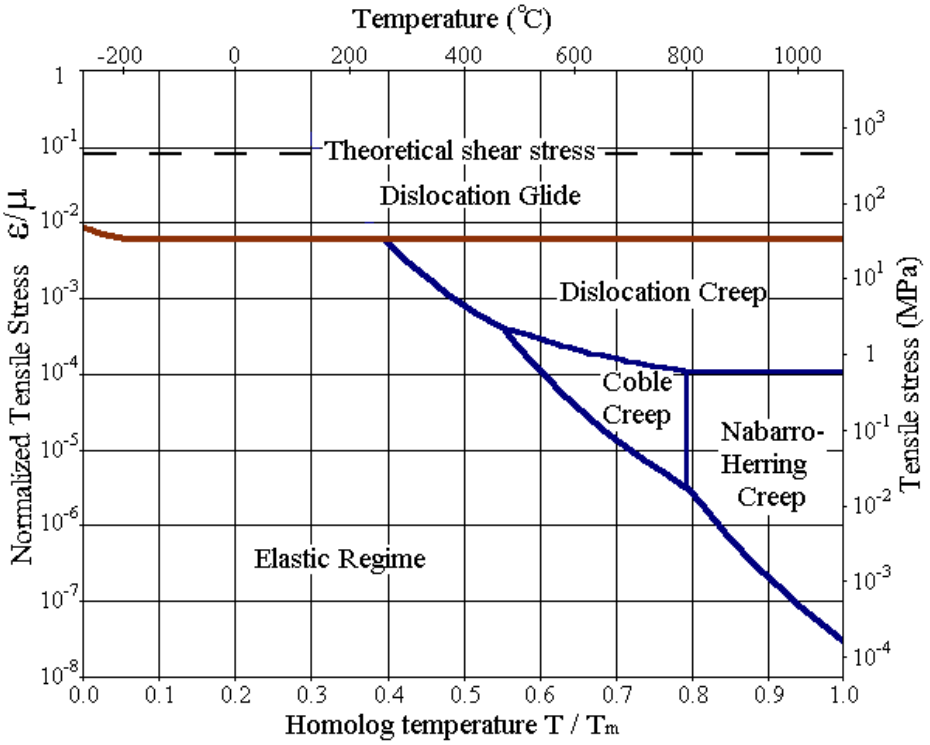

Figure 12: Ashby diagram for pure copper, constructed from constitutive equations and data from [2]. The standard microstructural state used includes a grain size of 32 μm and an obstacle spacing of 50 nm.

Of the creep mechanisms dislocation creep is by far the technologically most important and it is this mechanism that is normally associated with creep fracture and deformation. Dislocation creep is also known as power-law creep as the creep rate, in the steady-state part of the deformation, can be described as dependant on stress like $d\varepsilon/dt = B\sigma^n$, with the creep exponent n usually ranging between 3 and 8. In dislocation creep it is movement of dislocations through the lattice, by climb as well as glide, which causes the deformation. In a certain respect it can be thought of as similar to conventional plastic deformation, where deformation is caused by dislocation glide (slip) only. In dislocation creep the dislocations furthermore have the ability to climb, thus enhancing their ability to overcome the obstructing effects of obstacles (e.g. solute atoms, precipitates or other dislocations) and effectively lowering the stress needed for strain to accumulate. The climbing process is as mentioned conditioned to the absorption/emission of vacancies and so dislocation climb is coupled to the rate of self

diffusion, which is why elevated temperatures is needed for this process to occur.

Before moving on to the diffusional creep model there is a third creep mechanism, which is worth mentioning, namely that of Harper-Dorn creep. Harper-Dorn creep was proposed on the basis of unexplainable creep result in aluminium [30] and has since been reported in other materials as well. The physical basis for the H-D creep mechanism is still not entirely worked out but it seems clear that it is the movement of dislocations that in some way are responsible for the deformation. On the basis of discrepancies in measured Harper-Dorn creep rates recent work have questioned the validity of this process as an independent mechanism altogether [31]. Harper-Dorn creep has never been observed in copper, which is why it is not marked on the above mechanism map, and further discussion of whether it exists as an independent mechanism or not will therefore be charitably left to others.

From hereon references to creep mechanisms will implicitly imply one of the two diffusional creep mechanisms unless otherwise stated.

The diffusional creep model

The model for diffusional creep was originally proposed by Nabarro back in 1948 [32] at a time where precious little was known about grain boundary structure, and as such the model was developed in a form that was the best possible at the time. The basic assumption was that all boundaries act as perfect sinks and sources for vacancies during creep deformation. The equilibrium concentration C of vacancies at a boundary under a stress σ can then be calculated by:

$$C = C_{eq} * \exp(\sigma\Omega/kT) \qquad \text{(Eq. 8)}$$

where C_{eq} is the thermal equilibrium concentration of vacancies as given by Equation 1 and Ω is the atomic volume. The stress value is positive for boundaries in tension and negative for boundaries in compression, thus causing an increase and decrease of vacancies in these boundaries respectively. A concentration gradient will therefore be set up in a grain under stress and this will result in a diffusional flow of vacancies from boundaries in tension to boundaries in compression corresponding to a flow of atoms in the opposite direction. Material will thus be transported from longitudinal (parallel to stress axis) boundaries to transverse (normal to stress axis) causing a simultaneous elongation and narrowing of the grain, as shown on Figure 13.

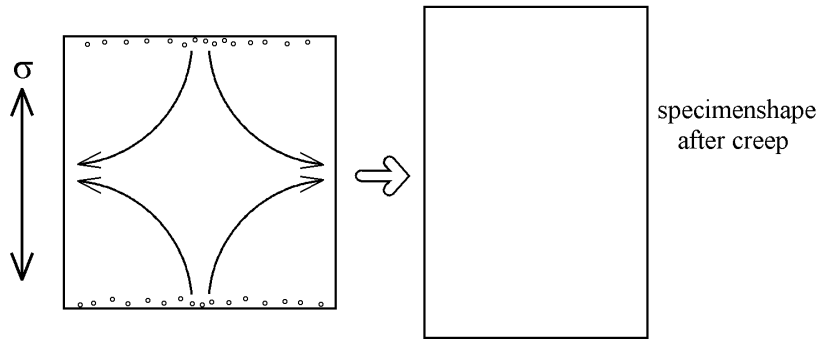

Figure 13: The diffusional creep principle shown for a specimen under a vertical stress. Vacancies diffuse from transverse boundaries (in tension) to longitudinal boundaries (in compression), corresponding to a flow of atoms in the opposite direction.

With the further assumption that the rate controlling process is the diffusion of vacancies through the lattice, Nabarro and Herring [33] derived the following rate equation for the mechanism:

$$d\varepsilon/dt = B\sigma\Omega D_L/d^2 kT \qquad \text{(Eq. 9)}$$

where B is a numerical constant of about 12, D_L is the lattice self-diffusion coefficient and d the grain size. Later Coble [34] pointed out that diffusion might just as well occur through the loose-packed grain boundaries as well, and that diffusion along the boundaries actually would be faster in some circumstances. In this case the rate equation takes the form:

$$d\varepsilon/dt = B'\sigma\Omega wD_{Gb}/d^3 kT \qquad \text{(Eq. 10)}$$

where B´ is a numerical constant around 50, w the grain boundary width and D_{gb} the grain boundary self-diffusion coefficient. The two types of diffusional creep are now recognised as independent mechanisms, known as Nabarro-Herring and Coble creep respectively. Comparing the expressions one will notice the stronger dependence on grain size in Coble's rate equation favouring grain boundary diffusion for decreasing grain sizes. Another important dependence comes from the dependence of the self-diffusion coefficients, which can be calculated like:

$$D = D_0 \exp(-Q/RT) \qquad \text{(Eq. 11)}$$

where D_0 is known as the frequency factor and Q is the activation energy (both specific for each diffusion type, naturally). As the activation energy for lattice diffusion is typically 1.5-2 times larger than for boundary diffusion, Nabarro-Herring creep will be favoured at high temperatures while Coble creep will be dominating at low temperatures, which shows in Figure 12 as well.

Discussion of the model

For a long time arguments have been exchanged concerning the validity of this model. Although there's a general consensus that the theory is elegant and founded on physically sound principles, experimentally measured values of creep rates have often been at odds with the rates predicted by the equations. Worse still the stress dependence on creep rate have in many instances been found to be more than unity (n=1), which is what the diffusional model clearly predicts. At the same time some of the more qualitative evidence have been questioned and found not quite unambiguous and conclusive. The reasons for these discrepancies are various and still somewhat unexplained.

First of all we have come to understand that the basic assumption of *all* boundaries acting as *perfect* sources and sinks for vacancies during diffusional creep is somewhat inaccurate. Special boundaries of sufficiently low energy exhibit strong resistance against creep deformation, and it is suggested that this behaviour be directly related to the efficiency of boundaries as vacancy sinks and sources. With the present understanding of grain boundary structure it has become clear that the ability to emit (or absorb) vacancies from the boundary is in fact due to the presence of secondary grain boundary dislocations (GBDs). For Σ boundaries it applies that the closer to perfect CSL a boundary lies, the fewer secondary GBDs will be present, and it would therefore seem reasonable that the ability to emit (absorb) vacancies will decrease proportionately. If special boundaries constitute a large fraction of the total boundary volume and are thus impeded in participating efficiently in the generation of creep strain, this would surely cause slower creep rates than predicted.

Another weighty reason for the discrepancies and lack of convincing qualitative evidence is the fact that the diffusion of vacancies are closely coupled to several other mechanisms, dependant or independent, that efficiently help smear the collective picture of diffusional creep. These are:

- Grain boundary sliding
- Boundary migration
- Grain growth

Grain boundary sliding (GBS) is inextricably linked to and plays an important part of diffusional creep deformation. We have suggested that it is the secondary dislocations that emit (absorb) vacancies during diffusional deformation, a process that eventually set the dislocation in motion. The actual emission (absorption) is a necessary consequence of negative (positive) climb of the involved GBDs (see Figure 3), but generally glide of the dislocations will follow. This is because the secondary GBDs are confined to the grain boundary plane, and thus any movement must be an interdependent combination of the two types of motion (except in special cases where the Burgers vector for the GBD is parallel or perpendicular to the boundary plane). Were it not so the movement would quickly bring the dislocation out of the grain boundary plane.

Moving of GBDs will displace the two grains with respect to each other (each dislocation causing a displacement of exactly their Burgers vector) and this is the phenomenon known as grain boundary sliding. The movement of the GBDs will be in such a way as to contribute positively to the overall creep strain *in conjunction with the absorbed (emitted) atoms*. Secondary dislocations in a transverse boundary will emit vacancies and thus climb negatively dictating the gliding movement this way. The direction of the GBD movement is thus governed by the emission (absorption) of vacancies and is *not* independent.

Unfortunately the coupling of vacancy diffusion and grain boundary sliding still suffer from a popular misconception. Too many times the schematic of Burton [35] has been reproduced (see Appendix A) accompanied by a variant of the quote:

> *"To accommodate the shape change of individual grains, relative movement of adjacent grains in the polycrystal must occur by the process of grain boundary sliding. If this sliding did not occur, material coherency could not be maintained and cavities would open up."*

A new way of putting the last phrase, calling to mind our present understanding of grain boundary structure would be:

> *"If this sliding did not occur, the secondary GBDs would not be able to emit (absorb) any vacancies to begin with and hence there would be no change of grain shape to worry about anyway."*

Even today the old misconception flourish though and has recently been used as the basis for a simplified model in an attempt to separate the individual strain contributions of diffusion and sliding [36], a rather pointless exercise as the present author see it.

It is possible and can be fruitful, as we will return to, by utilisation of scratch marks, to measure the amount of sliding done by a particular boundary during creep. To subsequently refer to this value as the *individual strain contribution from grain boundary sliding* is erroneous.

Boundary migration is closely coupled to diffusion creep as well. In the general case the dislocation core of secondary GBDs will be associated with a step in the grain boundary plane to conserve the grain boundary structure on either side of the GBD [37]. An example is visualised on Figure 14 with A and B displaying the position of the boundary on each side of the dislocation. The

step naturally moves with the dislocation and in general the movement of secondary GBDs therefore leads to motion of the entire boundary, normal to the plane, a mechanism known as boundary migration. It is important to note that boundary migration in no way contributes to the creep strain, but only affects the respective sizes of the involved grains.

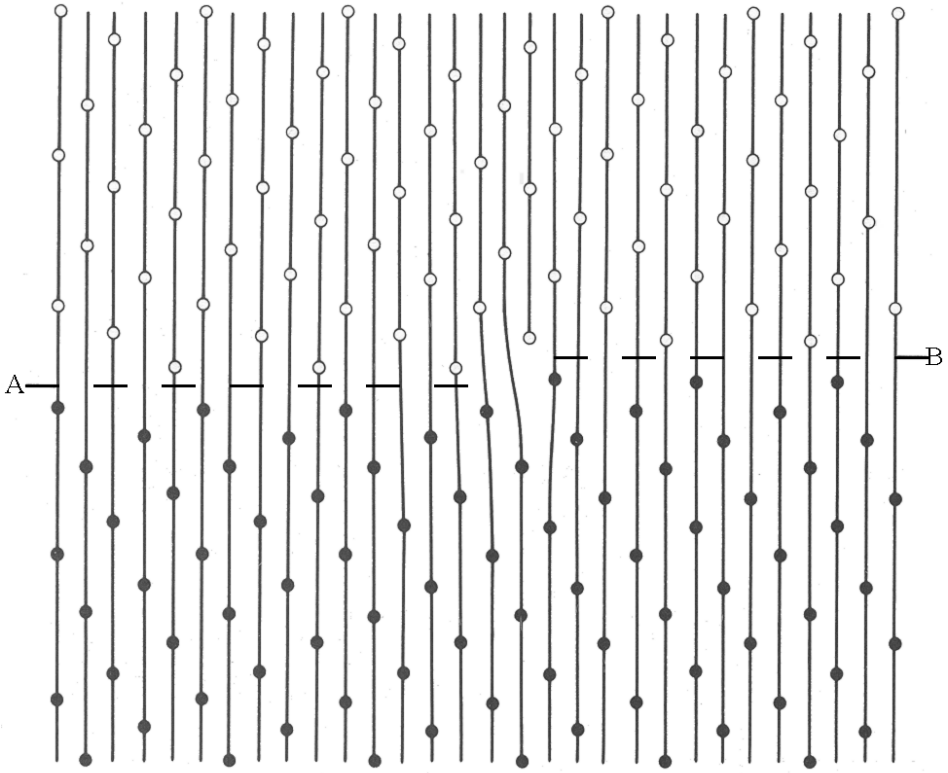

Figure 14: Illustration of a secondary edge dislocation with Burgers vector 1/10[130] producing a step in the $(3\bar{1}0)$, $\Sigma 5$ boundary (from Hull and Bacon [13]).

Grain growth is an independent mechanism that may or may not occur during diffusional creep testing. It is characterised by an increase in average grain size as some grains grow at the expense of other grains resulting in fewer, larger grains. As grain sizes and thus diffusion length increase as a result of grain growth one would expect it to result in a slowing down of creep rates. However experimental evidence have suggested that this is not the case and that grain growth during diffusional creep may actually have a positive effect on strain rates, presumably due to modifications on the stress redistribution [38].

Notice that absorption and emission of vacancies occur only at grain boundary dislocations in the context of diffusional creep. Free dislocations in the grains are able to absorb or emit vacancies as well during climb (as it happens during dislocation creep), but the higher stresses needed for this to play an important role usually places this outside the diffusional creep regime [39]. For now we will therefore exclude this process as irrelevant.

Diffusional creep phenomena

The just described mechanisms and influences all help complicate the quantitative or qualitative picture drawn in the original model. The reality of diffusional creep is therefore not as easily described as one might have hoped, but even as

some doubt can be cast on the original assumptions for diffusional creep, the basic physical principles behind remain unchanged and unchallenged.

With improved knowledge of grain boundary structure and properties we can go back to the basis and with no further assumptions attempt to reformulate the original mechanism. Taking into consideration the possibility of boundaries not partaking in the deformation process at all, the fundamental processes can tentatively be formulated as:

- The equilibrium concentration of vacancies will be raised at *active* boundaries under a tensile stress and lowered at *active* boundaries in compression.
- The concentration gradient will cause vacancies to diffuse from *active* grain boundaries in tension to *active* grain boundaries in compression, corresponding to a flux of atoms in the other direction.
- Material (i.e. atoms) will be removed from *active* boundaries in compression and deposited at *active* boundaries in tension.

Of the three above-mentioned processes the first two are clearly very difficult to observe or otherwise verify directly by experiments. The third process, on the other hand, has macroscopic effects that, given a properly designed reference system, can be readily identified. It is crucial to note here that the deposition or removal of material can be caused *only* by diffusion i.e. there is no other known mechanism that can account for deposition and removal of material.

To recapitulate the creep section it could be fruitful to examine some of the phenomena associated with diffusional creep deformation, in the light of our present understanding of grain boundary structure and diffusion processes. In particular, one could expect to find:

Inactive boundaries. First of all we would expect to observe special behaviour from stable boundaries such as CSL and near-CSL boundaries. It would be reasonable to expect a threshold stress, as it is seen for other low-energy boundaries, namely low-angle boundaries, under which no detectable vacancy sink/source activity occur [40]. Adopting the Gleiter equations to $\Sigma 3$ boundaries, a threshold stress of 970 MPa can be roughly estimated, implying that these boundaries should be completely inactive at normal creep stresses. The presence of secondary GBDs should cause this threshold stress to be lowered considerably for increasing CSL deviation.

One has to be aware, though, that the presence of inactive boundaries in no way is a characteristic of diffusional creep. Low energy boundaries such as CSL will, as earlier noted, display extraordinary stability against many types of deformation or degradation.

Negative glide/climb. GBDs may have their Burgers vector oriented relative to the stress axis in such a way that the forces acting on the glide and climb components have opposite signs. A grain boundary may therefore be forced to slide in the negative direction in order for the GBD climb to make a larger positive contribution to the overall deformation. Theoretically this is expected to occur predominantly at boundaries that are almost perpendicular to the stress axis [41]. Likewise negative climb may occur at boundaries almost parallel to the stress direction, in order for the grain boundary sliding to make a larger, positive contribution to the deformation [42]. Doing surface examinations (such as SEM) one has to be very careful though and note that longitudinal boundaries will here be competing with the free surface for the role of vacancy sink. For this reason it might be more fruitful looking for the phenomenon (negative glide) at the transverse boundaries instead.

Denuded zones. One of the most debated effects of material deposition is the occurrence of denuded or precipitate free zones. This phenomenon occurs in materials containing inert ”particles” (e.g. inclusions of foreign atoms, precipitates or voids as a result of radiation damage) evenly distributed in the main

material phase (known as the matrix). Diffusion of vacancies leading to deposition of new material at a transverse boundary will invariably lead to a zone where no such particles are present, as typically only the matrix element will diffuse (se Figure 15).

It has been postulated [43] that the diffusional creep model predicts denuded zones of equal width on each side of transverse boundaries. This is however not the case as we understand the process today. The depositions of atoms will as mentioned occur exclusively at the secondary dislocations in the boundary during climb of these. The exact nature (Burgers vector) of the dislocation will thus determine on which side of the boundary the deposition will actually occur (which of the two grains will grow) and each subsequent atom will be deposited on the same side by this exact dislocation, regardless of where the interstitial came from or the vacancy afterwards diffuses to. For a boundary with only a single type of secondary dislocations the entire deposition will thus occur exclusively on one side of the boundary, while boundaries with multiple arrays of dislocations can have a divided, but not necessarily equal, deposition. Simultaneous migration of such boundaries will invariably help to further complicate the picture and make generalisation impossible.

At longitudinal boundaries where the matrix material is removed one should likewise expect an accumulation or enrichment of precipitates, though this is generally a bit harder to establish.

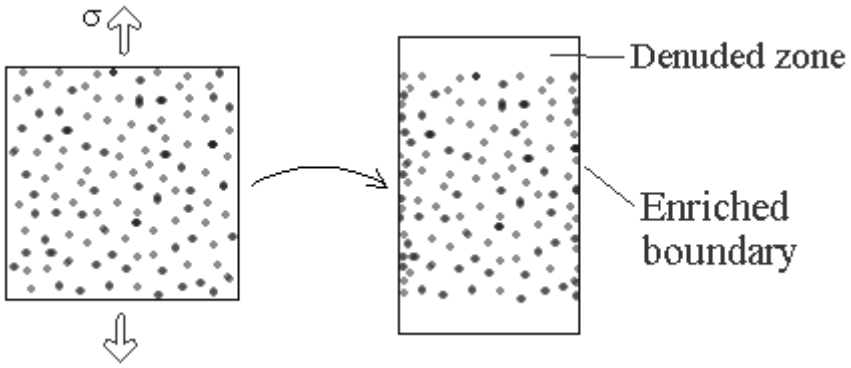

Figure 15: The formation of denuded zones by diffusional creep.

Other mechanisms than diffusional creep can be thought of to lead to occurrences similar to diffusional–based denuded/enriched zones and making the distinction have been the cause of much controversy. Boundary migration can be caused by e.g. grain growth or pure dislocation glide and a migrating boundary can ‘sweep’ a zone free from precipitates. As a moving boundary typically will not be able to simply pass encountered precipitates, these will instead be ‘pushed’ along leaving a denuded zone behind. A denuded zone created in this way would therefore be expected at the same time to show enrichment at the boundary, and the occurrence of this phenomenon should not show any dependence on stress axis (e.g. only occur at specific boundaries such as transverse).

The possible occurrence of denuded zones by other mechanisms makes this phenomenon unreliable to trust as direct evidence for the occurrence of diffusional creep.

As a final note it is necessary to stress that although we usually talk of the diffusional creep regime as being strictly low stresses and high temperatures, this is not necessarily the case. Diffusion takes place in all ranges and when nanoscale grain sizes are involved the field of Coble creep will expand dramatically (compare Figure 12 to Figure 16) and become the dominating mechanism for a large range of temperatures and stresses. Thus newer evidence points to diffu-

sional creep deformation for nanocrystalline gold and copper at temperatures of only 20–250°C and at rather high stresses of 200-140 MPa respectively [44,45].

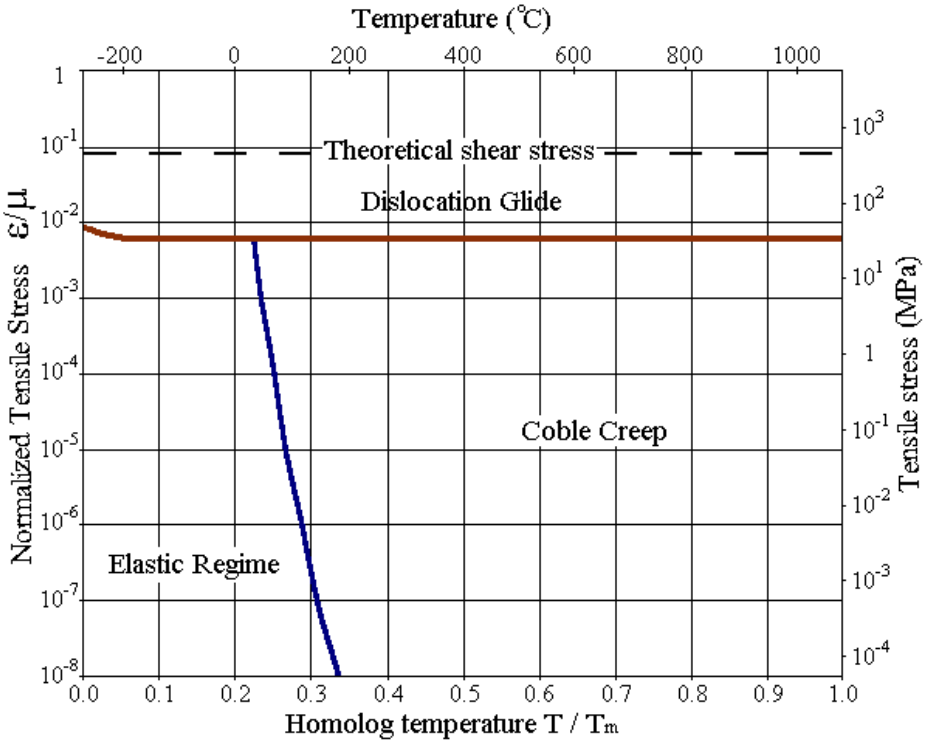

Figure 16: Strain mechanism map for pure Cu, constructed from constitutive equations and data from [2]. Grain size 30 nm, obstacle spacing of 50 nm.

1.3 Review

This short review will examine a few selected papers containing some of the important discoveries and novel experiments in the field of diffusional creep and grain boundary structure, including the work of Peter Thorsen. Additionally some of the papers and arguments of the diffusional creep opposition will be examined.

Denuded zones

During metallographic examination of a Mg(0.5w.%Zr) alloy for what they believed was corrosion attack, Squires, Weiner and Phillips [46] were the discoverers of denuded zones. The sample had been creep tested for 4734 hours at 450-500°C and a stress of 0.76 MPa after which zones along transverse boundaries were formed in which no Zr-precipitate was present. X-ray analysis showed that the zones were in fact completely denuded of zirconium, ruling out the possibility that the precipitates had somehow been dissolved and absorbed in the matrix of the denuded zone. In the interior of the grain the Zr-precipitates where evenly distributed and examination of unstressed parts of the sample showed no signs at all of denuded zones. This was a clear-cut example of a severe microstructural breakdown at a low supposedly ”safe” stress level and really brought attention to the technological importance of diffusional creep.

Efficiency of boundaries as vacancy sources

Jaeger and Gleiter were the first to report a relation between grain boundary structure and the efficiency of the boundary as a vacancy source [47]. Their experiment was done with bamboo structured Cu specimens with a vapour deposited layer of Al_2O_3 on one side. After creep deformation for 100 hours at 1075°C under a tensile stress of 0.1 MPa, they observed that cracks had developed in the Al_2O_3 layer at some, but not all, of the copper grain boundaries. The reason for the cracks was, they concluded, deposition of new material at the boundaries resulting in new free surfaces without Al_2O_3 and an overall elongation of the creep specimen. Closer examination shoved that all the boundaries, which had been inactive in the deformation, were low energy boundaries of the Σ3, 5, 7, 9, 11 and 15 types whereas all active boundaries were non-CSL (general). The crack width was measured for the general boundaries and varied between 0.1-5 μm.

A doubling of the stress and creep time used did not cause fracture of the Al_2O_3 at the CSL boundaries and Jaeger and Gleiter suggested that a threshold stress (which they obviously didn't exceed) seemed to exist for the vacancy emission at these boundaries.

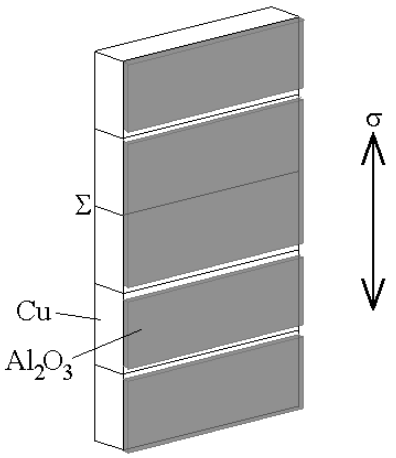

Figure 17: Bamboo structured Cu creep specimen coated on one side with Al_2O_3. After creep the uniform coating is cracked at most boundaries but intact at Σ boundaries.

The CSL boundaries in the study were unfortunately not further characterised by their deviation from exact CSL.

Creep anisotropy

Timmins and Arzt [48] examined the creep anisotropy arising in a material as a consequence of grain shape and texture. Their specimens of MA 6000 (Ni-Cr based super-alloy dispersion strengthened with Y_2O_3) have a structure with grains highly elongated in one specific direction and they were creep tested under compression in all three directions.

At high stresses (>200 MPa), where dislocation creep supposedly controls the deformation, they observed comparable creep rates between the longitudinal and the transverse stress loading. As the stress is reduced below "the dislocation creep threshold" though, large differences in creep rate are observed. With tensile stresses parallel to the long axis of the grains creep rates were very slow, which they formally ascribed to the very long diffusion distances. With com-

pressive stresses parallel to the long axis of the grains, diffusion distances were greatly reduced and creep rates a 100 times higher were measured.

Additionally precipitate free zones were widely observed at transverse boundaries for low stress tests, a phenomenon that didn't show at higher stresses.

Structure of ledged twin boundaries

Wolf, Ernst, Muschik, Finnis and Fischmeister [49] made a combined theoretical and experimental study of the influence of grain boundary inclination on the structure and energy of Σ3 boundaries in Cu.

Atomistic simulations were performed on 16 different twin boundaries defined by the inclination angle Φ. Starting with the coherent twin boundary at Φ=0° the boundaries were modelled by rotating the boundary plane about the $[00\bar{1}]$ axis ending up with the symmetric incoherent twin boundary (with boundary plane {211}, see page 26 for details) at Φ=90° as illustrated schematically on Figure 18. In addition they prepared nine different grain boundaries with well defined orientations, corresponding to nine of those simulated, and these were investigated by grain boundary grooving and high resolution TEM.

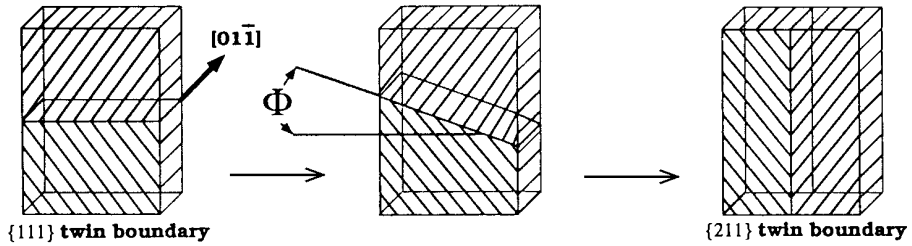

Figure 18: Definition of the various boundaries examined in terms of the inclination angle [49].

In addition to demonstrating the very low boundary energy of the {111} twin, they found the existence of another energy minimum, by simulation as well as experimentally, for a boundary inclined 82° to the coherent twin (see Figure 19). This boundary, termed M, they found to be more stable than a boundary exactly on the {211} plane (Φ=90) and in relaxation simulations the ideal symmetric incoherent twin indeed shows microfacetting into two structures – coherent twin and M boundaries. Wolf et al find the M structure to give rise to rather broad (1-2nm) boundaries and the boundary structure is explained by the structural unit model in terms of a rigid sandwich of rhombohedral 9R phase forming between blocks of FCC material.

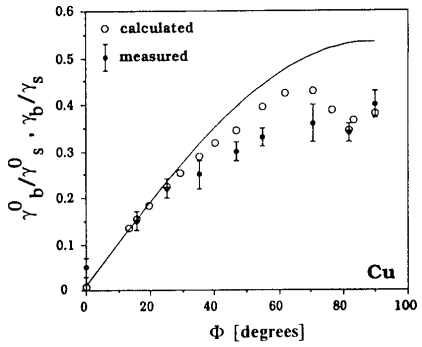

Figure 19: Grain boundary energy against inclination for Cu Σ3, [011] grain boundaries.

Observation of scratch displacement

A structural approach to diffusional creep evidence was taken by McNee, Jones and Greenwood [50]. Their specimens of Cu had purposely retained scratches from polishing, which after creep testing could serve as an inert reference. Careful 3-dimensional examination of scratch displacement across boundaries provided very convincing evidence for material deposition and removal.

Figure 20 is sketched from one of their actual boundary triple points after creep deformation. AFM scans showed this area to be almost smooth surfaced, which means that the grain movement relative to the surface during creep has been negligible. This effectively means that the 3-dimensional movement of the three grains can be interpreted solely in the two dimensions given by the figure. Taking a closer look it soon becomes evident from the positions of the scratches that grain 1 and 2 has moved apart and material therefore must have been deposited at their mutual boundary. Grain 3 has, apart from a bit of sliding, moved up towards the other grains and thus material must have been removed from its boundaries.

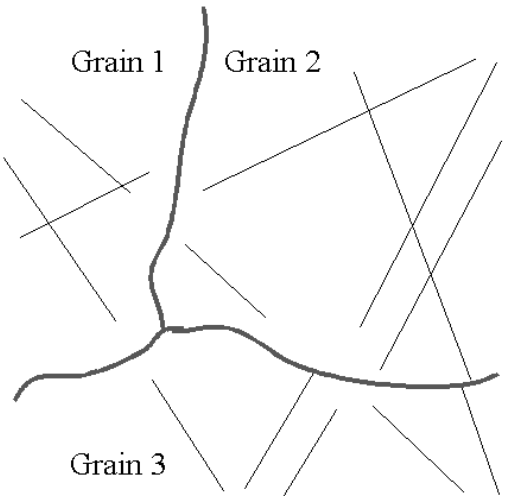

Figure 20: A sketch of a grain boundary triple point with surface scratches showing the creep deformation. Stress axis is horizontal

Evidence of this kind is hard to dispute and McNee, Jones and Greenwood claim intent to expand their line of investigations into composite materials and alloys as well.

Material deposition and inactive boundaries

Experiments by Peter Thorsen and Bilde-Sørensen [51,52,12] were made on specimens of Cu (99.99%) alloyed with 2wt% Ni (99.999%). Creep specimens were polished and provided on one side with a fine meshed grid of Al_2O_3 deposited with a photoresist technique. Linear intercept length for grain boundaries (coherent twins excluded) was 165 μm in longitudinal and 147 μm in transverse direction. Creep was performed at 1073K at 1.14 MPa to a total strain of 2.4%.

Surface investigations using the alumina reference grid showed the deformation to have occurred solely on grain boundaries while leaving the interior of grains largely undisturbed.

Misorientations of selected boundaries was calculated from electron backscattering patterns and it was revealed that all inactive boundaries were low energy boundaries, that is either low angle boundaries or Σ3 and Σ9 boundaries with a very low deviation. Amongst the active boundaries several CSL boundaries with high deviations were found. Characterisation was originally done by the

Brandon criterion, but has been converted to Palumbo-Aust deviations for easy comparison (in the process discarding half the measurements as v/v_m increased beyond 1). The results can be summed up as:

Inactive boundaries		
No.	Σ	v/v_m
28	3	0.03 - 0.21
3	9	0.27 - 0.31

Active boundaries		
No.	Σ	v/v_m
7	3	0.14 - 0.81
2	9	0.58 - 0.64

Table 3: Deviation range (Palumbo-Aust criterion) found for the given number of active and inactive Σ boundaries.

Despite the rough statistics there seem to be a clear correlation between low deviation from CSL, and thus low energy of the boundary, and the ability of the boundary to act as a vacancy source.

One of the extras was the demonstration of negative slide on a transverse boundary on the edge of the creep specimen (hence the poor surface quality) as seen on the figure below. From the grid displacements it is found that a layer of 4.8 μm new material has been deposited on the boundary and concurrently the boundary must have slid 1.8 μm in the negative direction.

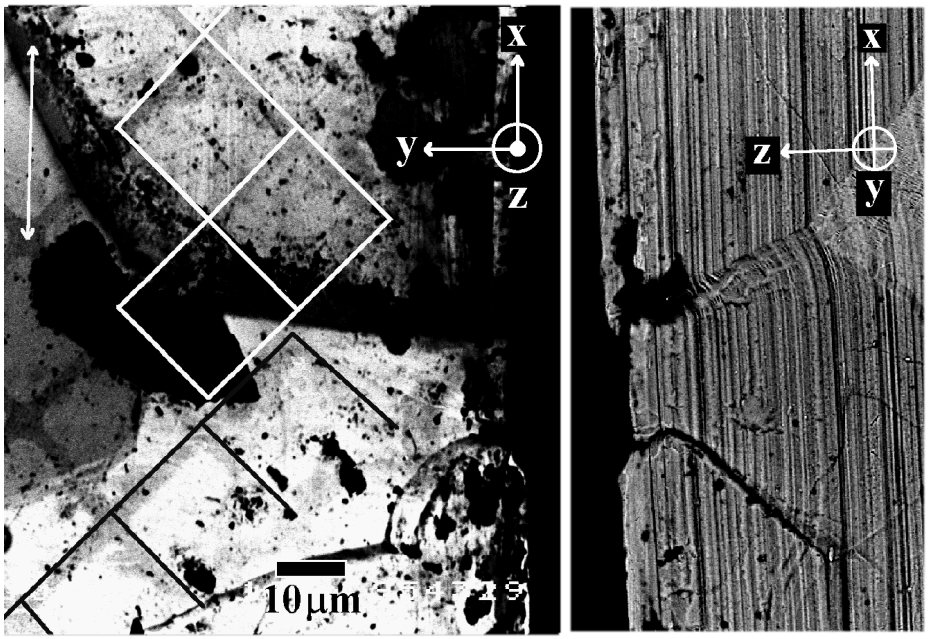

Figure 21: Example of negative slide. (a) The grid covered surface with grid redrawn for clarity. (b) Same part of the sample seen from the side. Traces from the machining can be used to evaluate z-motion of the grains.

Critical views on evidence for diffusional creep

As mentioned some of the ”creep fundamentals” described in section 1.2 have long been and to some extent are still quite controversial. The objections to experimental findings being interpreted as diffusional creep were initially raised by Ruano and Sherby in 1982 [53], and they have continued to lead the ”diffusional creep opposition” to the present day. In a recent paper with Wadsworth [54] they sum up two decades of controversy in an extensive and somewhat biased table, reproduced below as Table 4.

	Diffusional Creep Described as Rate-Controlling Process	– Alternative View – Grain Boundary Sliding and Dislocation Creep
1.	Coble diffusional creep is proposed as the deformation mechanism for several metals at intermediate temperatures by Jones et al.; these are Cu [55], α-Fe [56], Mg [57], β-Co [58] and 304 stainless steel [59]	Coble diffusional creep is rejected as a deformation mechanism for Co, α-Fe, Cu, Mg and 304 stainless steel at intermediate temperatures (0.4 to 0.6 T_m); GBS accommodated by grain boundary diffusion "(GBS-D_{gb})" is instead proposed [53]
2.	The conclusions of the 1982 paper [53] are rejected by Sritharan and Jones; new data on Co are presented to indicate evidence for Coble diffusional creep [60]	The new data on Co is used to show further confirmation for the GBS-D_{gb} model; the range of "GBS-D_{gb}" creep as influenced by grain size is illustrated [61]
3.	Creep of fine-grained austenitic stainless steel at 0.7 T_m is explained by the Coble diffusional creep mechanism but requires the introduction of a threshold stress by Yamani et al. [62]	The grain size dependence and the actual creep rate are shown to not agree with the Coble diffusional creep model; a GBS model for creep at high temperature is introduced in which accommodation by slip is controlled by lattice diffusion (GBS-D_L); dislocation pipe diffusion is also included in the analyses [63]
4.	Creep of α-Zr at intermediate temperature is attributed to the Ashby-Verrall model for diffusional creep; a GBS model is rejected by Fiala and Câdek [64] as not fitting the data	The creep data for α-Zr, in combination with other published data on low stress creep of α-Zr [65] reveal that all data are in fact best described by GBS (GBS-D_{gb}) [66]
5.	Several materials are considered to be controlled by N-H diffusional creep at low stresses; these are Cu [67], Ag [68], γ-Fe [69], Cr and Mo [70], β-Co [71,72], Ni [73], α-Ti [74] and α-Fe [60]	These metals are shown to deform by a H-D creep mechanism; the creep data are well described by an internal stress-assisted dislocation creep model [75]
6.	Diffusional creep is considered the dominant creep process in fine-grained Al-7475 alloy in the temperature range 400 to 515°C by Hamilton et al. [76]	Analysis of data, together with additional studies on the same material, indicates that a GBS process (GBS-D_L) dominates deformation [77]
7.	Creep of UO_2 at low stresses is "conclusively shown" to be dominated by Coble diffusional creep by Knorr et al. [78]	Creep rate of UO_2 is shown to be much faster than predicted by Coble diffusional creep; H-D creep is proposed as the deformation mechanism [79]
8.	Creep in Mg-ZrH_2 showing denuded zones is considered proof of existence of diffusional creep [80,81,35,82]	Denuded zones are shown to be only observed at high stress exponents (n = 4 to 6); hence slip creep is rate-controlling; soaking time shown to dominate over grain size effect; evidence for diffusional creep of Mg-ZrH_2 at 500°C is shown to be invalid [83,84]
9.	The conclusions presented by the present authors in their 1988 paper [75] are considered to be in error; new data on creep of Cu (Pines and Sirenko, [85]) are presented by Fiala and Langdon [86] to indicate evidence for diffusional creep rather than H-D creep	The new creep data on Cu are shown to be totally unrelated to N-H diffusional creep; data are quantitatively assessed by GBS-D_L and H-D creep; soaking time effect shown to dominate over grain size effect on creep [84]

10.	The analyses of Jones [87] on nine metals (Ni, Co, α-Fe, Cr, Mo, Ag, Cu, δ-Fe and Au) are considered by Fiala and Langdon [86] to be the "widely cited" data which support a N-H diffusional creep model	Seven of the nine metals (Ni, Co, α-Fe, Cr, Mo, Ag and Cu) creep faster than predicted by diffusional creep theory and are shown to deform by H-D dislocation creep [75,84]; creep of δ-Fe and Au can be controlled by either N-H diffusional creep or H-D dislocation creep [84]
11.	Burton and Reynolds present a detailed defence of the diffusional creep theory; these include a discussion of denuded zones, superplasticity, creep of Cu (data of Burton and Greenwood [88]) and grain boundary grooving in creep of UO_2 [89]	The arguments of Burton and Reynolds are categorically rejected; GBS accommodated by slip is the principal deformation mechanism for fine-grained materials backed by extensive experimental and theoretical evidence; the Burton and Greenwood data on creep of Cu is shown to be controlled by power-law creep, by GBS, and by H-D dislocation creep [90]
12.	Greenwood consider the evidence for denuded zones and for anisotropy of creep strength in dispersion-hardened materials is best explained by a diffusional creep process [91]	The creep flow of dispersion-hardened materials is best explained by dislocation creep with a possible contribution from a threshold stress (the latter is not yet fully understood) [90]
13.	New evidence is introduced by Langdon to show that diffusional creep is responsible for denuded zones in creep of Mg-0.5 wt% Zr at 400°C; creep experiments of Pickles [92] at 350 to 450°C are given as proof of N-H diffusional creep as the deformation mechanism [93]	The creep rate-stress curve for Mg-0.5 wt% Zr at 400°C shows that denuded zones are observed in the power-law dislocation creep range where solute atoms interact with moving dislocations, and therefore the diffusional creep process is rejected. Pickles observation that denuded zones appear on both longitudinal and transverse boundaries at low stresses are interpreted to indicate that GBS, accompanied by grain boundary migration, is the principal deformation process [94]

Table 4: Summary of Papers on Plastic Flow at Low Stresses Related to Diffusional Creep vs. Grain Boundary Sliding and Dislocation Creep (from [54]).

They have so far never disputed the physical basis for the diffusional creep mechanism and indeed continue to recognise it as a rigorous and elegant model, which represent a theoretical possibility at low stresses and fine grain sizes. The various evidence for diffusional creep (Coble and Nabarro-Herring), which have accumulated over the years, they have on the other hand tried vigorously to refute. In many cases they have sought to show that the given experimental results fits better with some other mode of deformation, namely grain boundary sliding (GBS) or Harper-Dorn creep (H-D), while in other cases they simply argue against the diffusional creep interpretation. In their 1993 paper with Wadsworth and Wolfenstine [84] provocatively titled *Evidence for Nabarro-Herring creep in metals: fiction or reality* they conclude that "there is in fact virtually no convincing evidence for N-H creep in metals"

Their opposition is based in three main arguments:

1. Creep rates measured experimentally are usually much higher than theoretically expected for diffusional creep
2. Grain size and stress dependencies are often at odds with predicted values
3. Denuded zones does not look and are not located as predicted in the diffusional creep model

Re pt. 1: The argument most often repeated is that experimentally measured values of creep rates rarely fit closely with theoretical calculations based on the original Nabarro-Herring or Coble model respectively. Measured creep rates are often found to be many times greater than thus expected and this trend has been thoroughly examined by Ruano et al. and used as a weighty argument against the model.

The procedure has been to take creep data as used by a "diffusional creep believer" and recalculate it to their own end. One of their standard techniques, which some might refer to as "a dirty trick", is the usage of "the generally accepted" geometric relation

$$d_{ts} = 1.776 \bullet L_{MLI} \qquad \text{(Eq. 12)}$$

in order to calculate the "true spatial grain size" (d_{ts}) for usage in the diffusional creep rate equations (Eq. 9 and Eq. 10). This results in theoretical creep rates of 3.2 or 5.6 times lower (for N-H and Coble respectively) than earlier calculated by the previous author or originator of the data. In this way the measured and theoretical values are moved further apart by Ruano an co-workers, lending more weight to the notion that the model doesn't apply in the given case. The reasonableness of using the mean linear intercept length (L_{MLI}) directly in Nabarro and Cobbles formulae can certainly be discussed (as will be briefly on page 61). Modifying other people's work using the "generally accepted relation" in Eq. 12 uncritically and with only sparse (if any) additional microstructural information can hardly be seen as anything but an attempt to further own beliefs. If anything the systematic work of Ruano and Sherby might actually be used to disprove the appliance of this relation as their calculations almost consequently leads to larger discrepancies between model and actual measurements than what is found using the MLI directly.

With or without modification though there is no denying that measured creep rates are often a long way off the theoretical predictions of the original model.

Re pt. 2: Another common discrepancy between experiments and model is that stress dependencies are often found to be larger than unity. In other cases where creep behaviour of samples with varying grain sizes have been explored the grain size effect has sometimes failed to show the proper dependence.

These are grave problems, which are hard to ignore or explain solely on the basis of difficult measuring techniques and experimental uncertainties. Together with the above-mentioned creep rate discrepancies these have put focus on the flaws of the original models and shown the need for evidence of another kind to accurately determine creep mechanisms.

Re pt. 3: The structural occurrence of denuded zones in two-phase materials had for long time been a phenomenon that was seen as solid evidence for diffusional creep. Wolfenstine, Ruano, Wadsworth and Sherby argued [83] against this commonly believed relationship on three counts.

First they conclude that in many cases where denuded zones have been observed the creep data doesn't fit the diffusional creep model due to discrepancies such as mentioned in pt. 1 and 2, and thus the denuded zones cannot be attributed to diffusional creep (as this was not the deformation mechanism in the given case). Secondly they argued that experimentally observed denuded zones doesn't appear and occur the way denuded zones produced as a result of diffusional creep should look. Especially they point to a) the findings of denuded zones on boundaries orientated far from transverse direction b) that denuded zones usually occur on only one side of the boundary and c) that the width of the denuded zones doesn't fit the theoretically expected. As a final point they give an account of how denuded zones can arise from alternative mechanisms such as a migrating boundary "sweeping" a zone free from precipitates.

The first of these is a pretty weak argument in terms of separating the phenomenon of denuded zones from diffusional creep, as it really is more critique of the basic formulae's capability to predict creep data (as in pt. 1 and pt. 2) and tells more about their general approach to the available evidence. Regarding the appearance of denuded zones it was soon pointed out by Bilde-Sørensen and Smith [95] that these phenomena a), b) and c) had earlier been predicted from an analysis of diffusional creep in particle containing materials [96] and was in no way inconsistent with deformation by diffusional creep (as examined on page 37). The last argument about alternative mechanisms being the cause of particle denuded zones still seems a viable option. It has been shown that dragging of particles by a moving grain boundary can happen as a natural consequence of the local sliding accommodation [97] and the occurrence of denuded zones can therefore no longer be said to be synonymous with diffusional creep deformation.

The "diffusional creep opposition" still hasn't responded to the latest, structural evidence for diffusional creep. These are the very convincing demonstrations of material deposition and removal (at transverse and longitudinal boundaries respectively) by usage of inert surface markings performed by Thorsen and Bilde-Sørensen as well as McNee, Jones and Greenwood.

1.4 Quantifying crystallographic information

This section will deal with why diffraction patterns arise and especially how they can be used to obtain crystallographic information about grain orientation and thus boundary misorientation. This text assumes a basic knowledge of transmission and scanning electron microscopy.

Diffraction basics

The phenomenon concerning diffraction in crystalline samples are both numerous and relative complex to describe. To give a mathematical description it is however often sufficient to use the convenient approach of Bragg. Bragg argued that the electrons of the primary beam behave as plane waves that are reflected off the atomic planes as seen on Figure 22. For the wave to scatter with constructive interference, the path lengths of electrons reflected at adjacent planes must differ by an integral number of wavelengths. On the figure the path difference between electrons scattered from the upper and lower plane equals AB + BC, and if this length corresponds to an integral number of wavelengths λ the scattered electrons will remain in phase after the scatter event. Basic geometry gives the length AB (=BC) expressed by the incident angle θ_B and thus Bragg's law:

$$n\lambda = 2d_i \sin\theta_B \qquad \text{(Eq. 12)}$$

where n is an integer, d_i is the interplanar distance and θ_B is known as the Bragg angle. Even though the notion of electrons being reflected is physically wrong, the equation is mathematically correct, and the diffraction type is still widely termed Bragg *reflection*.

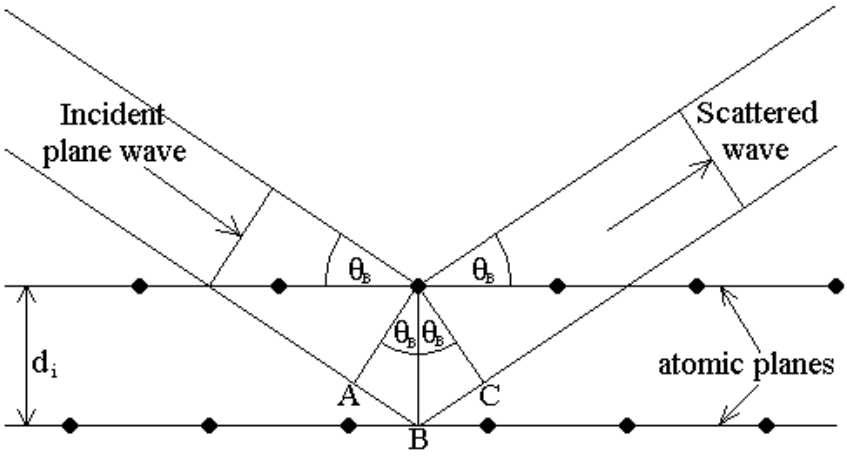

Figure 22: The Bragg description of diffraction as reflection of a plane wave in a couple of atomic planes.

Notice also that the angles on the figure are grossly exaggerated. For {111} planes in Cu, where d is 0.21 nm and with 200kV electrons of $\lambda = 0.0025$ nm the first order (n=1) Bragg angle can be calculated to $\theta_B = 0.34°$. As a rule of thumb the Bragg angles relevant for electron microscopy are usually below 1°.

The consequence of the integer n in the equation is that many orders of reflection exist for each set of planes and wavelength conditions. This shows clearly in the common spot pattern where several orders of diffraction spots are usually seen at the same time.

To make spot patterns in a transmission electron microscope (TEM) a parallel beam is normally used and a small aperture is used to limit the area from which the signal is obtained (known as selected area diffraction – SAD). The incident parallel beam is then diffracted in planes that fulfil the Bragg condition (i.e. planes that is almost parallel to the beam direction) and thus the beam is split up in multiple diffracted beams making a symmetric pattern of spots on the viewing screen. The distance between spots in such patterns is proportional to the interplanar distance of the planes fulfilling the Bragg condition.

The appearance of such diffraction patterns cannot be described sufficiently for real materials by the rigid rules of Bragg's law however. The limited size of the crystals we examine in the TEM means that the diffracting planes are not mathematical points in reciprocal space, but rather rods of a certain extension. Using the construction known as the Ewald sphere to examine which planes will give rise to diffraction spots, one therefore finds that a greater number of spots can be expected. Tilting the specimen will likewise influence the shape of the reciprocal rods and thus how the diffraction pattern will look in the microscope. The bottom line is that planes that doesn't exactly fulfil the Bragg condition, but are sufficiently close, can still give rise to diffraction spots and that several orders of these will often be seen simultaneously.

Kikuchi patterns

Among other things spot patterns are used extensively to select specific diffraction parameters for imaging in TEM (e.g. a particular diffracted beam for dark field microscopy). Spot patterns are however not suitable for the accurate measurement of orientation because as the positions of reflections (spots) can be largely unchanged over several degrees of tilting [98]. If the diffraction arises from a thicker crystal or alternatively by usage of a microdiffraction technique

such as CBED, an additional diffraction effect occurs, known as Kikuchi diffraction. As the name implies the Convergent Beam Electron Diffraction (CBED) technique utilises a converging beam, making measurements possible on very small areas. This additionally means that there will always be a proportion of scattered electrons, which impinge on all lattice planes at exactly the Bragg angle. Diffraction from a lattice plane in these circumstances means that an entire plane of incident electrons is diffracted creating a set of parallel lines on the otherwise grey background – one deficient of electrons (black) and one with surplus intensity (white). These are known as Kikuchi lines, they are approximately linear (really conic sections) and their positions are highly dependent on the orientation of the measured grain.

Essentially a Kikuchi pattern is a limited section of a projection of the geometry of *all* the lattice planes in the crystal. In other words a very precise "map" of the distribution of the lattice plane geometry. A measured "flat" Kikuchi pattern is thus a so-called gnomonic projection of only a small fraction of the complete pattern that is 3-dimensional and sphere shaped. Radius of the pattern sphere is represented by the equipment parameter 'camera length' (i.e. specimen to screen distance) which therefore can be used to control the size of the pattern section.

In practical terms a Kikuchi pattern is thus a map of the angular relations between directions and planes in the crystal with linear distances measured on the pattern representing angles in the crystal. With today's computers the calculation/simulation of such maps are almost a trivial matter and when the crystal structure of the sample crystal is known the determination of crystal orientation thus becomes a "simple" matter of comparison between measured and calculated Kikuchi pattern as illustrated on the figure below.

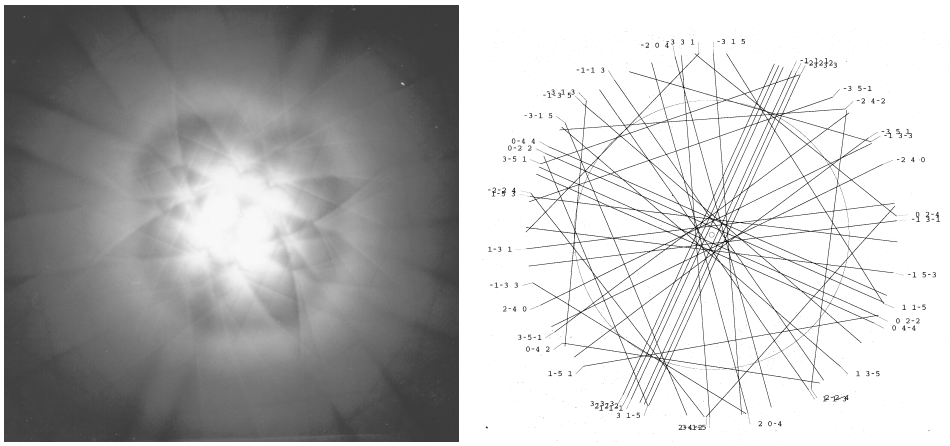

Figure 23: Kikuchi pattern comparison. A) Kikuchi pattern (112 pole) obtained by CBED B) Kikuchi simulation created by "Electron Diffraction".

Our equipment and software allowed this comparison to be executed automatically making the entire orientation determination of thin foil grains a relative simple procedure.

A CCD camera (576•384 pixels) incorporated into the TEM allowed for easy obtaining of Kikuchi patterns such as that of Figure 23A. Provided certain standard settings of the TEM hardware (intensity, camera length etc.) are respected these patterns can subsequently be analysed automatically by computer software (Texmeter by N.C. Krieger Lassen).

The Kikuchi lines are first enhanced by background subtraction and detected in black/white pairs by a convolution procedure known as a Hough transform. In order to perform this in a reasonable time frame the original pattern is reduced in resolution by a factor of 3 by a simple averaging manoeuvre. The

software additionally contains some large tables containing all possible Bragg angles and interplanar angles between pairs of crystal planes in the families of {111}, {002}, {022}, {113}, {133}, {024}, {224}, {115}, {135}, {244}, {026} to which the experimentally found bands are compared. The indexing is then found through the use of a special *evidence accumulator table* and the most probable solution is given along with a value describing the quality of the indexing. Finally the suggested solution may be validated manually by a display of a simulated pattern (the solution) on top of the actual pattern, agreement of which indicates correct indexing. The result of this procedure is a determination of the measured crystal (grain) orientational given in Euler angles. More information can be found in [99].

The accuracy of misorientation calculations on the basis of the here described digital orientation determination has been estimated experimentally by repeated determinations to be approx. 0.1°. This inaccuracy is thought to be mainly due to mechanical slip of the CCD camera arm and slight errors in the automated band detection because of the limited resolution of the digital Kikuchi patterns. If absolute orientation (relative to specimen surface) of a grain is needed, the coupling to the mechanical tilting devices probably increases this value somewhat. The accuracy is though still superior compared to "manual" determinations made on the basis of electron micrographs of Kikuchi patterns. In this case the error limiting the accuracy is that individual film slides may move slightly inside the photo box.

Electron Back Scattering Diffraction (EBSD)

EBSD is the less-known SEM equivalent to the Kikuchi patterns produced in the TEM. Similarly we have a focused beam of electrons creating Bragg diffraction in a wide range of atomic planes giving rise to bands on the diffraction pattern. As the electrons used for imaging such patterns are backscattered the total process is somewhat more complicated than for Kikuchi scattering. While Kikuchi lines come in black and white pairs the EBSD lines are grey/grey pairs. Despite the different mechanics of EBSD patterns the information contained in these are almost equivalent to what can be obtained from Kikuchi patterns and can thus be a highly useful tool for obtaining orientational information.

A necessary condition for creating EBSD patterns is to tilt the specimen heavily (70°) towards the detector in order to get sufficient backscattered electrons.

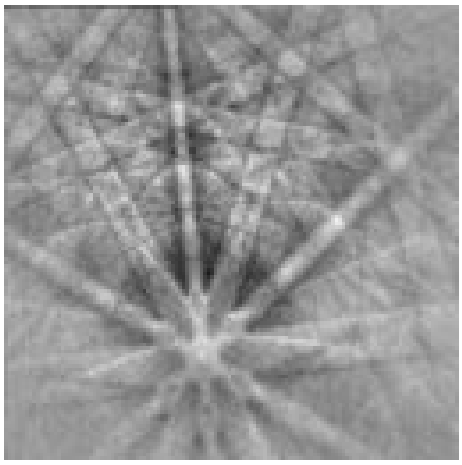

Figure 24: A measured EBSD pattern.

Equipmentwise our process for making orientational determinations in the SEM is also quite similar as EBSD patterns are obtained digitally and automatically

processed by an image analysis program. This program (Cromatic by N.C. Krieger Lassen) is specifically designed for the purpose and utilises almost identical principles for band detection and indexing [100,101], although they are obviously modified for the slightly different pattern type. Again the results are given in the form of three Euler angles for each measurement along with a quality parameter describing the number of correct bands used for the indexing. Simultaneous automated pattern acquisition and control of sample movement is possible in this software as well as we will explore in the next chapter.

The accuracy for misorientation measurements using the EBSD procedure has in this project been evaluated to approx. 0.3°. This is somewhat more than for orientation determinations by usage of Kikuchi patterns, and this is mainly due to the significantly larger sample volume of the SEM technique.

The final step from two independent orientation measurements to a misorientation is taken by yet another program. Based upon the program AXANG.BAS by Valerie Randle the software has been modified by Peter Thorsen and myself to fit present purpose and need for automation. The orientation input of two sets of Euler angles (no matter whether from Kikuchi or EBSD measurements) is transformed into matrix description and from which the misorientation matrix is calculated. The search for CSL up to Σ=51 is performed and results of misorientation angle/axis and deviation according to the Brandon as well as the Palumbo-Aust criterion is given.

2 Experimental

As mentioned earlier, the work done for this thesis has in many respects been a continuation of the earlier work by Peter Thorsen, briefly described in Section 1.3. The main consequence of this has been that some groundwork had already been laid and that in the making of creep specimens we wanted to imitate the previously used procedures in order to keep the new results consistent with the earlier results and thus easier to interpret.

Apart from this restriction the scope of this thesis have from the beginning been quite ambitious and the aim of the experiments have as a consequence been manifold.

2.1 Making of creep specimens

The making of new creep specimens was the natural first part of the experiments, a part not to be taken lightly, as the procedures used here reflects directly in the properties and microstructure of the final samples.

Material and Casting

The material chosen for the tasks was Cu-2wt%Ni. Originally the nickel addition was chosen to suppress the extensive grain growth, which was displayed by pure copper specimens during creep testing. This had seemingly proved a sound choice, and for the sake of consistency with earlier results and observations, it was decided to continue the investigation with this alloy. The alloy had earlier been shown to exhibit linear stress dependence at low stresses [102]. According to the rather simple phase diagram nickel and copper can be alloyed in all compositions in solid solution.

The alloy was melted and cast in a vacuum furnace, using a carbon mould, and the alloy was subsequently cooled to room temperature in the oven. Used was 695.9 g plated copper (99.999% purity) and 14.31 g nickel wire (99.999% purity) for a final composition of 2.0 wt% Ni. The feed head contained shrinkage grates and was therefore cut off and discarded. The ingot was afterwards milled slightly on the sides to remove the outer ½ mm layer, resulting in a nice clean slab.

Rolling

Next step in the process was rolling. Here the aim again was to mimic the procedure of the previous batch made by Peter Thorsen as closely as possible, in order to achieve a comparable grain size in the final samples. The old procedure called for a total thickness reduction of about 60% in 5 consecutive rollings, which however had resulted in grains that were slightly elongated in the rolling direction.

To avoid this grain elongation it was decided to try alternating the rolling direction between each pass of the rolls. The catch was that this would result in the ingot being enlarged in width as well as length, exceeding the maximum dimensions the available machinery could handle (Cu-contamination to the larger rolling machines could not be risked). The ingot was therefore cut in 2 near-equal sized pieces, which were given the exact same rolling. The maximum reduction achievable in a single rolling was about 0.6 mm why it took 9 consecutive rollings to reach the overall thickness reduction of 60%. The rolling was carried out at The Technical University of Denmark.

Rolling direction	Piece 1 (9.1*57*52)		Piece 2 (9.1*57*58.5)	
1st : L	9.10 → 8.55	6.0 %	9.10 → 8.55	6.0 %
2nd : W	8.55 → 8.00	6.4 %	8.55 → 8.00	6.4 %
3rd : L	8.00 →7.43	7.1 %	8.00 →7.44	7.0 %
4th : L	7.43 → 6.82	8.2 %	7.44 → 6.83	8.2 %
5th : W	6.82 → 6.23	8.6 %	6.83 → 6.22	8.9 %
6th : W	6.23 → 5.61	10.0 %	6.22 → 5.64	9.3 %
7th : L	5.61 → 5.05	10.0 %	5.64 → 5.04	10.6 %
8th : W	5.05 → 4.40	12.9 %	5.04 → 4.47	11.3 %
9th : L	4.40 → 3.73	15.2 %	4.47 → 3.73	16.6 %
Total reduction		59.0 %		59.0 %

*Table 5: Overview of the rolling procedure, giving the starting dimensions (thickness*width*length), the rolling direction (W: along the width, L: along the length of the piece) and thickness reductions. All measurements in mm.*

The actual reductions after each rolling can be seen on Table 5 along with the rolling directions. Alternating the rolling directions meant that approx. 56% of the overall deformation was applied by rolling along the L axis and the remaining 44% along the W axis.

Preliminary grain structure observations

Small samples of the cast and rolled material were cut off and ground with SiC polishing paper of increasing fineness #500, #1000 and #4000. The finishing polish was obtained with a polishing etchant, giving a smooth surface with a nice twin contrast. Finally the samples were heat treated 4 hours at 400°C + 4 hours at 800°C and examined by SEM.

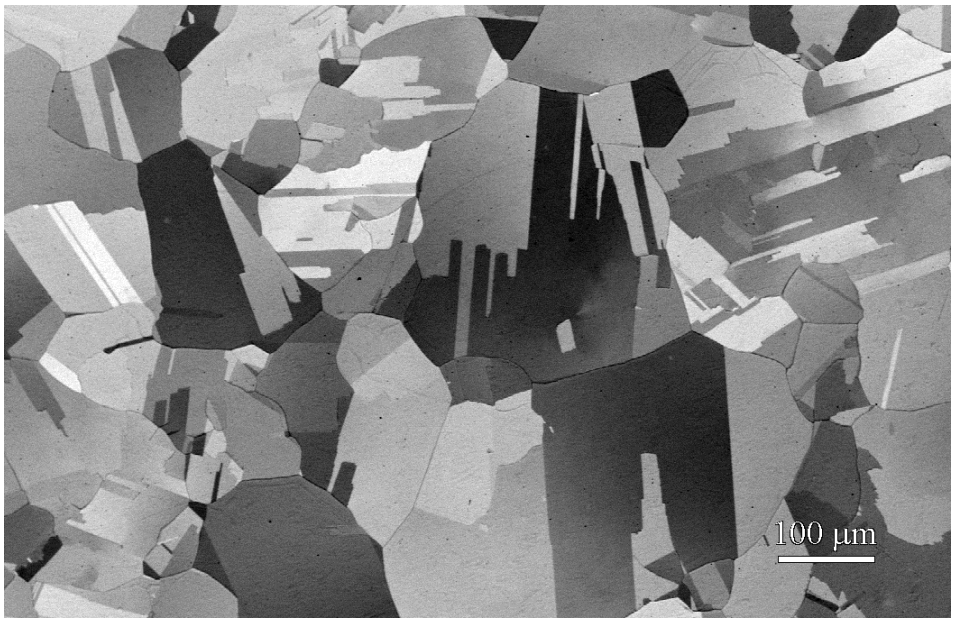

Figure 25: Typical SEM picture of the surface of the Cu(2%Ni) material after polishing etch and a single heat treatment. Notice that almost all grains contain one or more twins. Rolling directions L and W are vertical and horizontal respectively.

Mean linear intercept length measurements (MLI) were performed (see next paragraph for details) on the samples for approx. 500 grains in each direction (L and W) with the result of

$L_{MLI}(L) = 123\ \mu m$
$L_{MLI}(W) = 121\ \mu m$

On this basis it was concluded that the alternation of rolling direction had been successful in achieving approximately equiaxed grains, and that it wouldn't matter which way the creep specimens would subsequently be cut from the two Cu(2%Ni) slabs.

Grain size measurement

As mentioned earlier the grain size has important influence on many of the properties of polycrystalline materials, not the least on creep mechanisms. The diversity and distribution of different grain sizes and shapes in a material can have important consequences as well but is much harder to define and incorporate into models. In practice the term grain size is usually referred to as a single measured parameter that supposedly describes the size of the average grain.

There are several parameters to choose from and the choice will necessarily be a compromise between what the grain size is needed for and what is practically viable in terms of the complexity of the measurements. Ideally one might want a distribution of grain volumes which then can be compressed down to a single number. Still one would have to make generalised assumptions about the shapes of the grains (ellipsoid, equiaxed, cubic etc.), and the way to average small and large grain sizes would depend on what the grain size ultimately should be used for. This could perhaps or perhaps not (depending on how good the extensive measurements have been made and how well the assumptions hold true) result in a parameter, which is pretty close to the "true" value looked for, but the parameter would be difficult to compare directly to other grain size measurements based on other shapes and distributions.

To avoid this we have chosen to use the mean linear intercept length (MLI) as the parameter to represent our grain size. The biggest advantage of the MLI parameter is that it is very well defined and it is additionally relatively easy to obtain from ordinary light or electron micrographs. For a given value of grain boundary density, the mean intercept length depends neither on the actual size of individual grains nor on their shape [103]. As a result, the mean intercept length is only a measure of the density of grain boundaries and very different size distributions can yield the same MLI length. It is therefore important not to confuse the MLI length directly with grain size but to use it only as a parameter giving information about the density of grain boundaries and from which the average grain size can be estimated but roughly.

In the present work however we are far more concerned about the qualitative than the quantitative (creep rates) evidence for specific creep mechanisms and to that end a rough grain size determination seems adequate.

Practical Procedure. Though the MLI parameter is rather well defined, the exact deployed practice for this work will now be shortly reviewed.

The measurements where done on SEM micrographs (1336*1000 pixels) with magnifications of x100-x500, depending on how well the grain boundaries stood out on the particular specimen surface. On to these micrographs a grid of lines were systematically superimposed – 3 horizontal and 4 vertical lines on micrographs with low magnification, fewer lines at higher mag. The lines were spaced so as to make the most use of each individual micrograph while at the

same time keeping them sufficiently separated so as to be reasonably independent (no grains were counted more than once in each direction).

Along the lines, which start and end arbitrarily inside grains near the border of the micrograph, all intercepting boundaries (except twins as noted below) were marked and counted. The total number of these intercepts divided by the total length of the line resulted in 3-7 MLI values for each micrograph which subsequently was averaged to mean linear intercept lengths for the specimen in the x, y and in one case z direction.

For practical reasons the MLI was not measured for each and every specimen. Instead of taking some micrographs of each specimen, no matter how well the surface was suited for this, and measure rough individual MLI values, a few specimens were thoroughly examined to give a good determination, and this was subsequently conferred to the sister specimens. Qualitative comparisons between specimens have shown them to be reasonably alike, and great care was taken to make the heat treatments identical for all specimens.

No twins. It is important to note that we have consistently excluded the many twin boundaries found in our specimens from all the grain size measurements. This was decided for several practical reasons:

First of all it is much more difficult to include than exclude twin boundaries consequently. This is because most twin boundaries will not be affected by the etching procedures, which are normally used to expose grain boundaries, as twins are very resistant to intergranular corrosion. Thus one will have to rely solely on the channelling contrast caused by the orientation differences of the twin grains. As seen on Figure 26 though, the shade of each grain changes as the sample is tilted and often twin boundaries will be invisible. Several pictures of each area with different tilt would therefore be needed to determine all twin boundaries with certainty.

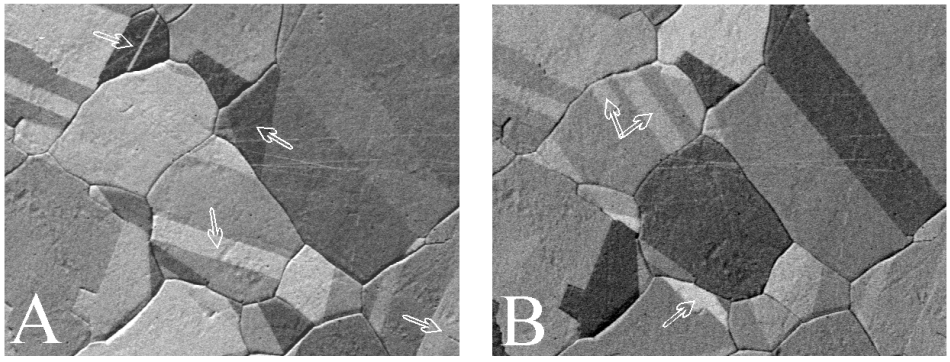

Figure 26: Two SEM pictures of an etched Cu(2%Ni) surface, tilted but a few degrees between takes. Some twins, marked with arrows, are practically invisible on the opposite picture.

Fortunately twin boundaries are relatively easy to recognise and distinguish from other boundaries in that they are usually very straight boundaries lying at specific orientations, often as bands and they show no topographical etching. In this way it is possible to exclude them altogether from consideration when making the linear intercept measurements.

The intercept length thus obtained will not give a real indication of the amount of boundary in the sample, as twins are very common in the used material. As we shall see though, twins play a rather passive role during diffusional creep testing, so by excluding these boundaries we actually get a better estimate of the real diffusion distances involved. One might say that the linear intercept lengths without counting twins indicate the density of *active* boundaries in the

material. Later will be shown some statistical calculations made to estimate the amount of twin boundary present in the samples and subsequent calculations of what MLI values we might have obtained if twins had been included.

Creep specimens

From the 2 rolled pieces a total of 14 creep specimens were cut out and milled to fit the strict specifications required for fitting inside the creep machinery (see Figure 27). Some of the earliest specimens unfortunately became too thin from the following excessive polishing. Therefore the last batch of creep specimens was made slightly thicker (1.3 mm) to compensate.

The additional deformation that was induced to the specimens as a consequence of cutting and milling was considered small compared with the 60% rolling reduction.

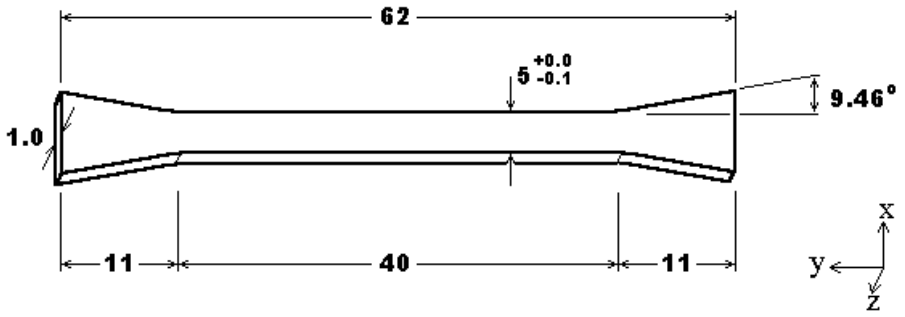

Figure 27: Creep specimen specifications, the defined x,y,z co-ordinates will be used consequently to refer to the respective axes. All lengths in mm.

Heat treatments

The purpose of heat treating (annealing) the specimens before creep testing is to relieve the accumulated inner tension, build up as a consequence of rolling. This relievance and stress redistribution is often accompanied by grain growth, which, as mentioned, is highly unwanted during creep. The exact annealing procedure used can help determine the "final" grain size obtained.

The 'old' standard heat treatment, which I decided to adopt, called for 4 hours at 400°C + 4 hours at 800°C. Unfortunately the raw creep specimens were slightly stressed and bend from the machining procedure (cutting and milling) and it was therefore deemed necessary to anneal them in order to relieve the stresses *before* polishing could commence. On the other hand it was important for the specimens to have completely undisturbed surfaces for MLI measurements and in particular for grid deposition. This spoke in favour of annealing *after* the polishing procedure, which could possibly induce slight mechanical deformation on the surface.

In the end it was therefore decided upon a double heat treatment procedure, one anneal before and one after polishing. The old standard heat treatment was used each time, a bit overly complicated one might argue but with the advantage that specimens could be annealed together even when they were at different stages of preparation (before or after polish).

For the first anneal the specimens were packed in the oven under a slight pressure from slabs of SiO_2 so as to straighten them out during the annealing. This

part was not necessary for the second anneal where specimens just lay openly in the vacuum oven.

The specimens were introduced into the oven enclosed in a vacated glass tube. The annealing was thus performed in a vacuum better than 10^{-5} torr so as to avoid an inevitable oxidation of the specimens and substantially prolonging the time taken for the specimens to achieve oven temperature during start and cooling. As is customary the oven was pre-heated before the specimens were introduced into it, while the cooling down, for practical reasons, were done inside the oven by cooling of the entire system. The following day the oven was pre-heated to the higher temperature and the specimens were re-inserted. To sum up:

Standard heat treatment
4 hours at 400°C (+ furnace cooling)
4 hours at 800°C (+ furnace cooling)

The heat treatment was carried out over 2 consecutive days and all specimens (*except* No1) were given this standard heat treatment twice, once before and once after polishing.

Polishing Procedure

The aim of the polishing procedure was to obtain a flat, undisturbed surface with a minimum of scratches, and with a good grain contrast.

The raw specimens bore heavy scratches from the milling procedure and after the initial heat treatment they were very soft and great care had to be taken so as not to bend or otherwise damage them. This proved more difficult than expected due to their flat, elongated geometry and several specimens suffered small or fatal bending in the course of polishing.

It was found that a silicon-carbide (SiC) polishing paper of roughness #500 [I] was adequate to get rid of the milling scratches and polishing continued on papers of increasing fineness #1000 and #4000. For this part of the polish it was found very useful to glue the specimens onto a holder of some sort, to provide the stiffness that the specimens lacked. Multiple specimens could be glued to a large disk, which fit into an automated polishing device, while single specimens were glued to the back of a small iron slab and polished by hand.

After polishing with #4000 paper the specimens had rows of very fine scratches. For the final treatment several possibilities were investigated, each of which had its advantages and drawbacks:

- **Electro polishing** (H_3PO_4 based electrolyte with ethanol, propanol, urea and 'Vogelsparbejdse', cooled to < 3°, 5V in 5-30 seconds): A reasonably simple and convenient procedure. Unfortunately the resulting specimens suffered from pitting and had no great grain contrast.
- **Polishing etch** (96% OP-S suspension w. 2% conc. H_2O_2 and 2% conc. ammonia): This is a combined chemical and physical polishing which was found very effective and could give beautiful results in terms of grain (and twin) contrast (see Figure 25). Practically though, it proved impossible to achieve this finish over more than a third of a creep specimen. Bad contact between the sensitive specimen and the rotating cloth (it wasn't possible to use a strengthening holder for this procedure) combined with the corrosive media caused pitting and over-etching on the remaining areas. For simpler

I The roughness given of the polishing paper follows the Struers Standard (FEPA) where the stated quality of #500, #1000 and #4000 corresponds to SiC grain sizes of maximum 30 μm, 18 μm and 5μm respectively.

or smaller samples the polish is deemed highly useful, although rather time consuming, and the nice contrast is largely (but not perfectly) preserved during the second annealing.

- **Diamond polish** (size 3μm): Surprisingly the diamond polish wasn't found to improve the surface significantly as scratches of comparable size was introduced from the diamonds as well.
- **No additional treatment** (thermal etch): Accepting the fine scratches from the #4000 polish paper as the final result was actually not a bad alternative, and was obviously the easiest. The grains would step in character upon the second annealing (known as thermal etching) with a decent result over the entire surface.

Which of the above treatments that was actually used will be noted for each different case in the following. Remember that all samples were annealed after receiving their final polishing in order to obtain a mechanically undisturbed surface before commencing the creep test.

The Creep experiment

The samples were crept individually in a vacuum oven, which was reconfigured to fit this specific purpose. The specimen was mounted in the oven as seen on Figure 28, with a similar arrangement at the lower end. The holder in the lower end was hanging freely on to the specimen providing the necessary stress for the creep test. On to the freeload holder, which weighed in itself 360 g, several kg of extra load could be placed, giving the option of providing the exact stress needed within the given limits. To the creep tests conducted for this thesis the exact extra load was calculated on the basis of each individual specimen cross section so that all specimens were subjected to the same stress (1.14 MPa).

The protection tube shown on the figure was necessary to avoid particle contamination from the oven walls to the specimen surface. The tube is standing freely on the lower holder and is included in the weight given above for this arrangement. The deformation was measured with a LVDT Strain transducer mounted below the sample, giving readings every 5 minutes.

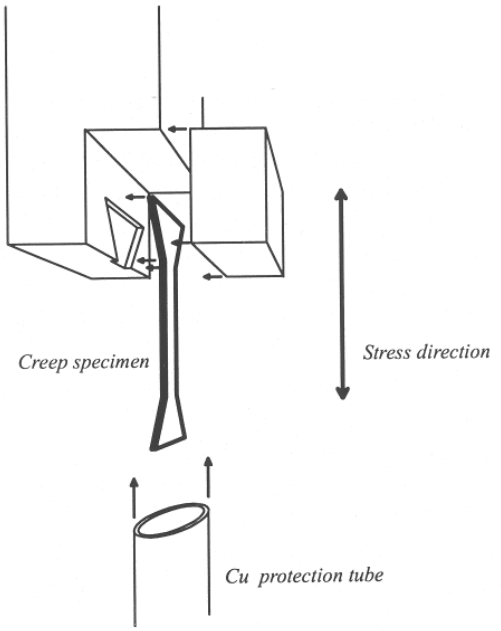

Figure 28: Sketch of the creep machinery (drawing from [104]).

Mounting of the specimens in the holder was a very delicate matter and great care had to be taken to avoid damage to the soft specimens (a single specimen was irrevocably destroyed in this process). After creep the specimen heads were usually welded to the holder and were consequently cut off in order to free the specimen.

A total of five specimens were successfully crept for the present work. In all cases the experimental conditions met were:

- Vacuum of approx. 10^{-5} Torr
- Temperature of 800 °C (controlled within ± 2°)
- Stress of 1.14 MPa (by constant load)

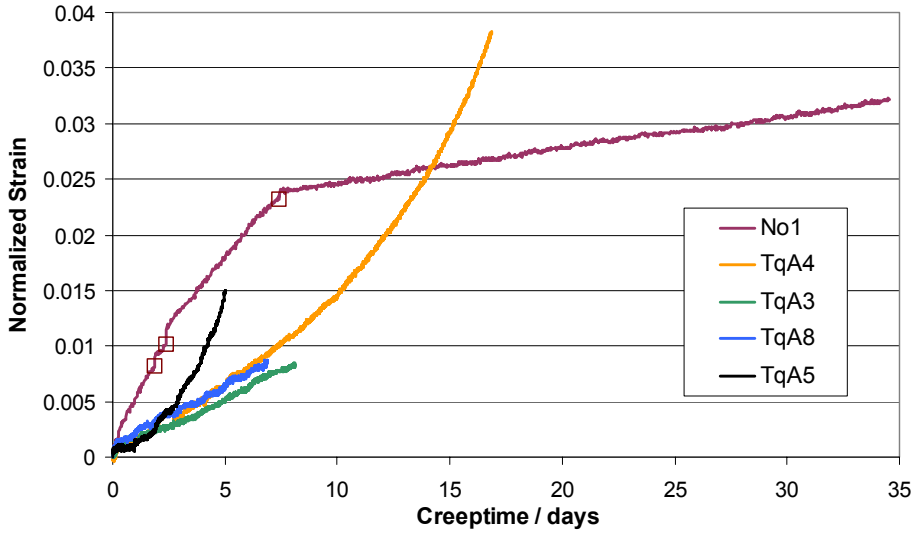

Figure 29: Creep curves for the 5 specimens

No1: The first specimen to be crept was the one designated No1. This was a specimen from a previous batch, prepared by Peter Thorsen using procedures (rolling/heat treatment) similar but not identical to those described in the previous sections. Consequently the microstructure is different for this specimen, giving rise to markedly different creep behaviour.

Most remarkable is what looks to be a very long primary creep phase, but upon closer examination more seem to be individual parts with a constant (higher) strain rate. Fact is that there were technical problems during the creep test and that it was interrupted three times (as marked on the figure) for a total of 58 days of standstill. The problems with the cooling water could perhaps have resulted in the test being run at higher temperatures than was intended in these first 7 days. The steady-state creep rate given in the table below is in any case measured from the long, straight period succeeding this first week.

TqA4: The first creep sample from my own batch was TqA4. Naïvely expecting creep behaviour similar to that seen for No1, this specimen was accidentally allowed to continue deforming into the tertiary creep phase.

Heavy creep damage could afterwards be observed on this specimen such as voids and cracks in many grain boundaries. The specimen was probably not far from failure when the creep test was terminated. The primary phase is observably pretty short (about 7 hours) followed by approx. 7 days of steady-state creep before the steady rising of creep rate.

TqA3 & TqA8: Samples TqA3 and TqA8 followed and they reproduced the behaviour of TqA4 pretty well, until these creep tests were deliberately ended before the onset of tertiary creep. No creep damage was observed in either specimen. These samples were the primary sources for TEM specimens.

TqA5: This last specimen had a markedly different behaviour from the other specimens of the same batch, which possibly is partly due to being crept at a slightly higher stress than the previous specimens. This was because it had been subjected to a chemical etchant (see section 2.3) prior to creep, which I may have been unable to account exactly for in the calculations of needed extra load for the lower creep holder (to obtain a stress of exactly 1.14 MPa).

The creep curve shows almost no steady-state creep phase as the strain rate is increasing continuously after a short primary phase. Voids and small cracks could be observed at some grain boundaries.

Speci-men	Cross section (mm^2)	Extra load (g)	Steady-state creep rate (s^{-1})	Total elongation (mm)	(%)	Grain size L_{MLI} (x,y,z)[§] (µm)
No1	4.85	208	$3.5*10^{-9}$	1.28	3.2	147,180, [¤]
TqA4	3.88	91	$1.3*10^{-8}$	1.53	3.8	104,105,88
TqA3	3.73	74	$1.1*10^{-8}$	0.33	0.8	
TqA8	3.08	0	$1.5*10^{-8}$	0.34	0.8	
TqA5	3.45	41	$1.5*10^{-8}$ [#]	0.55	1.4	

Table 6: Creep data for the 5 specimens. ([#] this value is a rough estimate, [¤] not measured, [§] the co-ordinates refer to the directions given on Figure 27) .

Deformation mechanism

The creep conditions of 800° ($T/T_m \approx 0.8$) and 1.14 MPa formally puts the deformation mechanism close to the border between Nabarro-Herring creep and dislocation creep (see Figure 12). For the present grain sizes Coble creep should be of no significance.

This border can be found experimentally by measuring the creep rate at several different stresses and make a plot. The transition from diffusional to dislocation creep is accompanied by a change in stress dependence, which should be easily seen as changes in slope on the stress/creep rate plot. In this fashion the transition stress have earlier been found [104] to be 1.8 MPa, for a sister specimen to No1, with slopes equal to n=1.4 and n= 3.1 for diffusional and dislocation creep respectively. As the new batch of samples are reasonably similar in properties (the smaller grain size they display should favour the diffusional mechanism) this transition stress result is considered adoptable. The used stress of 1.14 MPa is pretty close to the transition stress, however, so one might expect some contribution from dislocation creep even though the diffusional process should clearly be rate controlling.

Calculation and comparing of the creep rate according to Nabarro's formula raises again the question of grain size. Let us start by stressing that *there is no reason to expect the MLI length to be equal to the average grain size*. The MLI is an average of randomly drawn secants measured on random cuts (the surface) of three-dimensional grains, and as such must necessarily be smaller than the diameters (in each direction) of the grains. If one has detailed knowledge of grain shapes and size distributions of the used specimens or is willing to make some assumptions about these (e.g. equiaxed grains, logarithmic size distributions etc.) the MLI measurement can be converted to an average grain diameter (d) through careful geometrical analysis. Thus conversion factors of about $d=1.77 \bullet L_{MLI}$ have been used in some instances [105, 106], but this is often done without any prior discussion or arguments to support the soundness of this choice.

When detailed shape and size distributions are not available though, the MLI value is often used directly and inserted in formulae as the average grain diameter, the argument being something like:

There's no reason to convert a value (that we know is inaccurate), by a procedure we are not sure really applies to our material, into something that therefore is just as inaccurate.

By this device we have also chosen to apply the MLI length directly into the formulae, as the average grain size. Calculations of creep rate according to Nabarro's formula (Eq. 9) using the conditions described in the previous section yields a "theoretical creep rate" of $1.6 \cdot 10^{-9}$ s^{-1} for a grain size of 180 μm. The experimentally measured rate for No1 is about twice as fast as this.

Likewise the "theoretical creep rate" can be calculated to $5.6 \cdot 10^{-9}$ s^{-1} for a grain size of 105 μm and $6.8 \cdot 10^{-9}$ s^{-1} for a grain size of 88 μm. Experimentally measured creep rates for specimens TqA3, 4, 5 and 8 is again approx. double these theoretical values.

Calculated creep rates are very often lower than the actual experimental rates and discrepancies of a factor 2 are absolutely not uncommon. For the given case I consider the match pretty close, and no cause for concern.

All in all, though, it is not very convincing evidence for the notion that the creep mechanism is indeed diffusional creep as we propose. But as stressed earlier, and one of the major points of this thesis, the deformation mechanism can only be determined with any certainty through examination of microstructural evidence. This we will turn to in the following.

2.2 Automated EBSP measurements

In earlier work by Peter Thorsen a correlation between activity of individual grain boundaries during diffusional creep testing and the grain boundary structure of these boundaries, was determined, as seen in Table 3. In order to expand the investigation to some of the rare Σ boundaries and get some better overall statistics, the work was continued and a way was sought to automate the time-consuming search and identification procedure.

Specimens

A single creep specimen (No1) was left behind from my predecessor, which was used in this range of experiments as the main specimen. This sample had a slightly larger average grain size and different creep behaviour than the new batch of samples (see Table 6).

The special thing about this old specimen was that it was equipped on one side with a thin layer of Al_2O_3 formed as a regular, quadratic grid. This grid was placed upon the annealed sample before creep and could thus be used as an inert marker for how the surface had changed and consequently for quantifying the creep deformation for single boundaries.

Looking at the crept specimen for the first time several observations sprang to mind. First of all it became clear that practically no deformation at all had taken place in the bulk of the grains, that is to say all the deformation had occurred at the grain boundaries. This is easily confirmed by noticing how the reference grid is disturbed only between grains, and it is a rather strong indication that dislocation creep has not played a significant part of the deformation. Other creep experiments at higher stresses, where dislocation creep were rate controlling, have shown a distinct wavy deformation of grid lines in the interior of grains, for specimens equipped with similar reference grids [107].

Secondly one notices that only some and not all boundaries display disturbances of the reference grid. Other boundaries, most of which are obviously twins, seems to have played no part whatsoever in the creep deformation. This phenomenon is what we in this section want to explore, by correlating these

inactive boundaries with grain boundary structure. Additionally we are interested in finding CSL boundaries that have deformed during the creep test in order to determine the critical deviation these boundaries are allowed before being "activated" to take part in the deformation.

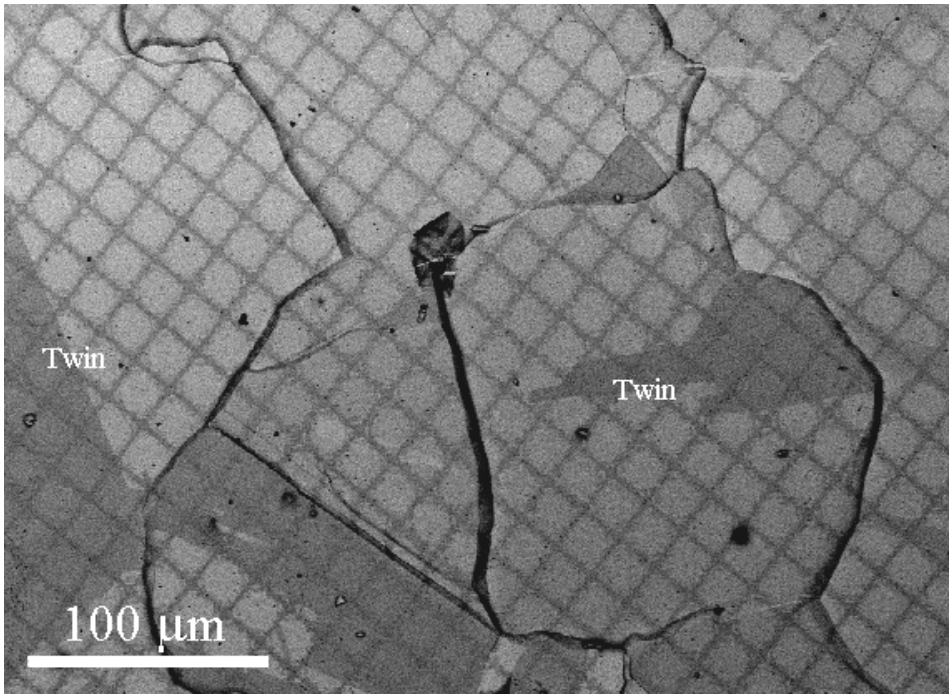

Figure 30: A backscatter micrograph of No1 after creep. In the interior of the grains the grid is largely undisturbed, while deformation shows distinctly across some boundaries. Other boundaries e.g. the marked twins show no deformation.

From the shadows on the micrograph it is clear that the grains have moved normal to the surface as well as in the plane creating the topographical contrast seen. This motion can be determined accurately by tilting the specimen and it is obviously necessary to take this movement into account if a detailed description of the deformation at individual boundaries is wanted.

Below is an example of three general and active grain boundaries. By manually expanding the reference grid from one of the grains into the domain of the others, as shown, the movement of the grains with respect to each other, becomes very clear. In the present case the C grain is used as reference, and it is obvious from the grid displacement to see that grain B has moved away from it and that the (transverse) boundary region between them has been filled with new material, upon which no grid is seen. The opposite is the case with grain A, which have moved towards grain C (and B) and it is just as obvious that here parts of the original grid covered surface is missing. The AB and AC boundaries are mainly longitudinal but near the triple line the boundaries are, for energetical reasons, relaxed to a near 120° angle. Examples like this are numerous and easy to find on this sample, and the evidence for material deposition and removal, that they represent, is clear-cut and hard to dispute. The grains have moved slightly out of the plane as well, but in the present case it is insignificant compared to the x-y movement.

Note that twins are not visible on this specimen (No1) surface under 'normal' circumstances, i.e. secondary electron imaging.

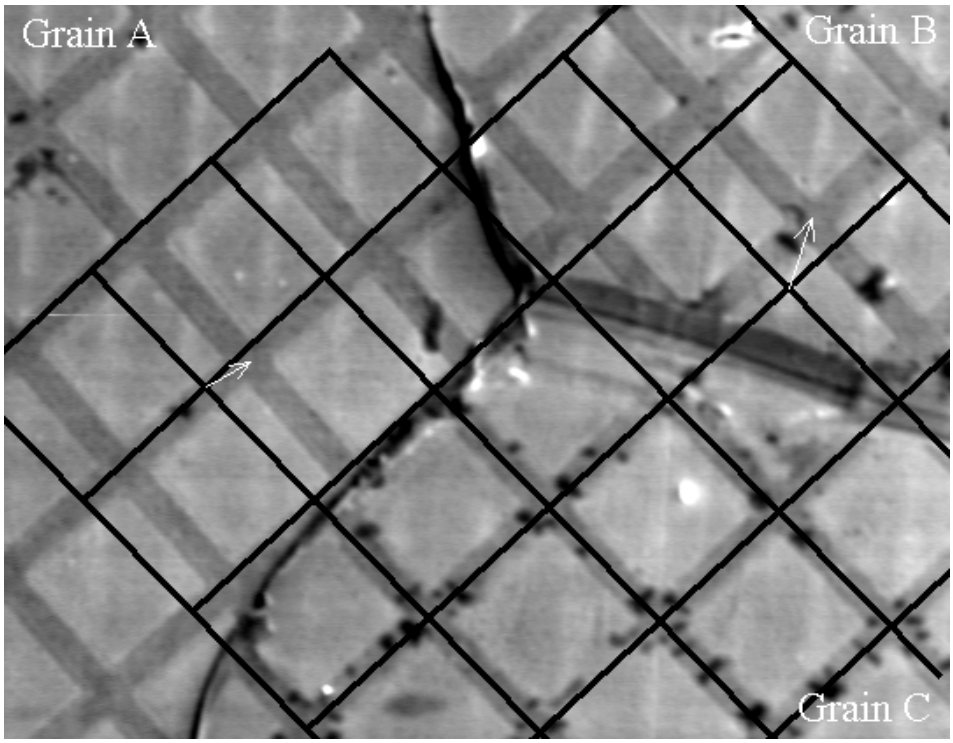

Figure 31: Determining deformation by usage of the reference grid. Using the superimposed black grid one can determine that Grain A has moved towards, and grain B away from, grain C during creep, as the white arrows indicate. Strain axis is vertical.

The manual EBSD procedure

The manual procedure for describing boundaries by misorientation and 'activity' was used in the early stages of this project in lack of something more efficient and can be described by the following 4 steps:

1. Taking micrographs of relevant (i.e. all even remotely interesting) boundaries along the edges of the specimen. Boundaries along the edge are chosen because they are relatively easy to find again at a later session, and because the characterisation can be immediately expanded to include the grain boundary plane, should the need arise.
2. Manual EBSP measurements on the grains earlier micrographed, marking the point of measuring on each printed micrograph.
3. Calculating the misorientations across grain boundaries.
4. Re-examining the micrographs of boundaries with "interesting" misorientations, determining whether deformation had taken place or not by help of the inert alumina grid (as on Figure 31).

The problem with this procedure is of course that in this particular investigation we are only interested in a fraction of the total amount of boundaries, namely the CSL. Thus a lot of hard work is used to take pictures and measurements on boundaries which turns out to be not particularly interesting, work that is consequently of little worth afterwards.

This could be accepted if the procedure was a fast and simple one but this is not the case, due to the very large amount of twin boundaries. The presence of the twin boundaries (and $\Sigma 9$) is easy to establish during the measuring session because of the pronounced chance in EBSD pattern, but they are predominantly invisible in the imaging mode. Therefore, in order to be certain of the measured boundary misorientation, one has to determine the twin areas by use of the

EBSD probe, which is an elaborate and time-consuming procedure. Thus to properly measure the misorientation around a single boundary it takes many carefully performed measurements in both grains in the vicinity of the boundary, and often re-measurements have been necessary to clear up the confusion.

The approx. 430 manual EBSD measurements initially made on grains along the two edges of the No1 specimen thus resulted in characterisation (by misorientation) of only 16 boundaries usable for Table 8. This is hardly the statistics of an effective procedure.

The automatic EBSD procedure

The automatic procedure evolved as the software was developed, which means that it was only at the very last stages of the work that the "final" procedure as it is described here was even available:

1. An automated surface scan is initiated.
2. Analysis on the accounted data, searching for boundaries with particular misorientations (specific CSL).
3. Microscope session where the interesting boundaries are located on the sample, micrographed and the misorientation is re-measured manually.
4. The deformation (if any) is determined from the micrographs.

Re pt. 1: Setting up the microscope for an automatic scan became a pretty standard procedure, as the controlling software (Cromatic by N.C.K. Lassen) was finalised. The sample has to be set up, tilted in position (70°) for the backscatter detector and aligned to x-y directions of the microscope stage. Then the image capturing system has to be calibrated and a background of noise is recorded and subtracted. Finally a set of start and end co-ordinates defines the area and the step length is chosen resulting in a specific amount of measuring points. The standard scans performed for this work used a step length of 10 μm and was of 131•131 points, which was approximately what could be measured overnight (15½ hours). As the sample focus is constant during the scan this sets an upper limit on how large areas can be scanned in each run, but as our specimens are pretty flat, areas up to 1.8•1.8 mm posed no problems.

It was quickly discovered that it was a very good idea to obtain a micrograph of the scanned area immediately after the EBSD session. At this point the scan lines are still visible as black lines of contamination on the surface (just visible a few places on Figure 34) pointing out the exact area of measuring. These lines faded gradually as the sample was readied for new sessions and cleaned by pressurised dry air.

Re pt. 2: The result of an EBSD scan is a rather large text file (3MB for a standard scan) containing the calculated Euler angles, x,y,z settings (with z being constant throughout each scan), quality parameters and time for each measurement. This file is handled by a program (Croplot), which apart from some input about the sample (lattice parameter and crystal system) automatically creates an orientation map as that seen in Figure 32.

Each measurement is individually given a colour based on their orientation, so that points with almost equal orientations become related in hue. The black points correspond to measurements where the EBSD pattern was too poor to be determined with any certainty and these are consequently excluded in any analysis. The latest version (1.55 Beta) of Croplot features an automatic procedure for 'cleaning up' the map by redefining the orientation of these points to those of a neighbouring measurement, thus making it much easier to grasp the boundaries of individual grains for comparing with micrographs. To enhance this, a feature in the program can mark out grain boundaries by calculating

misorientations between all neighbouring grains and putting a boundary where this fall in a specified range, a feature that can be roughly used to locate specific CSL. For example one can draw all boundaries with misorientations between 15° and 180° with black and on top of this mark all boundaries of misorientation 57-63° with white as is seen on Figure 33. A problem with this procedure is that it catches not only the wanted twin boundaries but also any general boundaries, which happen to have a misorientation in this range (around another axis than <111> obviously). Afterwards one will have to make sure in each individual case if the axis is right for CSL, as will be the case for almost all of the near 60° boundaries. When searching for rarer sigma this will not be the case as most boundaries in a given window of misorientations will be general and thus it will not be a convenient procedure to use. Unfortunately Croplot has (yet) no dedicated CSL determination incorporated.

Search for CSL in the automated EBSD maps have therefore primarily been done by data handling of the raw scan files. First the measuring points are picked out and paired by an algorithm and secondly this series of orientation pairs are run through a CSL determination program. How the measurements are paired must be a compromise between catching as many of the CSL boundaries as possible and avoiding too many double determinations and ”false” boundaries (pairing of measuring points which are part of grains that have no mutual boundary on the sample). Because of the many bad measurements, this was a bit complicated. Pairing of every third measurement in an interlocking system and skipping every other column (or row) proved reasonable.

The misorientation calculation and CSL searching program following came up with a list of some thousand ”boundaries” per scan. In a lot of these at least one bad measurement was implicated and these were subsequently discarded. Another great deal were (very) low-angle boundaries as the two measuring points had been taken from within the same grain. The rest of the boundaries were divided into general, Σ3, Σ9 and other (rare) Σ. The lists of Σ boundaries were scrutinised and the actual boundaries they represented were marked down on the EBSD map for manual measurement.

The raw EBSD files were used for some statistical examination as well and for this the scan points were paired neighbourwise so as to get the most correct misorientation values and all columns were used. Pairs including bad measurements were discarded along with boundaries < 15°.

Re pt. 3: Comparing the EBSD map with a micrograph of the scanned area is no trivial matter. When the exact area is found, cut out and sized comparably as Figure 33 and Figure 34 it is still no easy task and takes some intensive studying to find common features on the two pictures. To even get there, it is crucial to be able to define exactly the scanned area, and therefore the area should be micrographed immediately after the scan session, as mentioned.

The interesting boundaries, which were marked down on the EBSD map, are thus transferred to the micrograph by careful analysis. In the following manual SEM session these boundaries are located and a final misorientation measurement is done by hand. This session is much easier than the corresponding pt. 2 in the manual procedure because we now have a map of all the elusive twin boundaries to begin with.

Re pt. 4: Determining deformation from micrographs is a pretty straightforward task, exactly like in the manual procedure. The grid of one grain is expanded by hand (and ruler) across the boundary to see whether it matches perfectly with the grid in the neighbouring grain. Micrographs for this procedure are taken at zero specimen tilt.

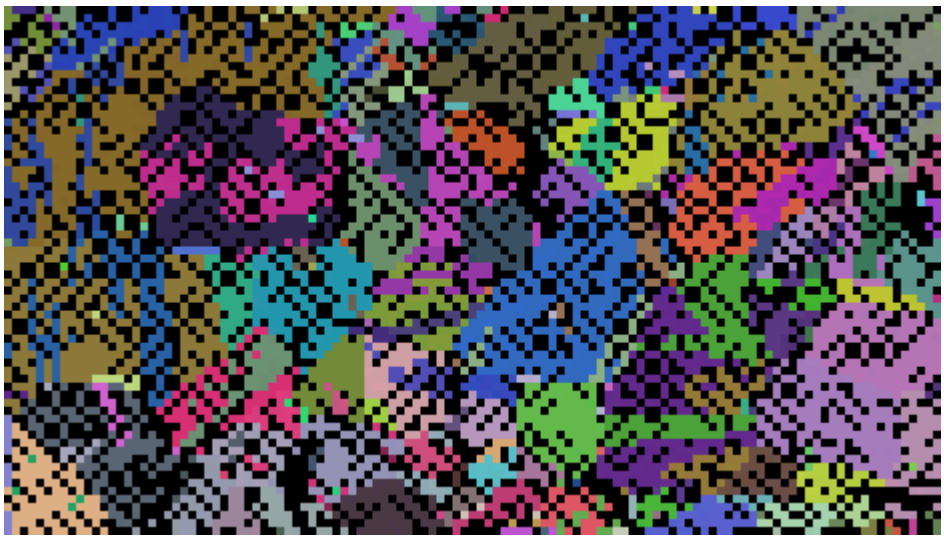

Figure 32: Part of an orientation map from an Automatic EBSD surface scan

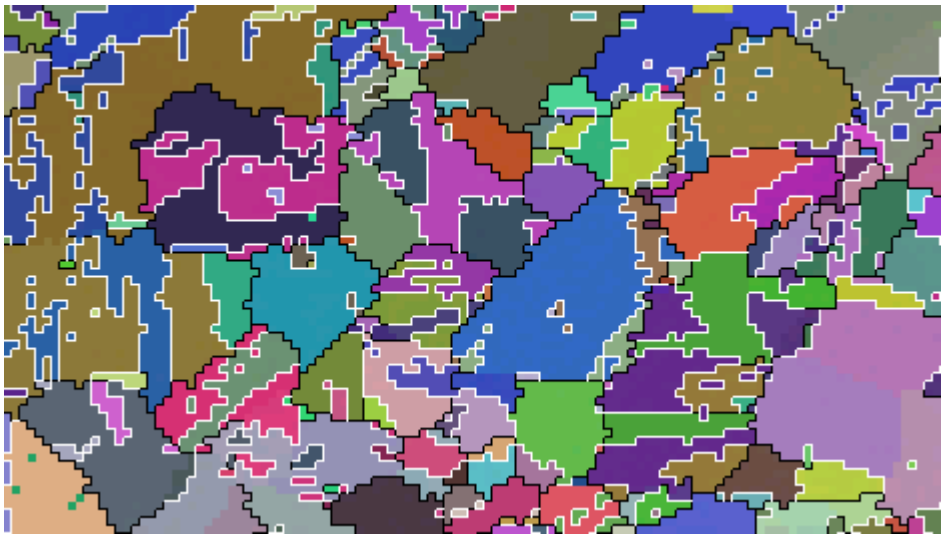

Figure 33: Same autoEBSD scan as above, cleaned for bad measurements and with boundaries marked. White = twin boundaries, black = other high angle.

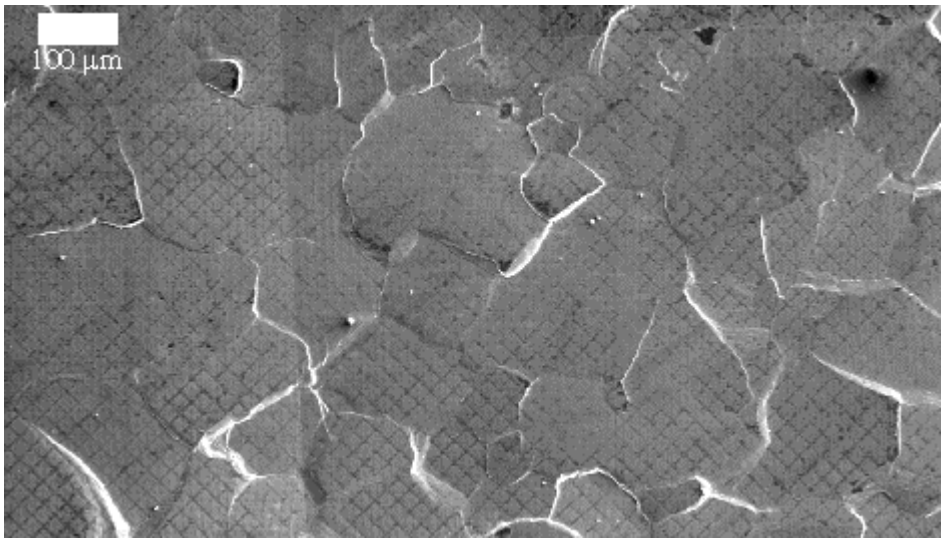

Figure 34: SEM micrograph of the exact area scanned for the above figures.

Results

The No1 specimen displayed a very high fraction (approx. 35%) of bad measurements well distributed over the entire surface and as suspected this showed to be directly related to the Al_2O_3 grid. Other specimens without the grid had a more acceptable ratio (approx. 7%) of bad measurements and these were predominantly (and understandably) found in the boundaries. An earlier mapped grain (lower right corner on Figure 33) was EBSD scanned again with a smaller step length (2 µm) allowing for a very graphic explanation to this discrepancy.

The below figure actually displays what could have been a single grain but which have undergone multiple twinning formation, with many of the twin properties clearly demonstrated. A grain can have up to four different twin boundaries (i.e. one for each of the four different 111 type planes) as displayed by the large violet grain. Where different twins 'meet' their mutual boundary is a Σ9, which is seen for the violet/brown boundary, as these grains are both twins to the yellow grain. Further complication yields Σ27 boundaries of which there is only a small example near the centre.

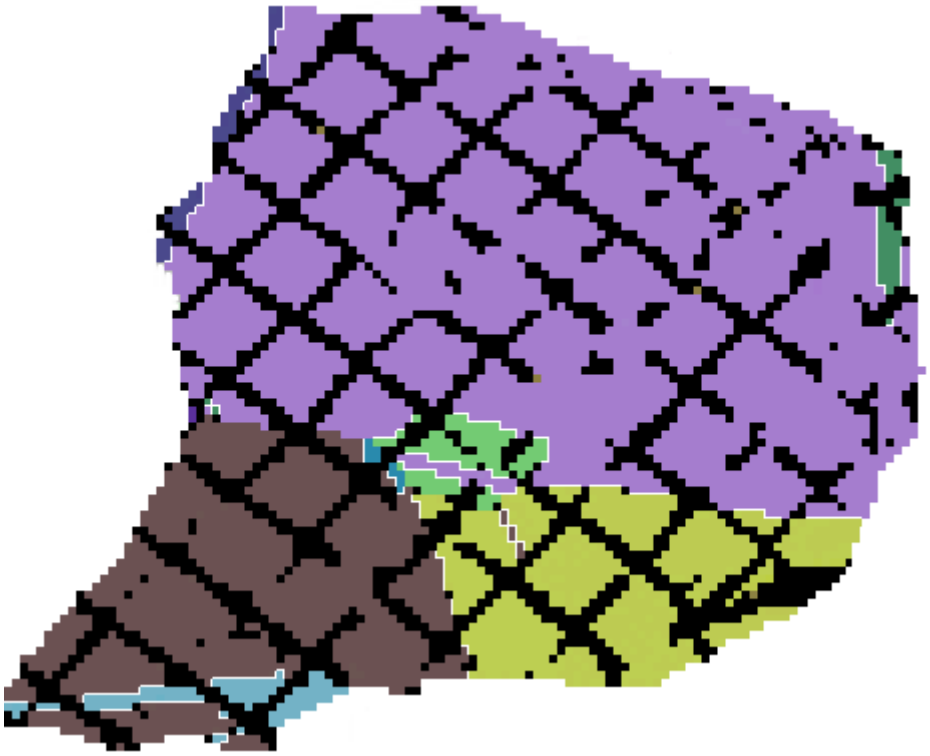

Figure 35: AutoEBSD scan showing a grain in detail (step length 2 µm). The grid clearly obstructs the pattern formation. Twin boundaries are marked with white.

The statistical examinations of the EBSD scan files showed the proportions between the different boundary types present in the sample as seen on Table 7.

	No1 (%)	TqAX (%)
General Boundaries	28.6	39.6
Σ3 Boundaries	67.8	56.8
Σ9 Boundaries	2.7	2.6
Other Σ	0.9	0.9

Table 7: Distribution of boundaries in the used samples.

As expected the amount of twin boundaries is very great, constituting well above half of the boundaries, in the new as well as the old samples. The presence of this many Σ3 is directly responsible for the large fraction of Σ9 as well and makes the fraction of other Σ even smaller comparably. Less than one percent of the total boundary volume is reserved for these rare Σ boundaries and this accounts for the sparse data on these and the fact that we have so far been unsuccessful finding rarer Σ with deviations below 0.5. Therefore it is not surprising either that the few encountered rare Σ that have been investigated all have been found to have been active during creep testing. Of the Σ3 boundaries 83% have deviations of 0.08 or below.

On Table 8 the entire list of boundaries that have been characterised by misorientation measurements as part of this work can be seen.

INACTIVE BOUNDARIES				
Axis	Angle	Σ	v/v_m	Name
0.5804 0.5785 0.5731	59.7	3	0.03	a01 06e-f
0.5803 0.5791 0.5726	59.7	3	0.03	Man B gr75
0.5809 0.5767 0.5744	59.8	3	0.05	Man B gr46
0.5820 0.5804 0.5696	60.0	3	0.05	a01 01b-c
0.5804 0.5765 0.5752	59.8	3	0.05	a03 05a-b
0.5784 0.5776 0.5761	59.7	3	0.05	Man B gr56
0.5852 0.5751 0.5716	59.7	3	0.06	a04 01b-a
0.5786 0.5777 0.5758	60.0	3	0.06	Man B gr84
0.5779 0.5772 0.5769	59.9	3	0.06	a01 03g-f
0.5817 0.5767 0.5736	59.4	3	0.06	a03 06c-d
0.5832 0.5806 0.5682	59.6	3	0.08	a03 02a-b
0.5860 0.5799 0.5660	59.9	3	0.09	Man B gr39
0.7074 0.7068 0.0001	38.9	9	0.17	a03 05a-c
0.7101 0.7041 0.0042	39.3	9	0.22	a03 04c-d
0.7111 0.7031 0.0036	38.5	9	0.23	a01 05a-b
0.7164 0.6976 0.0031	38.7	9	0.26	a03 02c-b
0.7130 0.7012 0.0058	38.1	9	0.34	a03 01a-c

ACTIVE BOUNDARIES				
Axis	Angle	Σ	v/v_m	Name
0.8579 0.3816 0.3440	5.9	1	-	Man A ga51
0.6883 0.6821 0.2470	6.5	1	-	Man A ga70-71
0.7277 0.6706 0.1438	8.4	1	-	Man A ga03
0.5885 0.5790 0.5643	11.2	1	-	Man A ga43
0.7918 0.5603 0.2430	14.6	1	-	Man A ga53-54
0.5810 0.5782 0.5782	59.4	3	0.07	a04 02k-l2
0.5879 0.5748 0.5692	59.9	3	0.08	Man B gs27-28
0.6149 0.5694 0.5456	54.7	3	0.80	a04 09b-g
0.6266 0.5772 0.5236	55.4	3	0.81	Man B gr14-15
0.6241 0.5880 0.5146	55.2	3	0.86	a04 06a-b
0.6576 0.5697 0.4930	60.2	3	0.89	Man A ga66-67
0.6733 0.5312 0.5143	59.8	3	0.95	Man B gr93-94
0.6514 0.5585 0.5136	55.3	3	0.96	a04 05b-f
0.7103 0.7039 0.0068	38.8	9	0.21	a01 02a-b
0.7146 0.6995 0.0058	39.8	9	0.39	a04 09c-d
0.7076 0.7065 0.0125	40.5	9	0.58	Man B gr62
0.7294 0.6840 0.0141	37.8	9	0.59	Man A ga55-56
0.7408 0.6718 0.0060	38.8	9	0.66	a04 07l-m
0.7291 0.6835 0.0349	36.5	9	1.03	a01 07b-c

Table 8: List of the boundaries, which have been characterised by misorientation and activity during creep deformation.

Some general boundaries have been investigated as well but all of these have consequently displayed creep activity and are therefore not listed. Quite a large number (approx. 30) of inactive, low deviation twin boundaries ($v/v_m<0.07$) have been characterised besides those displayed.

Generally CSL (Σ=3 and 9) boundaries with low deviation are observed to be inactive while higher v/v_m values give rise to active CSL boundaries. Inactive boundaries range up to 0.09 for Σ3 and 0.34 for Σ9 while the active boundaries are found down to 0.07 and 0.21 for Σ3 and Σ9 respectively. Thus there is a slight overlap in deviation values between the inactive and active group of boundaries. The uncertainty on orientation measurements has been estimated (experimentally in this work) to approx. 0.3° for misorientations. An angle of 0.3° corresponds to deviations of 0.05 and 0.12 v/v_m for Σ3 and Σ9 respectively and thus the overlapping can actually be explained almost entirely by this uncertainty. It is however not unreasonable to expect a real overlap between the two groups when recalling that no consideration has been taken to include influences such as boundaries inclination with respect to the stress direction. All in all the range of active and inactive boundaries fits pretty well, as they ought, with the results obtained earlier by Peter Thorsen (Table 3)

It is notable that some of the boundaries lying close to (on either side of) the active/inactive deviation border have been hard to categorise rigidly as either active or inactive. The deformation displayed by these boundaries was sometimes so small as to be difficult to establish with any certainty.

Notice that a few low angle boundaries with quite low misorientation ($\theta < 6°$) displayed clear activity during creep testing.

Method evaluation

The manual procedure certainly works but is rather troublesome because of its inefficiency and need for long, careful, manual labour. Once a decent alternative arose it soon became unbearably tedious.

Aside from these complaints there are also technical considerations talking in favour of the automated procedure. The manual is to some degree limited to boundaries at the rim of the specimens, where the surface because of the mechanical polishing generally is more irregular than in the middle.

Additionally the results from the manual procedure are biased from what is readily visible on the surface of the specimen. Therefore the manual procedure generally gets more results on boundaries that are active because inactive boundaries are often invisible on the surface and thus one never stops to measure anything at this exact spot. All the inactive Σ3 that have been characterised by the manual procedure were discovered by accident during investigation of another – visible – boundary.

Contrary to this the automatic procedure picks up all boundaries, visible or not and allows you to search for exactly the kind of boundary that you want to study. Only the rarity of these puts a restriction on how easy the results can be obtained and how many measurements are needed.

A powerful extra is the option to examine earlier obtained EBSD maps for specifics, which were not part of the original investigation. Some of the statistical possibilities I have examined here are but a small part of what an increasingly creative research could achieve from the immense information stacked in each EBSD map.

All in all a very powerful tool with only a few points of critique such as the notion that it can tax heavily on microscope time. This can be partly overcome by making overnight measurements, which has become very popular at our lab, and made booking in advance more of a necessity.

On the software side there is still room for development and improvement. Primarily it would be nice to get rid of the computer breakdowns during scans, which have been frequent for my measurements and may be due to the many bad measurements arising from the No1 sample. These bad patterns are often almost uniformly grey (no pattern what so ever) making it difficult for the software to identify even false lines and construct a set of Euler angles for the measurement, maybe causing a crash.

Another nice addition would be the incorporation of CSL determination into the program, which would be a bonus especially for investigations such as these and would ease the amount of data handling significantly.

2.3 Grid etching and 3D boundary description

The correlation of boundary structure with activity of boundaries during diffusional creep had so far been quite successful. The purpose of this new line of work was to expand this investigation to include determination of grain boundary plane, by eliminating some of the limitations of the earlier procedures.

The concept

It is obvious (see Figure 6, page 20) that observation of grain boundary planes requires more than 2 dimensional access to the boundary. This has earlier been achieved by exclusively examining boundaries at the rim of a specimen, but this practice has some severe limitations. For our specimens this means that only a small fraction of the total boundaries are readily accessible, and in order to expand investigation into the inner part of the surface an inefficient, destructive grinding is necessary. On top of this the characterisation technique for boundaries along the edge must necessarily be manual, which isn't the most efficient of procedures, as discussed in the previous section.

To avoid this, we devised another procedure for obtaining the third dimension of the boundary plane, namely by usage of topographical features on the surface. It has earlier been found that surface scratches are retained during creep testing and such has been successfully used as marker lines for determining grain deformation (see page 41). We wanted to take advantage of this by creating well-defined scratches deep enough to measure the inclination of grain boundaries, by the surface offset of a boundary crossing such a groove (as shown on the figures below).

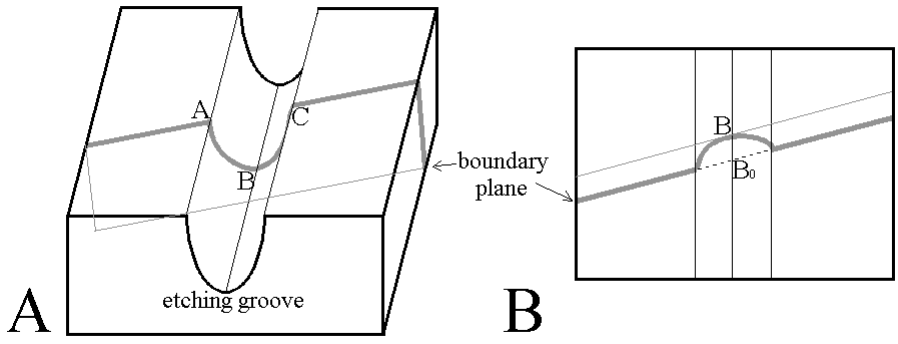

Figure 36: Measuring the boundary inclination using a surface groove A) 3D representation of the boundary (grey) crossing a groove B) Boundary seen directly from above. The distance B_0B represents the boundary inclination.

To do this one needs but to determine the x,y,z co-ordinates for the three points A, B and C (Figure 36A). If the depth of the scratch (or groove rather) is already known, it can be achieved by a single picture taken directly from above (Figure 36B) by measuring the distance B_0B, provided the inclination is sufficiently far from the surface normal. For grain boundary planes inclined near 90° to the surface, the length B_0B will be very short and thus the determination will hold great uncertainty on the angular calculation. In this case tilting of the specimen will be necessary and stereo imaging can be used to determine the appropriate parameters. Likewise more than one micrograph is needed if the depth of the groove is not known beforehand.

As described in the Auto EBSP section the usage of an inert reference grid had been highly successful for qualitatively determining creep deformation. We wanted to achieve the same effect with the grooving procedure, so that the Al_2O_3 grid was simply replaced by a complete grid of grooves.

The resist deposition technique

The procedure chosen to accomplish the goal, was a resist deposition technique that is otherwise highly used to achieve very fine patterns on disks of silicon. A similar procedure was used for the old specimens for appliance of the Al_2O_3 grid but that particular collaborator was no longer available and some of the technical problems thus had to be overcome once again.

The four steps of the procedure is as follows:

1. Photoresist deposition: The core of the entire principle is the deposition of a thin layer of a light sensitive polymer, known as photoresist, on to the surface of the specimen.
2. Illumination: The resist is subsequently illuminated selectively, using a patterned mask to shield parts of the surface.
3. Development: The development removes the illuminated parts of the resist and the surface is thus left with a layer of photoresist shaped exactly as the used mask.
4. Etching: Final step in our process is the selective etching of the surface, with photoresist protecting partly, achieving the final pattern.

Experimental procedure

The three first steps of photoresist deposition were done in collaboration with the Optics and Fluid Dynamics Department at Risø.

The specimens used for these experiments had no final surface treatment (i.e. the #4000 SiC paper was final) and they were all annealed twice after the standard heat treatment procedure. The second anneal, which became standard, is especially crucial for these specimens because of the need for a surface completely at rest. Any induced deformation will in theory be able to cause false movement of the grid structure as a result of relaxation, which could afterwards be interpreted (wrongly) as creep deformation.

The photoresist (S1813 –200MPR) is initially a liquid of medium viscosity and a crucial point of the procedure is to spread it in a uniform layer of equal thickness all over the specimen. This is normally achieved by fast rotation (spinning) of the specimen while the resist is applied onto the centre, relying on centrifugal forces to get an even distribution. This works very well with round and square specimens but yields poor results on awkward geometry's such as that of our specimens. To modify our geometry into a square, a copper plate was produced, which had a cut in the middle made to fit exactly the proportions of the creep specimens. With the specimen inserted into the copper plate so that

the surfaces are level, the resist finally had a chance to spread out in a fine layer covering the entire surface of both pieces.

The fit between the plate and the specimen was however not perfect on a micrometer scale and edge effects could not be avoided. This meant that the layer thickness of the resist was approx. 1.6 µm on the majority of the specimen but somewhat thicker in a band near the edges of the specimen. After spinning the photoresist was hardened by heating to 90° in 30 minutes.

The wanted pattern is introduced by the selective illumination of the photoresist and thus the design of the mask is a crucial point. It is clear that a grid pattern which is turned 45° with respect to the x and y directions of the specimen is preferable as this allows for easy examination of transverse as well as longitudinal boundaries. The width of the grooves should be sufficient to allow a reasonable depth, but on the other hand they shouldn't dominate the surface entirely. The distance between grooves should be so as to allow several squares in each grain for the sake of deformation measurement. An extra detail, in the form of the numbers 0-9, was added to the otherwise homogeneous grid structure, to help navigate on the creep specimens. The final design of the mask can be seen on the figure below

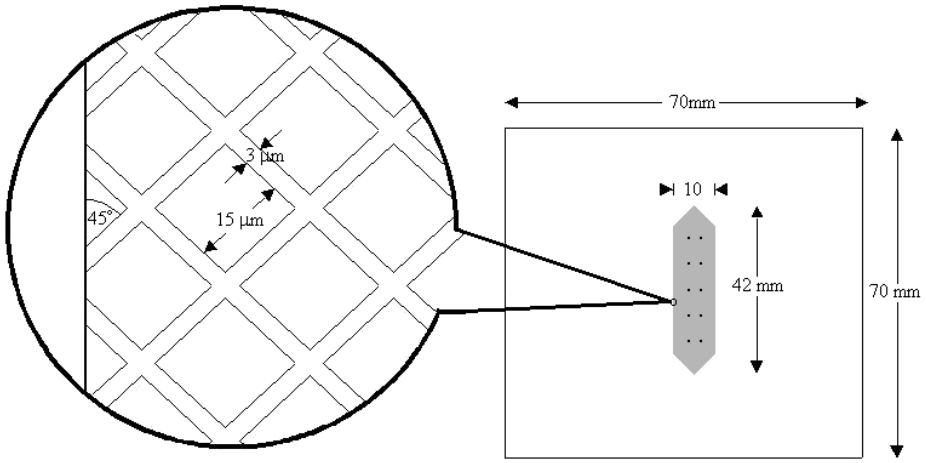

Figure 37: Specifications for the creep mask. The dots represent the numbers 0-9 incorporated into the grid.

The mask was produced and bought from a vendor in Holland, but due to an unfortunate misunderstanding during the ordering process, the received mask was equipped with *the inverse of the initially wanted pattern*. As the project was a bit strapped for time at this point it was decided to make due with the delivered mask as was.

The mask, which consists of a glass plate with a thin layer of patterned chrome, was pressed tightly down to the specimen (still fitted into the Cu plate) and illuminated for approx. 10 seconds. Immediately afterwards the photoresist layer was developed (2 min. in 15% Microprosit 351 developer) thus dissolving the illuminated parts.

Several acids were tried and by far the best results were achieved with the following copper etchant:

400 ml HNO_3 (65%)
100 ml distilled. H_2O
1 g $NiCl_2$

This acid gives a nice and homogeneous etching and does not dissolve the protecting photoresist prematurely. The only real problem is that the acid reacts

very vigorously with the copper. For our need the etching time is therefore well below 1 second making it quite difficult to control the etching precisely. For longer etching times the pattern rapidly degrades as the walls are dissolved completely, blurring the overall picture. Dilution of the acid was observed to cause a markedly slowed, but also markedly poorer etching and was no realistic alternative.

Results

After etching the lines of the mask design stood out on the specimen surface like sloped walls framing thousands of small, enclosed squares (see Figure 38). The corners where walls meet are small 4 pointed stars with a plateau of the original specimen surface were old scratches from the final #4000 polish could still be seen. All scratches in the etched areas had disappeared as intended. Each square is almost flat bottomed with a slight rise in the centre. Height difference between the floor and the top of the walls is about 1-2 μm.

The etching seemed to be pretty even across the surface although some parts of the sample displayed slightly thicker walls as a result of less etching while a few other parts displayed walls that were etched through at the top. Preferably the walls should have remained of a certain thickness, say about 2 μm, to provide a better comparison between the boundary positions at the top and bottom. With the present mask parameters that was not possible if an etch depth of at least 1 μm is wanted, as the dissolution of material happens simultaneously in all directions during etching. As seen on Figure 39 though it is still possible to measure boundary inclination with the walls as they turned out (exact height differences still have to be measured obviously). If a wall height of 1 μm is assumed the upper displacement of the boundary trace of approx. 0.6 μm gives by simple geometry a calculated angle of 59° between the boundary normal and the surface normal for the present example.

Some clear edge effects from the spinning could also be observed. Along both edges of the sample the resist layer had been too thick to be illuminated completely through and thus had only been partly removed during development resulting in an imperfect etching. Sometimes the pattern was largely intact anyway and the limited size of these areas makes this problem acceptable.

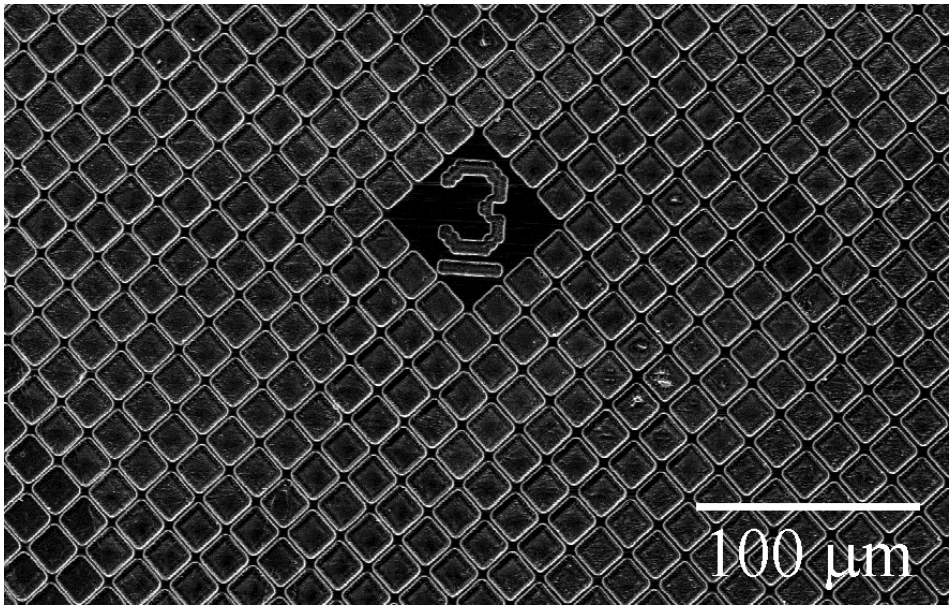

Figure 38: SEM micrograph of the etched surface. The design of the mask is clearly and beautifully implemented into a three-dimensional pattern.

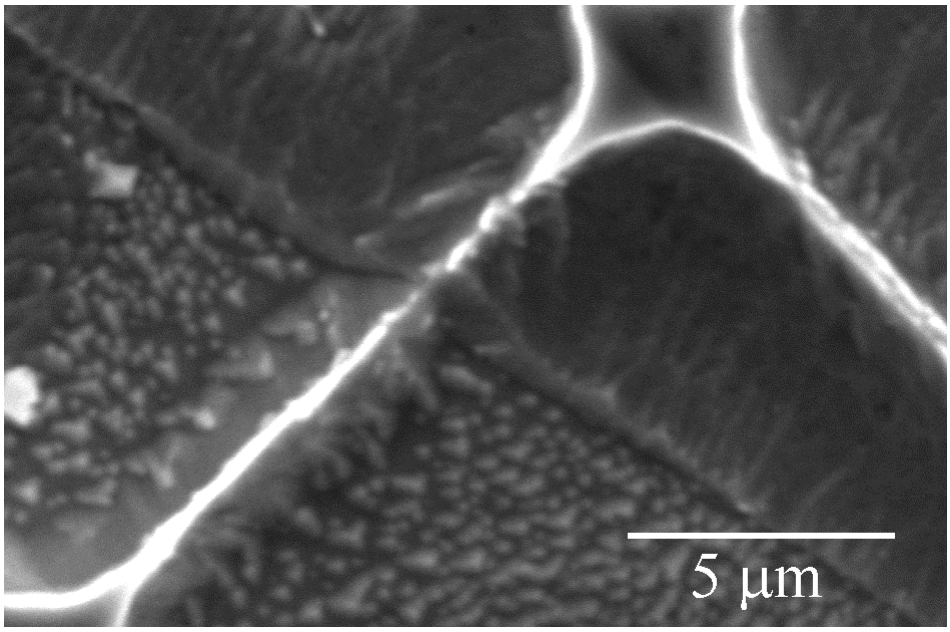

Figure 39: Zero tilt micrograph of the specimen before creep showing a boundary crossing an etch wall, revealing it's inclination by the slight bend of the boundary trace.

Degradation of the grid

A sample (Tqa5) with the aforementioned etch grid was crept under the conditions discussed on page 59. The creep behaviour was markedly different from that exhibited by the sister specimens for reasons which are not exactly clear at this point, but may be due to instabilities in the old creep machinery and a larger creep stress than intended.

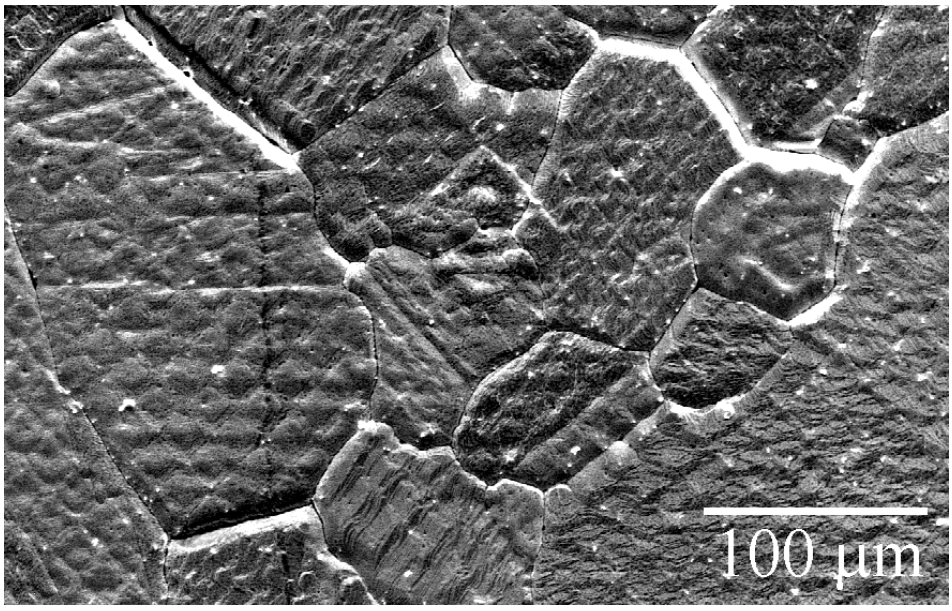

Figure 40: Specimen after creep, showing approx. the same area as Figure 38. The grid is heavily degraded and the number (3) is almost unreadable at this point.

The grid structure suffered unfortunate, heavy degradation during the creep testing, to an extent that was somewhat surprising. Comparing Figure 38, which shows an area of the sample before creep, with Figure 40 showing the same area afterwards, almost says it all.

Grain boundaries are now clearly visible because of thermal etching and deformation. Several boundaries show creep damage such as voids and small cracks (e.g. Figure 41). The grid structure however is now worn down to the extent of being almost unrecognisable in many grains. Other grains still display most of the original pattern but the walls have clearly diminished in height as well as thickness.

Conclusion

Some degradation of pattern had been anticipated beforehand but certainly not to the devastating extent that is seen here.

It is clear that a walled pattern such as this have a high surface energy compared to a perfectly flat surface. At elevated temperatures this energy can be diminished by diffusional relaxation, causing a reduction in the total surface area. The question remains how damaging this effect is.

We have earlier observed small (unwanted) scratches be retained practically unharmed through an entire creep test of similar length and temperature. Scratches have also been used deliberately and with success as inert markers in pure copper at temperatures of 773K [50] as described in section 1.3. While scratches may be somewhat more resistant to diffusional relaxation than an etched wall structure, it seems reasonable to seek another explanation to the observed degradation.

Looking closer at the degraded surface it is found that many grains display parallel lines not part of the etched pattern and which looks suspiciously like slip bands. In many cases these bands are very close to the 45° angle of the walled pattern and can thus be difficult to spot, but careful examination reveals a lot of such bands. In some grains the original pattern has been distorted in a way that has created a different kind of pattern, as seen on Figure 41. It is hard to perceive how such a pattern could have been produced without deformation of the grain interior. Such distorted patterns could e.g. have been produced by slip along a lot of different bands inside the grain, spaced only few μm apart.

If we consult Figure 29, it is clear from the creep curves that the sample with the etch pattern (TqA5) behaved differently during creep testing, than the 'identical' specimens named TqA3, TqA4 and TqA8. As mentioned we suspect this to be due to a higher stress unintentionally used for this particular creep test.

Combining the evidence it seems plausible that the main operating mechanism in this sample may in fact have been dislocation creep instead of diffusional creep as intended.

Thus hope is still preserved for the basic idea of grid etching even though some further investigation may have to precede another creep experiment. The resist deposition procedure and etching process has in any case been rather successful and we see no reason why these shouldn't work perfectly with any other perceived pattern. One might perhaps want to look for another etchant, which is easier to control, but the uniform level of etching is ultimately what counts.

On another count the etched sample was found very suitable for automatic EBSD scanning and displayed a much lower fraction of bad measurements than the sample with alumina grid (No1) and could in this respect not be distinguished from a perfectly flat (without grid) specimen.

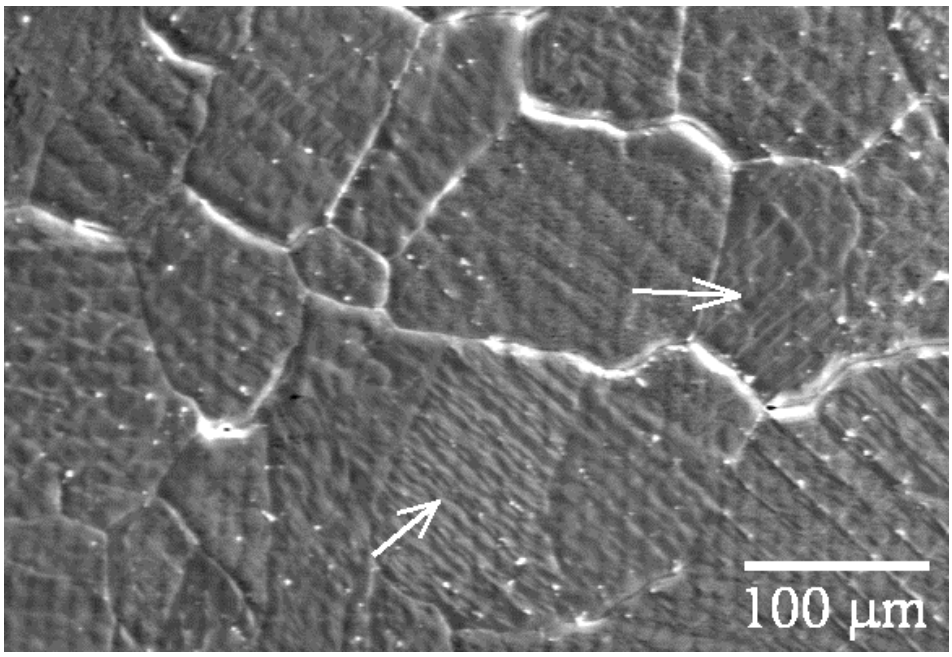

Figure 41: Etched sample after creep. Several grains display what looks like slip bands. Deformation along the slip bands has distorted the original pattern.

Finally the simple numbering put into the quadratic pattern certainly proved a very good idea and greatly helped locating specific areas on the sample. For future designs though, I would highly recommend the numbering (or lettering) be expanded as ten characters tends to disappear somewhat among the approx. 800 000 regular squares present on the sample.

2.4 TEM observations

The purpose of the TEM examination was to get a closer look at a material, which we beforehand (from the SEM investigations) knew to be deformed predominantly by a diffusional process. The idea was to obtain a deeper understanding of the diffusional and accompanying processes in order to explain some of the discrepancies and phenomena that still puzzled.

The investigations yielded many curious observations of which the most important will be examined in the following. Due to limited time and sample material some of these features where observed only a single or few times and can therefore hardly be explained satisfactorily yet. These will thus be described in as much detail as the observations allowed, with the hope that future comparison with further observations may help to shed some light on some if not all of these.

Specimen preparation

Thin film samples were prepared from the various creep specimens described in section 2.1. Parts of these specimens were cut off and preliminarily thinned down until thin discs of about 3 mm (diameter) could be readily punched out. These discs were subsequently jetpolished by hand in a mixture of 200 ml H_3PO_4, 200 ml ethylene glycol and 400 ml H_2O until they were exactly etched through (usually in the middle).

Nearly all samples were made from the successfully crept specimens of TqA3, TqA8 and No1. The latter of these provided only a few as it had to be used extensively for the SEM investigation as well.

Two TEM samples were made from the TqA4 specimen. This specimen had been creep tested way into the tertiary creep phase and showed heavy damage in the grain boundaries. For this reason the TEM samples were very hard to make sufficiently thin as the voids in the grain boundaries were attacked heavily by the thinning etchant, with a less than satisfactory result.

No TEM samples were made from specimen TqA5.

Observations

A total of 10 TEM samples of various qualities were investigated for this thesis. Working at magnifications of x20.000-120.000 even the modest macroscopic size of a single TEM sample becomes immense and makes ample room for many interesting features. In the best of our samples, where a relative large area is electron transparent, the grain size allowed for up to 15-20 boundaries to be investigated. Unfortunately buckling of the thin samples easily reduces this number by a factor of 2 as strong bending contours tend to complicate the observations, often beyond comprehension. No qualitative differences could be observed between TEM samples from different creep specimens, as the different samples from the same specimen showed just as large a diversity as seen when comparing samples from different creep specimens.

Looking at the specimens it was found that the interior of grains generally contained only few dislocations, as seen in the examples of Figure 42. Some grains seemed completely devoid of free dislocation while others had some bundles or single dislocations present. The exception to this was in areas that showed buckling or bending and where dislocations could sometimes be seen distributed uniformly throughout the grains. In close proximity to boundaries one would often find an increased density of "free" dislocations as well, in a way that seem to suggest that they have been emitted from the boundary as examples will show in the following.

The presence of reasonably few free dislocations fits very well with what is expected for well-annealed specimens such as ours, which have subsequently been deformed by diffusional processes only. If the specimens had undergone dislocation born deformation, this would have required some extent of dislocation multiplication and subsequent movement of these throughout the grains - thus more free dislocations would be expected. Therefore this is another indication that dislocation creep has played a secondary and minor role in the total deformation of our specimens (sample TqA5 excluded).

A lot of $\Sigma 3$ boundaries were observed and they sure came in many different disguises. From wide and strangely layered boundaries over the very long and straight to jagged boundaries with a lots of steps.

Only a single $\Sigma 9$ boundary was seen and characterised, which we will return to in the following section. Of rare sigma boundaries only one were characterized, namely a short piece of $\Sigma 27$ boundary found where a twin lamellae encounters the before mentioned $\Sigma 9$ boundary. All other rare sigma had deviations placing them outside the Palumbo-Aust criterion for CSL and are in this sense not rare sigma boundaries after all.

Sigma boundary ledges

One of the interesting and recurring observations seen in almost all samples, were the presence of steps (or ledges) found on low deviation $\Sigma 3$ and $\Sigma 9$ boundaries (see figures below). The phenomenon was actually so common as to be the rule rather than the exception, as the majority of the many twins displayed at least a few ledges unevenly spaced along the observable part of their

boundaries. Only a single Σ9 was found and this boundary displayed ledges as well (Figure 43A), although of a slightly different nature.

While all Σ3 ledges displayed almost, but not quite, a right angle between the different plane facets (the exact angle has to be measured looking straight down along the boundary planes obviously), the Σ9 boundary ledges were angled more like 45° (or 135° depending on definition).

On some boundaries the ledges were less obvious, than the shown examples, but looked rather like microfacets giving the otherwise perfectly straight boundary minute displacements along the length and thus changing the overall "macroscopic" grain boundary plane.

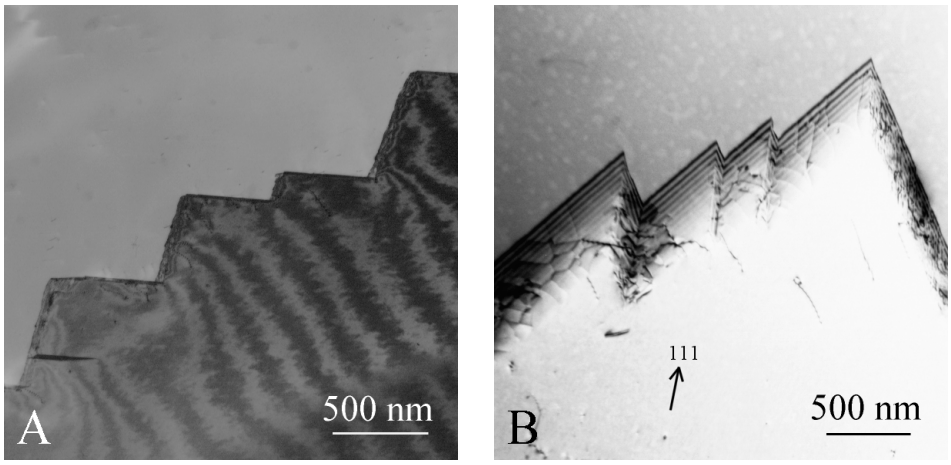

Figure 42: Σ3 boundaries with ledges. A) Notice the peculiar, small feature on the lower left, which could perhaps be an area with a stacking fault.

The occurrence of ledges on near Σ3 boundaries is a clear consequence of the very low energy structure that is particularly connected to the {111} boundary planes compared with other possible Σ3 boundary planes. Thus for a an odd angled boundary plane it is energetically favourable to "dissolve" a straight plane into two components of lower energy at the expense of making the boundary longer than strictly necessary. A necessary condition for this to work is that the ledge planes are of sufficiently low energy. As the energy relates closely to the deviation from perfect sigma one would expect an upper limit of deviation to which ledges can appear and after which it is no longer energetically feasible to extend the boundary this way. All ledge containing twin boundaries, which have been characterised for this study, have deviations of $v/v_m < 0.1$.

Common to all these boundaries is that they consist of only two different boundary planes, both of which are almost perfectly straight, meaning that all ledges on a single boundary were of exactly the same kind (or mirror images). Furthermore we find that the ledge angle on all observed Σ3 boundaries lies at about 80-85°. This suggests that it is in fact the same two types of plane that all ledged twin boundaries consist of. The obvious choice for one of these planes is the very low-energy, coherent {111} twin boundary, but what of the other plane? As mentioned, the Σ3 misorientation has another type of mirror plane namely the {211}, which stands at exactly a right angle onto the {111}. More likely though, the ledge plane is the so-called M-plane suggested by Wolf et al [7], which seemingly have a lower energy than the {211}.

Another interesting observation on some low-deviation Σ3 was that bundles of dislocations seemed to be emanating from the boundary ledges as seen on Figure 43B-D. The dislocation bundles seem to be lying in continuation of one or both of the boundary planes enhancing the impression that they have indeed been emitted from the boundary. This was a rather puzzling discovery as the

phenomenon was only observed on ledged Σ3 boundaries with rather low deviation ($v/v_m < 0.1$) and which we knew from the SEM investigation to be macroscopically inactive, thus taking no significant part in the deformation process. The presence of the dislocation bundles shows that these boundaries have at least been active on the microscopic level, even though they probably haven't contributed much to the strain of the sample.

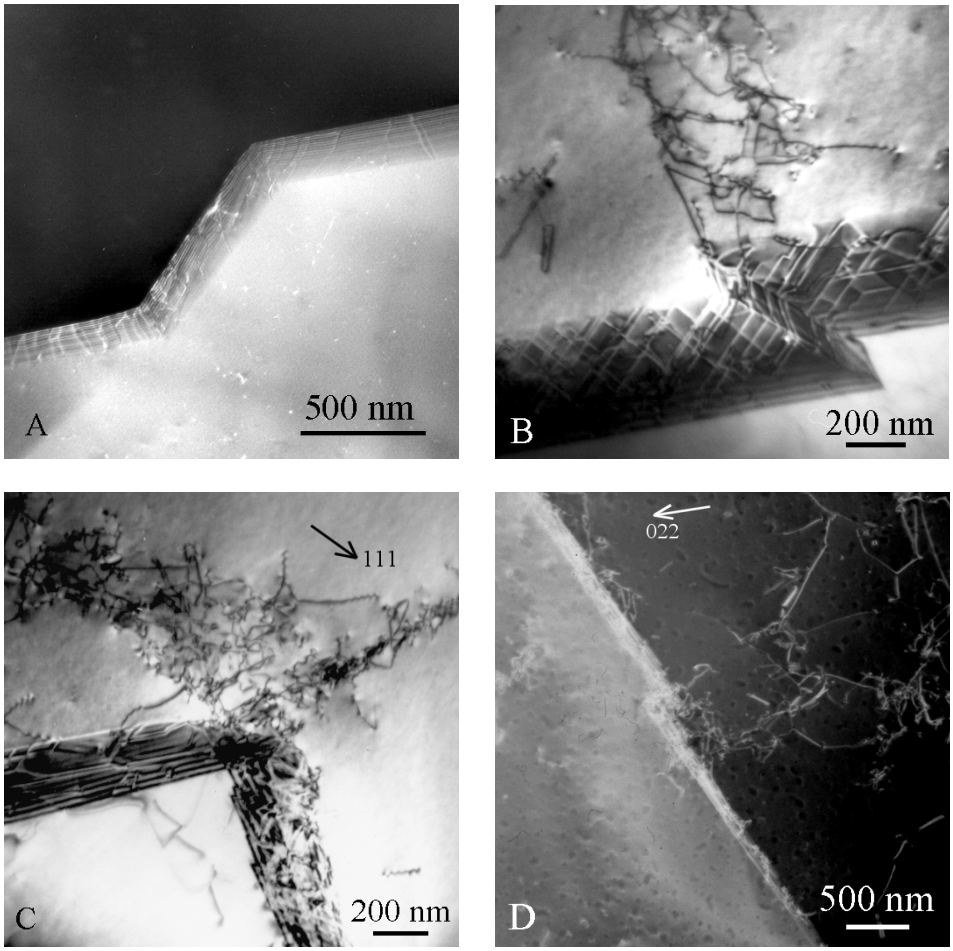

Figure 43: A) A Σ9 boundary (v/v_m=0.18) displaying ledges and secondary dislocations. B-D) Dislocations emanating from Σ3 boundaries (v/v_m=0.04, 0.06 and 0.06 respectively) at a ledge in continuation of one or both of the boundary planes.

Several unusual phenomena were observed as part of or in the vicinity of twin boundaries, as will be examined in the following sections. One of these was the small shade seen on the lower left of Figure 42A. It is a parallelogram in shape and seems to lie exactly in one of the twin boundary planes. Although the nature of the defect wasn't examined further than this, the evidence seem to suggest that it is an area with a stacking fault created by the propagation of a partial dislocation (Shockley) from the boundary. Stacking faults have earlier been reported forming near twin boundaries in metals like copper and nickel [108,109].

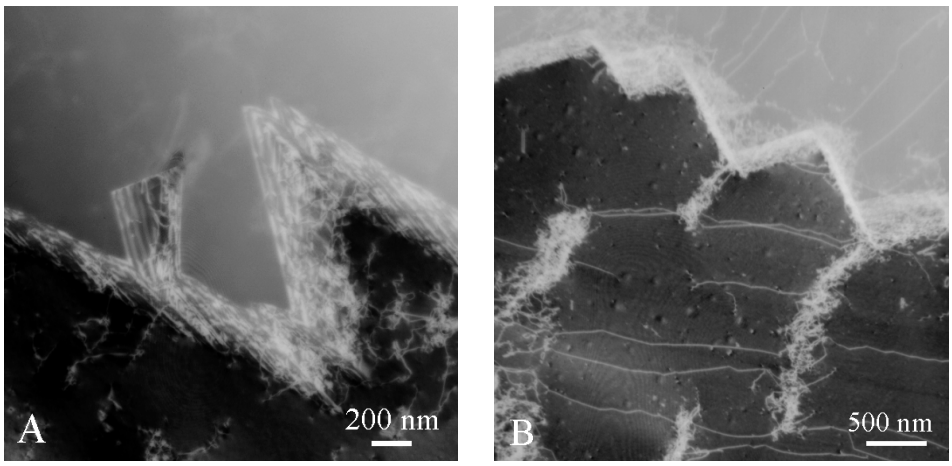

Figure 44: More Σ3 boundaries with unusual features.

'Layered' twin boundaries

A variety of strange looking twin boundaries were observed. Most of these were found in relative thick areas of the samples and usually in areas displaying bending contours as well. This made for difficult investigations and ambiguous interpretation of the phenomena.

On Figure 45 a twin boundary is shown, which seemingly consists of multiple overlapping, parallel layers. Each layer seems to begin inside one grain, gradually becoming more substantial before fading into the other grain. Along the line of the boundary the number of layers alternate between 1 to 5 layers, making for very thick-looking boundary at some places.

On Figure 46 is shown another example of a twin boundary, which seemingly expands in thickness along some parts of the boundary. This boundary is one part of a pair; together the two are creating a twin lamella (about 30 nm thick). The other boundary (not shown) is completely straight, with normal, uniform boundary thickness along the entire length.

Both of these examples were found in relative thick parts of the sample and bending contours are present as well in both cases.

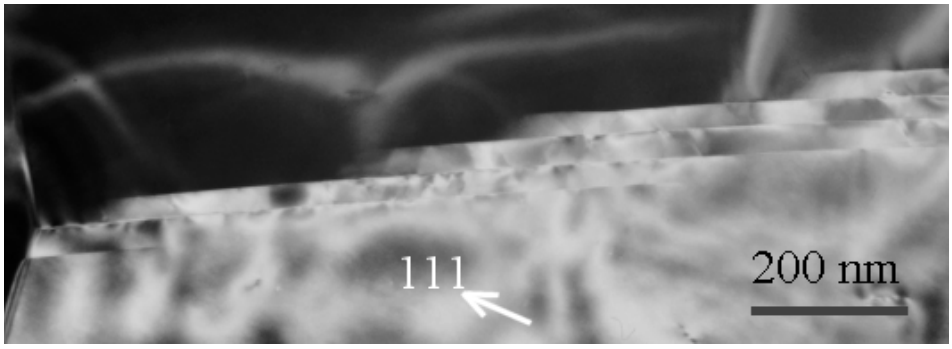

Figure 45: Dark field image of a twin boundary (v/v_m=0.13) displaying displaced layers.

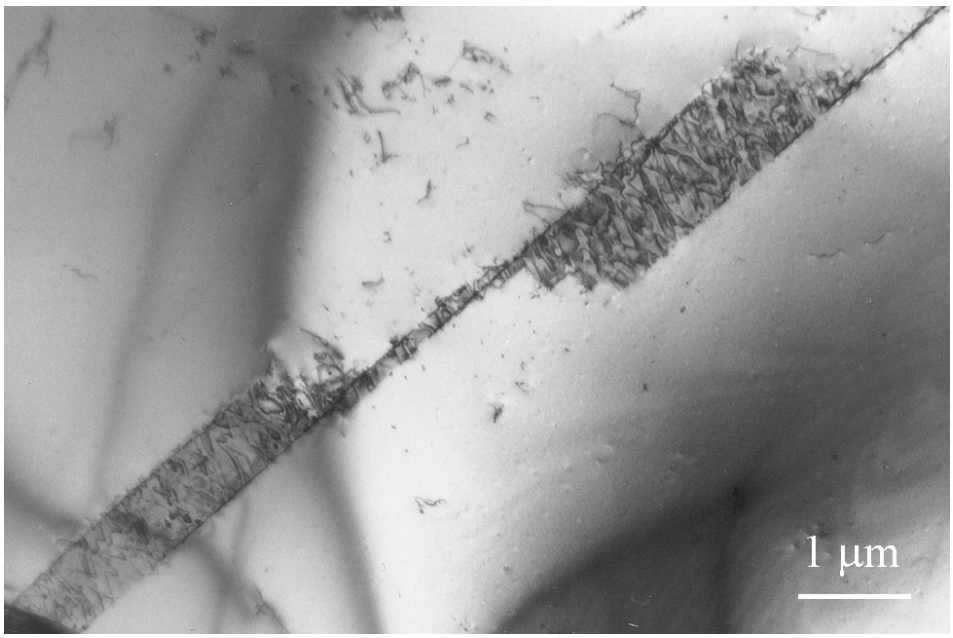

Figure 46: One of the more bizarre Σ3 boundaries (v/v_m=0.02) observed in an area with bending contours.

A third twin boundary is seen on Figure 47. Before tilting this boundary has the same type of layered appearance as the boundary on Figure 45 although this boundary looks somewhat simpler, displaying only 1-2 layers at a time at regular intervals. By heavy tilting of the specimen we managed to bring the boundary planes approx. edge-on to the viewing direction (Figure 47B) and it becomes clear that the boundary contains small ledges. The ledges appear to lie at approx. 80° to the main boundary plane like all previously found ledges on Σ3 boundaries. These ledges appear regularly along the boundary and it seems obvious that they are responsible for the layered appearance of the boundary at zero tilt.

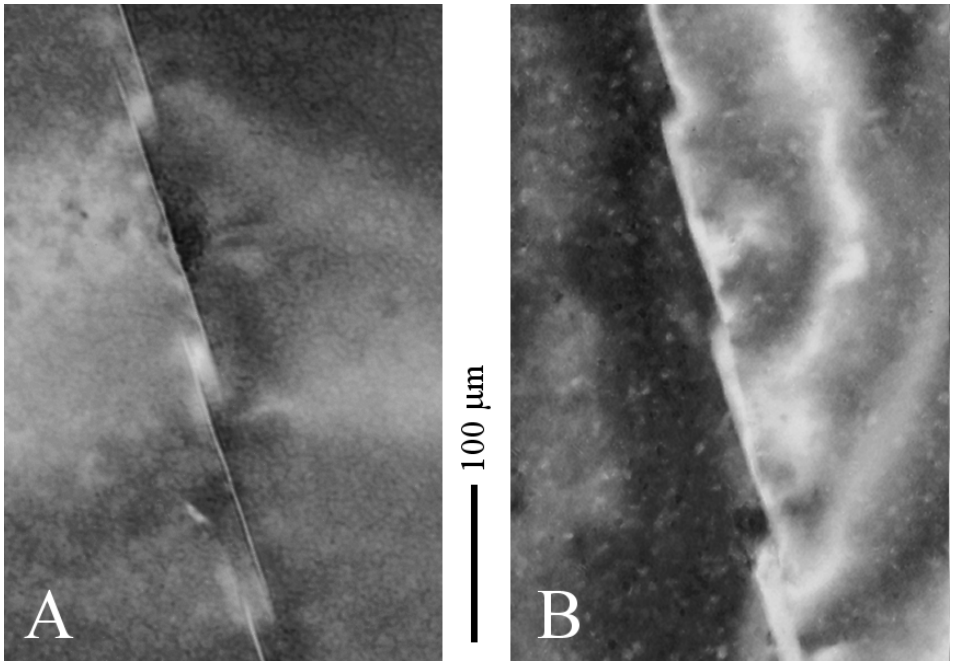

Figure 47: A layered boundary, before and after tilting.

This same procedure was not viable for the earlier described boundaries (Figure 45 and Figure 46), as the sample in these cases was so thick that the electron signal faded rapidly with even minor tilting. It seems reasonable to propose, though, that also in these cases it is actually the presence of small ledges on the boundaries that is the cause of the unusual appearances. In all the cases it seems to be that one of the ledge boundary planes is angled far from the thin foil normal, thus smearing the image of these ledges.

It is worth considering the possibility that ledges can occur in several directions in a single grain boundary. As the presence of ledges make up for a "macroscopic" boundary orientation away from the low-energy {111} it is clear that a single type of ledges can only compensate for certain rotations of the boundary plane. For a general boundary rotation at least two sets of ledge planes will be needed to compensate.

On geometrical grounds it would seem possible to have ledges in up to three different directions from a {111} plane, although one would be hard pressed to demonstrate this in a single example. In thin TEM samples it would be highly unlikely to find more than one type of ledge whereas in thicker samples it should be possible to observe ledges lying almost in-plane with the sample surface. This would effectively tend to smear the image of the boundary, making it look uncommonly thick.

From the present work it is perhaps a bit premature to unambiguously conclude that the puzzling appearance of the boundaries on Figure 45 and Figure 46 is partly due to such in-plane ledges. It is characteristic however that the most complicated-looking twin boundaries, such as the aforementioned, are always found in rather thick areas of the samples.

Secondary boundary dislocations

Focusing on the grain boundaries it was in many cases possible to observe the arrays of secondary dislocations that accommodate the deviation from perfect CSL structure and thus keeps the energy of the boundary low.

If the boundary takes part, even slightly, in the deformation processes the secondary dislocations will move as they absorb (or emit) vacancies. As they move they will often bend slightly, which can allow us to determine what way they have been moving. An idea arose, namely to correlate this movement with the overall deformation of the boundary (stress direction) in order to determine whether the dislocations were contributing constructively to the overall deformation as we would expect.

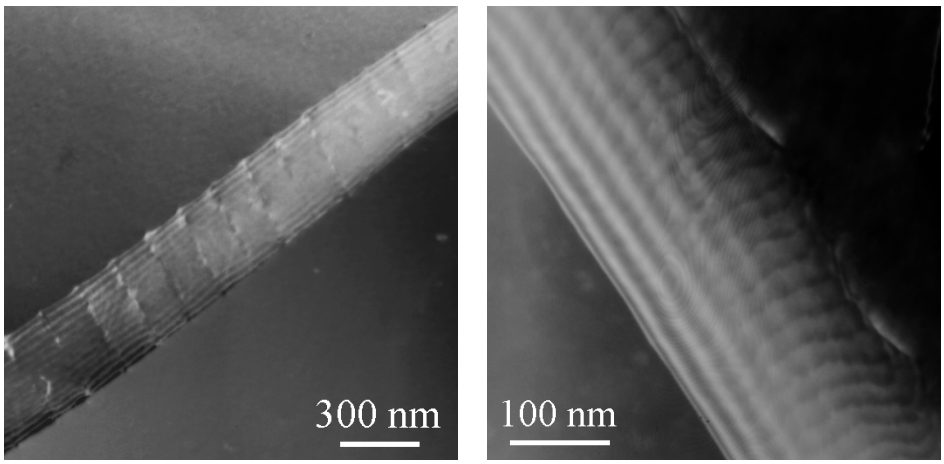

Figure 48: Secondary dislocations in grain boundaries. A) Σ27 (v/v_m= 0.15). B) General boundary.

Several attempts have been made to identify the secondary dislocations in different CSL boundaries, by usage of the invisibility criterion and weak-beam techniques [110]. At some boundaries several different types of secondary dislocations was present forming dislocation networks and thus making identification of the individual dislocations rather difficult. At present all of the attempts to identify secondary dislocations have failed, possibly due to my limited abilities as a microscopist

Rectangular Loop

An unexpected feature was captured by accident in a micrograph of a grain boundary (see Figure 49). The feature closely resembled a rectangular dislocation loop, and this was highly unexpected as such curious phenomena had only earlier been reported to form in certain irradiated materials [111,112,113]. Some of the reported materials were Cu-Ni alloys as it happens and the occurrence of this phenomenon has lead to the suggestion that rectangular loops form from clusters of Ni atoms. Hence the complete solid solubility between Cu and Ni, which is normally thought to exist, may actually be somewhat more complex on the nanoscopic level.

Looking at the rectangular feature it seems that two of the corners are "cut off" leaving a small length of dislocation lying at 45° to the sides of the rectangle – a characteristic phenomenon that is often observed on radiation induced rectangular loops as well.

During further investigations in an attempt to determine the exact nature of the feature it unfortunately disappeared very suddenly. In some sense this lends further credibility to the notion that it in fact was a rectangular dislocation loop as these are known to be unstable e.g. they can dissociate spontaneously into two glissile a/2<110> loops that can disappear to the surface (especially under the energetic glare of the electron beam). On the other hand it made further examination futile, and as no other such loops have yet been found in our samples, the exact nature of the feature will continue to remain somewhat a mystery.

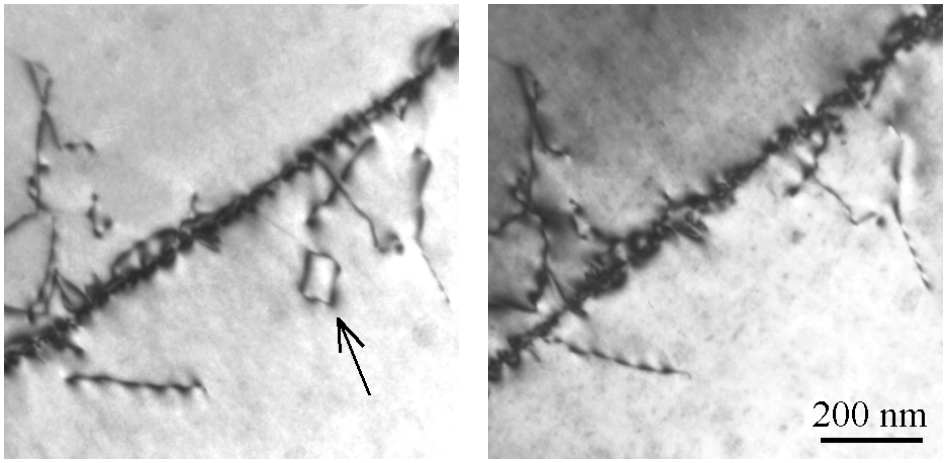

Figure 49: A Rectangular dislocation loop? A) The loop-like feature B) The same sample area after annihilation of the feature.

2.5 The gold experiments

This range of experiments were performed separately at the University of Purdue, Indiana as further development on earlier work [114,115,44]. The aim was to examine the grain growth of nanocrystalline specimens during creep at relative high stresses in an attempt to understand and quantify creep behaviour and determine the deformation mechanisms. If possible it was the intention to correlate grain growth and movement with grain boundary determination and classification.

Specimen preparation

10 TEM gold samples were made by vacuum deposition. 31 mm (0.7 g) gold wire was thermally evaporated under vacuum and deposited on freshly cut surfaces of NaCl single crystal. The thin gold layers were cut in smaller pieces (approx. 2*2 mm), lifted off the rocksalt and cleaned carefully several times in distilled water before being placed on gold TEM specimen support grids.

These grids were 3 mm disks divided into hundreds of smaller units labelled on the grid bars to facilitate identification of interesting areas.

The creep experiment

The samples were annealed at 250°C (in air) for 1 hour at a time, the development being investigated and TEM micrographs taken between each heat treatment.

The nanocrystalline gold films are found to weld strongly to the support grids at an early stage of annealing and at the same time extensive grain growth is observed. This combination results in the creation of a bi-axial stress in the plane of the films, as the total amount of grain boundary is diminished and replaced by the denser structure of the lattice. As the sample excess volume is thus diminished the film would tend to shrink, but is constrained from doing so by being welded to the support grid, which is comparably substantial and rigid. The resulting stress can then be seen relieved by the formation of voids or cracks in the thin films.

Specimen development

The annealing resulted in a columnar microstructure and a two-component <111> fibre texture as described in [114]. This texture comprises distinct regions in which the mean deviation of the <111> direction with respect to the surface normal is either approx. 1.5° or 4.5°. Apparently these two textures correspond to regions on the NaCl substrate, which are completely plane or rugged (containing steps on the crystal) respectively.

Mean linear intercept measurements showed the development in grain size as a function of annealing time. The starting grain size (0 hours annealing) could only be roughly estimated, as initially the grains were so small as to lie in several layers through the thin film.

Annealing time	0 hours	1 hour	2 hours	3 hours	4 hours	5 hours
Grain size (MLI)	< 20 nm	63 nm	72 nm	74 nm	91 nm	93 nm

Table 9: Overview of grain size development.

Crack growth often initiated in the 4.5°-texture regions of the film and grains near the tip of cracks were micrographed after each annealing session. This allowed for a closer look at how cracks developed and propagate through the

specimen. Even though the deformation from hour to hour is relative modest comparing images is rather difficult due to the great amount of twins and the different diffraction conditions one happens to use from microscope session to session (see figure below).

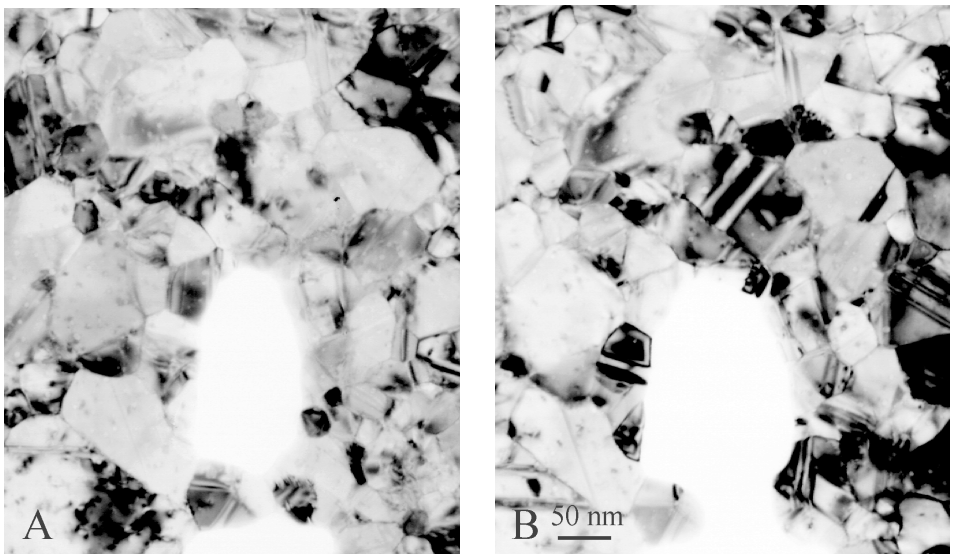

Figure 50: Grain and crack growth. A) Sample after 1h annealing. B) Same area after another hour (2h total) of annealing.

No free dislocations at all are observed in these specimens or any other signs for that matter that a dislocation mechanism should be responsible for the occurring deformation. The stresses in the film have earlier [44] been estimated to 140 MPa, much lower than the estimated yield stress for the samples of 900 MPa. By this exclusion of alternatives the proposed deformation mechanism must therefore be diffusional creep.

On the basis of microscope pictures some not altogether successful mapping of strain on single grains was performed. Likewise area strain maps were made from the basis of triple point movement these but proved equally inconclusive.

Misorientation measurements could not be performed consequently, as most grains were too small to yield proper Kikuchi patterns. As the above figures show the few relative large grains are usually surrounded by small grains making misorientation correlation difficult.

The thickness of the thin films was determined by CBED (Kossel-Mösselstedt fringes) to 34 – 41 nm, somewhat thinner than intended and one of the reasons suitable Kikuchi patterns were hard to produce.

3 Discussion

Here we will re-examine some of the performed work in an attempt to reach some clear understanding of the collective observations.

Determination of creep mechanism

Looking through the gathered evidence there can be no doubt in my mind that our specimens have indeed been deformed by processes which are based on the diffusional transport of vacancies from transverse to longitudinal boundaries, i.e. diffusional creep.

Micrographs of grains, which have moved apart at transverse boundaries displaying fresh material in the boundary trace, or grains that have moved together and where part of the original surface has disappeared are many (example at Figure 31). Not that many are really needed as a careful analysis of the rigid grain movement in a single example, actually gives very hard evidence for the fact that material has been deposited and removed at the respective boundaries. Until another mechanism is proposed that can predict this phenomenon, we must interpret it as indisputable proof that diffusional creep has occurred and is seemingly responsible for the induced deformation.

Let us for a minute consider alternative creep mechanisms such as Harper Dorn creep - the favourite mechanism of Sherby, Ruano and co-workers [116]. These people would presumably disagree with our conclusion regarding the creep mechanism. They would perhaps even seek to show, as they have done many times before, that our experimental creep data would fit just as well or perhaps even better with their chosen model for Harper-Dorn creep. Should we even begin to accept this reasoning it would have to be in the face of structural facts. The Harper-Dorn creep mechanism is supposedly born by dislocation movement - in the grain interior as well as in the grain- and sub-grain boundaries - with the strain rate being determined by diffusion controlled climb. Such a mechanism would cause deformation of the grain interior as well as across boundaries and this should be evident from structural investigation. Dislocation mechanisms such as H-D creep do not cause deposition or removal of material at grain boundaries.

Our SEM investigations indisputably show the surface grid to be completely undisturbed (beyond measuring anyway) in the interior of the grains meaning that no prominent deformation has taken place in the bulk of the grains. Furthermore the TEM investigations show only small amounts of free dislocations in the grain bulk, which, also indicate that there have been no mentionable dislocation activity here. This must lead us to conclude that deformation has occurred exclusively in the boundary regions of the samples and that dislocation creep therefore has played an insignificant role in the deformation process of our specimens.

The sole exception to this is the pattern-etched specimen TqA5, which we suspect to have been crept at a higher stress than the rest of our specimens. This sample displayed a markedly different creep curve and there was SEM evidence for creep deformation in the interior of the grains, and traces of slip bands. Unfortunate as this damaging of the sample was, it thus gives a gives a good counter example to the other specimens as these signs fit rather nicely into the theory for diffusional and dislocation creep.

We feel that the measured creep rates fits reasonably well with calculations done after the original model for Nabarro-Herring creep (grain sizes are too large for Coble creep to be relevant), although approximately a factor of 2

higher than expected. As stressed earlier however we don't consider this to be a weight carrying argument neither for nor against this particular mechanism, because of the many uncertainties concerning these formulae.

It seems clear that in regard to the theoretical formulae the diffusional model is still far from resolved. The structural evidence presented here, especially that of the SEM investigation, however seems to leave no room for explanations outside the diffusional creep principles. A consequent denial of diffusional creep as a viable operating mechanism in metals seems absurd.

Creep activity and boundary deviation

The SEM investigation of near Σ3 and Σ9 boundaries has confirmed the clear connection between CSL deviation and creep activity, which earlier work (by Peter Thorsen) had discovered. The new results have not moved the earlier determined limit between active and inactive boundaries significantly, but only added to the evidence giving better statistics.

Apart from a few exceptions there seem to be a wide gap between the groups of Σ3 examined for this work. Statistically it is reasonable that a lot of twins are found with deviation below 0.08 as copper is a known twin rich material. The many created coherent twins are very stable and take no or very little part in the subsequent deformation and therefore largely stay unchanged after creation. It is thus very easy to expand the statistics with more of this type of stable (inactive) twins. Stranger it seems that in the wide and interesting range of twins with deviations of 0.08-0.5 Only few are found, while another large group of the investigated twin boundaries are the active ones with deviations above these values. This could be simply coincidental, but a possible explanation could be the instability of the boundaries in this "transition" region.

As vacancies are emitted and secondary dislocations start moving in a twin boundary the two implicated grains are moved with respect to each other. If this movement is more than just rigid translation, i.e. grain rotation the misorientation will be affected. The activity that occurs can thus result in changing the boundary towards greater stability (lower v/v_m) or towards a more disordered state (higher v/v_m). Energetical reasoning would talk in favour of the first but as the boundary is taking part in a deformation these considerations might carry little weight. Basically the change is in the 'hands' of the vacancy emitting (absorbing) secondary dislocations and how their forced movement consequently alters the neighbourship of the implicated grains. On top of this one must not forget the fact that a single grain in the bulk of the sample has numerous neighbours. Thus many different boundaries will be affected simultaneously by e.g. rotation of a grain, building stresses. Statistically one would say that the odds are in favour for changing a boundary towards larger deviation, as generally there is only one way towards greater stability (the perfect CSL structure) but many away from. Thus many of the high deviation Σ3 that have been observed may initially have had smaller v/v_m values at the time before creep testing.

Another concern is the exchange of grain boundary dislocations across triple points. It is very possible (depending on the three boundaries that meet surely) that dislocations can be transferred fairly easy out of a twin boundary, but that dislocations moving the other way will have difficulties entering the twin segment, because of the restrictions on such particular dislocations. Thus a twin boundary might theoretically be 'emptied' for secondary dislocations as a consequence of the dislocation motion occurring during diffusional creep lessening the deviation (v/v_m) and creating a more stable boundary.

For boundaries having deviations in the 0.08-0.5 border area (between active and inactive) it is also a question whether they are truly inactive or just greatly

hampered in participating efficiently. With overall strains of only 1-2% on the creep specimens it is doubtful if any deformation could be observed in a boundary working at only a few percent efficiency. If this is the case it is also probable that these boundaries could be fully "activated" by a heightened creep stress, so that the limit between active and inactive boundaries is lowered.

In any case it is clear from watching the movement of grains by use of the surface grid that some grains do rotate quite significantly. This lends credibility to the notion that misorientations of some boundaries can change so as to change their "creep activity" during the test. In some cases one would therefore expect low activity boundaries to become more active while the test progresses and perhaps even becoming general boundaries in time. In other (clearly fewer) cases one might find boundaries, which after some initial strain has changed slightly into a more stable (low deviation boundary) configuration and subsequently stopped (practically) participating further.

The sufficient number of GBDs needed for boundaries to work as efficient vacancy sources or sinks has been discussed by Siegel, Chang and Baluffi [117]. From their model of sink efficiency it is hard to explain why twin boundaries with deviations up to 0.08 are inactive, as even small amounts of dislocations should make boundaries able to function, at least to some extent, as vacancy sinks or sources. An explanation for this discrepancy leads directly to the next part of the discussion.

Boundary ledges as creep impeding feature

One of the very pronounced features of our TEM investigation were the ledges present on the majority of low deviation ($v/v_m<0.08$) Σ3 boundaries.

Ledges on twin boundaries in Cu have also been studied by Huang and Mishin [118,119], who observed them exclusively on boundaries having deviations of less than 2° from the perfect CSL misorientation. A deviation of 2° corresponds to a value of $v/v_m=0.33$ (assuming a {111} misorientation vector) and this therefore fits nicely with our own observations.

The finding of ledges on low-deviation boundaries only is a clear indication that there is a natural upper limit for when it is energetically feasible for a twin boundary to decompose into low-energy facets. This upper limit has been experimentally found to be approx. $v/v_m = 0.1$, which is suspiciously close to another experimental finding, namely the deviation border between active and inactive boundaries found in the SEM investigation. This border, which is recapitulated on Table 8, is found to be approx. 0.08 and the notion that the two transitions are related is an obvious and intriguing thought.

The work of Wolf et al. [49], some of which has been briefly recounted on page 41, dealt with the nature of the individual facets on ledged Σ3 boundaries. It was found that the common companion to the coherent twin is a boundary inclined 82° to the {111} twin plane. This boundary, which they term M, is found to be more stable than the incoherent twin on the {211} plane and constitute an energy minimum in their relaxation simulations. They find the M type boundary to be surprisingly broad and comprised of partly FCC partly rhombohedral (9R) structural units.

That the energetically favourable boundary plane is inclined 82° (or 98° depending on 'which way' the facets are pointed) fits very well with our own observations of ledges on Σ3 boundaries. All the ledges we have found show facets inclined almost, but not quite, at a right angle and it seems reasonable that it is indeed the M boundary plane that our samples display.

It should be intuitively clear that a rhombohedral phase constituting part of a boundary could act as a major obstacle for the movement of secondary dislocations. In the given case of diffusional creep the GBDs also have to be trans-

ferred from one facet of the ledge to the other in order to keep moving. This transference can be very difficult if the specific dislocation isn't allowed on both facets and thus have to undergo some kind of reaction first. We therefore propose that the presence of grain boundary ledges could be an inhibiting factor in diffusional creep deformation. The ledge will obviously not affect the process of vacancy diffusion itself, but the necessary glide and climb motion of GBDs and the accommodating mechanisms of grain boundary sliding and migration could be greatly hindered. Obstructing the glide and climb motion of GBDs would effectively prevent these dislocations from absorbing or emitting vacancies effectively, thus keeping the boundary "macroscopically" inactive. Increasing stress could help overcome the obstruction presented by the ledges, and result in activation of boundaries, which would be inactive at lower stresses. This notion was already introduced on account of the SEM investigation (previous section).

Even without this more or less 'impassable' rhombohedral structure on the ledges, just the very presence of boundary facets would in some instances obstruct the motion of dislocations. This follows from the movement of dislocations, which is dictated by the need for negative or positive climb on transverse and longitudinal boundaries respectively. Depending on dislocation type and stress direction this can result in dislocations of the same type (same Burgers vector) moving in opposite directions on the two boundary facets. In the example below the dislocations could be a/3<111> with dislocation A lying on the coherent grain boundary plane. Under the indicated stress, dislocation A must move downwards to the right in order to contribute positively to the deformation, while dislocation B for the same reason will move upwards to the left. Meeting at the corner none of the dislocations will have any incentive to move further as that would contribute negatively to the overall strain.

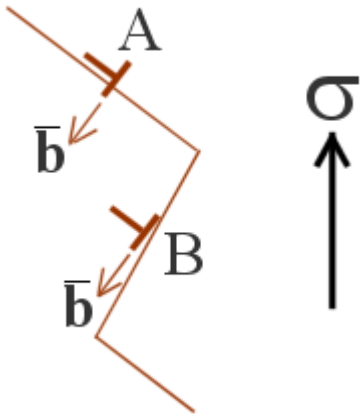

Figure 51: Sketch of two identical dislocations. Under the indicated stress the dislocations will move in opposite directions (meeting at the ledge corner).

In this way one might anticipate the dislocation movement in a ledged boundary coming to a halt thus preventing further vacancy emission or absorption. Notice that even though this is just an example, twin boundaries are often found as lamellae ending inside grains (as the cover micrograph) and in these cases the problem will necessarily occur on some of the corners (ledges).

It should be clear that these certain ledge corners would then experience a build up of dislocations and local stresses, to degrees depending on the specific circumstances. This may again help explain some of the observed phenomena with ledges apparently emitting dislocations (see Figure 43B-D). This could be seen as a sign of stress relievance in such corners, where the accumulation has

exceeded the boundary's ability to maintain coherency. If a particular secondary dislocation on one facet is not allowed on the other, it can perhaps undergo a suitable reaction so as to transfer onto the "forbidden" facet. Such a reaction will inevitably yield a "residual" dislocation in order to conserve Burgers vector. The emitted bundles of dislocations from ledge corners could perhaps be such residual dislocations.

It is still not clear exactly why some twin boundaries have few and some many ledges. Some display large and some display microscopic ledges of only few atomic steps. It is evident that the spread is wide and the exact configuration could probably influence the rigid determination of activity during diffusional creep. If we thus accept the hampering influence of ledges on diffusional creep it would not be unreasonable to suggest that a completely straight twin boundary with a deviation of $v/v_m=0.05$ may be active while another ledged boundary of $v/v_m=0.1$ may be inactive. Hence we get a reason for the slight overlap between the groups of active and inactive Σ boundaries that is not only based in measuring inaccuracies.

With the nice observations of ledges on low deviation Σ9 the obvious question remains whether they can be found on other (rarer) Σ boundaries as well. It is clear that such boundaries must fulfil the strict requirement of having (at least) two preferred planar orientations. That is to say the boundary planes of which a ledge is composed must be of sufficiently low energy compared to some average plane between the two.

Reasons for creep rate discrepancies

The main argument against the evidence for and occurrence of diffusional creep is that the measured creep rates and stress dependences are often very much at odds with the theoretically predicted values. Without presuming to know the details of the work of others, I will here present some of the possible explanations, to these discrepancies, as we have encountered them for our own experiments. They are:

- Grain size and shape distributions
- Grain size in z-direction
- Significant amounts of inactive boundaries
- Boundary activity dependent on stress

When working with real polycrystalline materials one is often faced with awkward size distributions and grain shapes far from geometrical beauty. The average diffusion distance that is needed for calculating creep rates is clearly affected by changes in shape and size distribution, compared to a material consisting of identical equiaxed grains. As a ground rule it should be clear that as a grain distribution widens (for constant arithmetic mean diameter) the creep rate should increase because of the non-linear dependence on grain size. Likewise as grain shapes become more exotic (for constant mean grain volume) the creep rate should increase as well, due to the average increase in grain boundary in the material as a whole.

The point of z-direction grain size measurements seems often to be forgotten or perhaps just neglected because of the difficulties in obtaining these measurements for certain specimen geometries. In our case the z-direction MLI was found to be only 88% of the length found for x and y directions. With the squared grain size dependence for Nabarro-Herring creep (and worse for Coble) assumptions about the grains being equiaxed would surely cause a minor error for creep rate calculations. Larger differences than ours could lead to serious discrepancies.

Another possible source of grave error to creep rates, which has been very relevant for our specimens, is when significant amounts of inactive boundaries are present. In the No1 sample more than half (56% actually) of the total boundary length is taken up by Σ3 boundaries with deviations $v/v_m < 0.08$, and which therefore supposedly is completely inactive during creep testing. Ignoring this fact in grain size measurements would give rise to errors of several orders. Even when working with non-twinning materials, one must remember that the fraction of special boundaries can increase dramatically in textured materials, and inactive boundaries can thus play an important role.

The possibility that certain low deviation Σ3 boundaries (which still constitute more than 50% of the total boundary length in our specimens) are "activated" at higher creep stresses would surely cause an unexpected increase in creep rate and thus a stronger creep rate dependence on stress. As some boundaries are activated the average grain size decreases and consequently the creep rate increases accordingly. According to Nabarro's (or Cobble's) model the stress dependence should be linear (n=1) but often higher values have been measured. Our own measurements of stress dependence gave a result of 1.4 as mentioned.

It should be clear from the previous that determination of creep mechanism on the sole basis of creep data requires lots of care and is at best a risky business. It is certainly no alternative to microstructural investigation.

Further research

Even though it has been rendered probable that the creep activity of low deviation Σ boundaries is dependant on stress, the transition from inactive to active is still somewhat speculative. I would therefore find it useful to try to describe the deviation limit from inactive to active as a function of a kind of threshold stress.

By use of the autoEBSP technique one could locate Σ3 boundaries with v/v_m values close to the active/inactive transition before creep. Subsequently creep testing the specimen at different (increasing) stress levels and noting when the transition to active occurs. At the same time it would be possible and very interesting to determine whether and how these boundaries change character (increased/decreased deviation from perfect Σ) during creep.

It is clear also that the TEM examination still has plenty more to offer. Many of the encountered boundaries cannot be explained satisfactorily and closer investigation is clearly needed. Identification of secondary dislocations should be possible as well and determining the way they have moved during creep would certainly be a novel way to demonstrate the theory of diffusional creep.

4 Conclusion

We have studied grain boundaries in creep-tested material by use of scanning and transmission electron microscopy. Disruptions of the reference grid is found exclusively at grain boundaries and relative grain movement demonstrate that material have been deposited at transverse and removed from longitudinal boundaries. The lack of lattice deformation and scarcity of free dislocations exclude dislocation born deformation as a significant mechanism. To the present author this shows beyond reasonable doubt that diffusional creep is the only significant deformation mechanism in the creep-tested specimens (one specimen excepted).

Manual and automated misorientation measurements were correlated with individual deformation activity. Σ3 boundaries with deviations (v/v_m) of 0.03-0.09 were found to be inactive during creep while active twins were found with deviations 0.07-0.96. For Σ9 boundaries the inactive boundaries were in the range of 0.17-0.34 while active boundaries had deviations of 0.21-1.03. It remains to be shown whether these limits depend on stress as suggested.

The resist deposition and etching experiment was partly successful. The actual transference of pattern from mask onto the surface worked very well and pre-creep examination of the surface indicated how the boundary plane can evaluated from an etched surface. Unfortunately the surface pattern was utterly ruined in the creep test process, presumably because of too high creep stress. SEM investigations revealed indications for pronounced dislocation creep in the sample. Thus hope is still retained for the basic idea of three-dimensional surface patterns, used for boundary investigation.

Studies and characterisation of grain boundaries by TEM have provided a glimpse of a microscopic world rich in strange and not easily explained phenomena. Ledges were found on low deviation Σ3 (v/v_m <0.1) and Σ9 (v/v_m=0.18) boundaries and the presence of such allowed for an explanation as to why these boundaries are inactive during creep testing. It is highly likely that such ledges act as an obstacle to the movement of grain boundary dislocations and that dislocations in certain circumstances will move in alternating directions on the different facets, thus being unable to absorb or emit vacancies. What could be interpreted as signs of such stress accumulation were seen on some of these ledged boundaries in the shape of dislocation bundles apparently being emitted from ledge corners. Further studies of these specimens could probably yield answers to some of the more puzzling observations.

A - The misconception of the role of GBS in diffusional creep

Below is a reprint of the original drawing by Burton [35], showing grain boundary sliding as a geometrically necessary accommodation step in diffusional creep. Although the understanding of the role of grain boundary sliding has changed a lot since then (see Section 1.2 for details) this intuitively seductive graphic is still causing confusion and misunderstanding.

Lets be clear that this is not how it works!

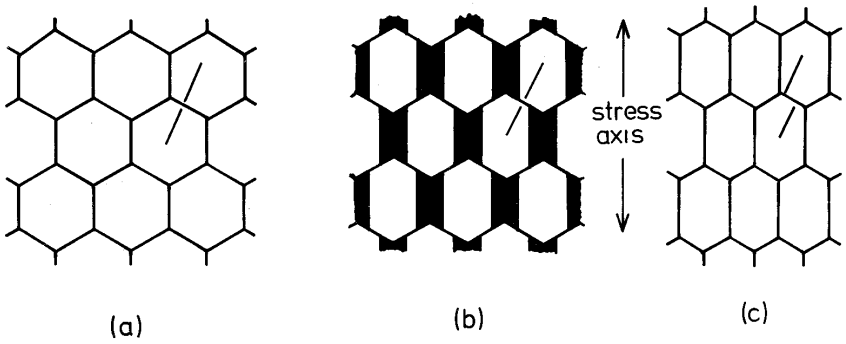

Figure 26 Schematic representation of marker off-sets by grain boundary sliding during diffusional creep. If sliding did not occur, cavities would open up as shown in (b).

B - Reprints of publications

From : Proceedings of the 9th International Conference on Creep & Fracture of Engineering materials & Structures (2001) pages 15-20

Σ=3 GRAIN BOUNDARIES IN Cu-Ni SUBJECTED TO DIFFUSIONAL CREEP

Thomas Nørbygaard and Jørgen B. Bilde-Sørensen
Materials Research Department, Risø National Laboratory,
DK-4000 Roskilde, Denmark.

ABSTRACT

In earlier work (Mater. Sci. Eng. **A265** (1999) 140) the behaviour of individual boundaries during diffusional creep was studied by measuring the deformation of the boundaries on the surface of a grid-covered sample in a scanning electron microscope. It was found that the boundaries deform by a combination of grain boundary sliding, grain boundary migration and deposition or removal of material at the boundary. For boundaries that can be described within the framework of the coincident site lattice (CSL) concept this behaviour can be understood in terms of the movement of grain boundary dislocations.

It was also found that $\Sigma = 3$ boundaries with a misorientation close to an exact lattice CSL misorientation were inactive during deformation. This cannot be understood directly on basis of the contents of GBDs. Therefore selected $\Sigma = 3$ boundaries in Cu-2wt%Ni deformed in the difffusional creep regime have been studied by transmission electron microscopy. The boundaries were found to contain ledges, and dislocation tangles were found to emanate from some of these ledges. The interior of the grains was generally found to contain only few lattice dislocations. It is suggested that $\Sigma = 3$ boundaries close to an exact CSL misorientation are inactive because the ledges act as obstacles to the movement of GBDs.

1. INTRODUCTION

The mechanism for diffusional creep was proposed by Nabarro [1] in 1948. He pointed out that the equilibrium vacancy concentration in the vicinity of a grain boundary under stress is given by $C = C_\circ \cdot \exp(\sigma\Omega/kT)$ where $C_\circ$ is the thermal equilibrium concentration of vacancies, Ω the atomic volume, k the Boltzmann constant and T the temperature. The stress, σ, is positive for tensile stresses and negative for compressive stresses. A concentration gradient will therefore be set up in the individual grains of a polycrystalline sample subjected to a stress, and this will result in a flow of vacancies from grain boundaries in tension to boundaries in compression (corresponding to a flow of atoms in the opposite directrion). Under the assumptions that the boundaries are perfect sinks and sources for vacancies and that the rate-controlling process is diffusion through the lattice, it can be shown that the rate equation is of the form

$$d\varepsilon/dt = B\sigma\Omega D/d^2kT \quad (1)$$

where B is a numerical constant around 12, D the lattice self-diffusion coefficient and d the grain size. At lower temperatures the grain boundaries may provide an easier diffusion path than the bulk lattice. Coble [2] showed that the rate equation for diffusional creep by boundary diffusion is of the form

$$d\varepsilon/dt = B'\sigma\Omega wD_g/d^3kT \quad (2)$$

where B' is a numerical constant around 50, w the grain boundary width and D_g the grain boundary self diffusion coefficient.

As mentioned, all boundaries were assumed to be perfect sinks and sources in these early models. Since then the understanding of grain boundary structures has increased considerably and it is clear that some of the phenomena observed during diffusional creep can only be understood in terms of the grain boundary structure.

In the following we shall use the coincident site lattice (CSL) model for our discussion of boundary structures [3]. The structural unit model provides an equivalent description, but the CSL model is chosen for the present purpose because it yields a more immediate illustration of some of the points. The basic concept of the CSL model is that some misorientations leads to a high degree of coincidence of lattice points on either side of the boundary. The fraction of coincident lattice sites is denoted by $1/\Sigma$. Such boundaries are often observed to have low energy. Small deviations from the CSL misorientation can be accommodated by secondary grain boundary dislocations (GBDs). These secondary GBDs have Burgers vectors that are translation vectors of the DSC lattice (the DSC lattice has translation vectors that preserve the grain boundary structure). The maximum deviation that can be accommodated by secondary GBDs, ν_m, will in the following be given by the Palumbo-Aust criterion [4] $\nu_m=15°\cdot\Sigma^{-5/6}$. The boundaries that cannot be described within the framework of the CSL model are termed general boundaries. These will not be discussed here, but it should be mentioned that recent research has shown [5] that even in general boundaries there is a significant degree of order and that structural units found in special boundaries also appear in general boundaries.

In the context of diffusional creep it is important to note that it is generally assumed that vacancies can be absorbed or emitted only at grain boundary dislocations. This assumption has been experimentally corroborated by in-situ experiments in a transmission electron microscope [6]. A GBD climbs when it absorbs or emits a vacancy. Since the GBDs are confined to movements in the boundaries they will in the general case have to move by a combination of glide and climb. The glide of GBDs leads to grain boundary sliding. GBDs are associated with a step in the boundary [7]. This step moves with the GBD and this movement of the step leads to grain boundary migration. The implication of the CSL model is thus that deposition or removal of material at the boundary during diffusional creep is coupled to grain boundary sliding and grain boundary migration. This theoretically expected coupling of the diffusional creep process to grain boundary sliding and migration was recently demonstrated experimentally by Thorsen and Bilde-Sørensen [8,9] who by scanning electron microscopy measured the deformation at individual boundaries in Cu-2%Ni deformed in the diffusional creep regime. They thereby demonstrated that material had indeed been deposited on grain boundaries loaded in tension.

Thorsen and Bilde-Sørensen [10] also examined the activity of various CSL boundaries as observed in the scanning electron microscope. It was found that active $\Sigma = 3$ boundaries deviated more than 0.14 from the exact CSL misorientation on the Palumbo-Aust criterion, whereas the inactive boundaries deviated less than 0.21. A similar result was found for $\Sigma = 9$ boundaries. This indicates a threshold value for active boundaries with ν/ν_m in the range 0.14 to 0.21. It is obvious on the basis of the boundary model discussed above that a grain boundary can operate as an efficient source or sink for vacancies only if it contains a sufficient number of grain boundary dislocations. The question what in this context is a sufficient number has been discussed by Siegel, Chang and Baluffi [11]. They found that the sink efficiency is given by

$$\eta = \frac{1}{1 + \frac{\ell}{2\pi W} \ln\left(\frac{\ell}{2\pi r_o}\right)} \tag{3}$$

where ℓ is the spacing of dislocation lines in the boundary, W is the distance of the boundary from a perfect planar source or sink and r_o the radius of the thin cylinder around the dislocation that acts as a perfect sink. This equation shows that the boundary should be an efficient sink as long as the spacing of GBDs is considerably smaller than W. It is disputable exactly which value to use for W. However, $\nu/\nu_m = 0.14$ corresponds to a dislocation spacing of appr. 14 nm, and any reasonable value of W will be considerably larger than this. In order to understand why the boundaries are inactive we have therefore examined $\Sigma = 3$ boundaries in Cu-2%Ni deformed in diffusional creep by transmission electron microscopy.

2. EXPERIMENTAL PROCEDURE

Cu-2%Ni was chosen as the material for the experiments in order to avoid the extensive grain growth during creep that was observed in preliminary experiments on pure Cu. After machining, the specimen was annealed in vacuum for 4 hours at 673 K and for 4 hours at 1073 K. It was then ground and polished and annealed for a second time. The specimen was finally given a combined etching and polishing treatment with a dispersion of 0.02 μm alumina in a mixture of 96 ml water + 2 ml 30% hydrogen peroxide + 2 ml 25% ammonia in order to obtain a smooth and clean surface. The grain size was measured to be 122 μm.

The specimen which had a reduced section with dimension 37.5x5x0.7 mm^3 was crept for 7 days with an applied stress of 1.14 MPa in a vacuum better than 10^{-5} torr to a total strain of 0.9 %. The strain was measured continually with a strain transducer. The creep rate before the onset of tertiary creep was $2 \cdot 10^{-9}$ sec^{-1}.

After creep, samples for transmission electron microscopy were prepared by jetpolishing a thin disc, cut from the sample, in a mixture of 200 ml H_3PO_4, 200 ml ethylene glycol and 400 ml water.

3. EXPERIMENTAL RESULTS AND DISCUSSION

Fig. 1 shows a near CSL $\Sigma = 3$ boundary. An obvious feature of this boundary is that it contains ledges. It is also noticed that the interior of the grains contains only few dislocations.

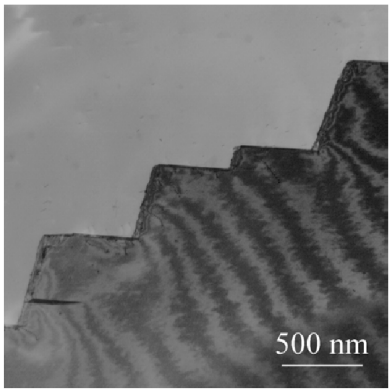

Fig. 1. Micrograph of a near CSL Σ=3 boundary exhibiting ledges inclined approximately 82° to the {111} facets.

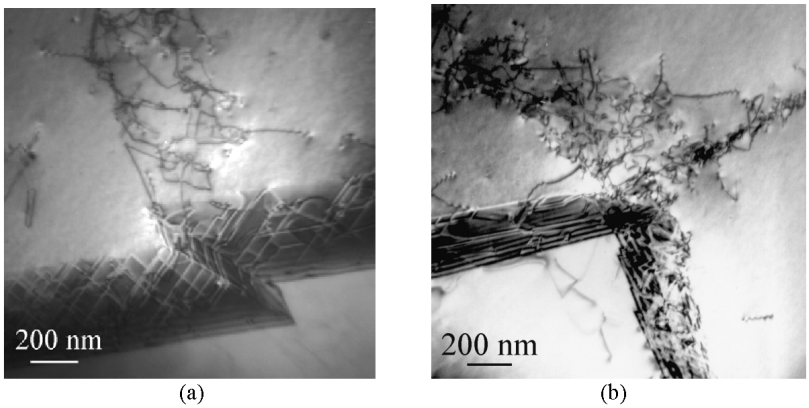

(a) (b)

Fig. 2. Dislocations emanating from ledges on a Σ= 3 boundary with an orientation close to the exact CSL misorientation. (a) $\theta = 59.94°$, $\nu/\nu_m = 0.062$ (b) $\theta = 59.83°$, $\nu/\nu_m = 0.040$.

This supports the view that the deformation has not taken place by a lattice dislocation mechanism. Another striking feature is seen in fig. 2 which shows that tangles of dislocations emanate from some of the ledges. In some cases the tangles lie in continuation of one of the planes forming the step in the boundary (fig. 2 (a)), in other cases in continuation of both planes (fig. 2 (b)).

Wolf et al. [12] performed an experimental and theoretical study of such ledges in Σ = 3, $[01\bar{1}]$ tilt boundaries in Cu. They found the existence of an energy minimum for a boundary with an inclination of 82° to the {111} boundary. This boundary exhibits a rhombohedral 9R structure formed in a 1 to 2 nm thick layer. The results were supported by high resolution electron microscopy.

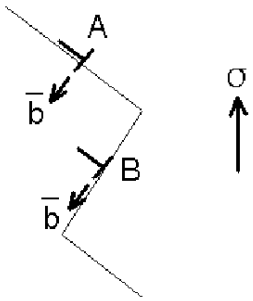

Fig. 3. Sketch showing two dislocations with identical Burgers vectors. Under the tensile stress indicated the dislocation marked A will move downwards to the right while the one marked B will move upwards to the right.

It seems highly likely that the presence of a rhombohedral structure at the ledges can act as an obstacle to the transfer of GBDs between the facets on the boundary. Even if the rhombohedral layer had not existed, there would be some configurations of the boundary for which it would be impossible to transfer secondary GBDs between the facets because dislocations with identical Burgers vector would move in opposite directions on the two facets This is illustrated in fig. 3. Two dislocations with the same Burgers vector are shown lying on two different facets of the boundary. The dislocation marked A could be a $\frac{a}{3}\langle 111\rangle$ dislocation lying in the coherent part of the boundary. Under the tensile stress indicated this dislocation must move downwards to the right in order to contribute positively to the deformation. The dislocation marked B, however, must move upwards to the right in order to contribute positively to the deformation. This sketch shows only one line orientation, but by considering these segments as parts of expanding loops on the two boundary segments, one can appreciate that the result applies to any line orientation: dislocations with the same Burgers vector will tend to move in opposite directions on the two boundary segments. It is therefore not possible to transfer GBDs from one boundary segment to another. The argument is only intended to show that ledges under certain circumstances can act as an obstacle to deformation. Transfer of this particular GBD could in principle occur if the ledge had turned the other way.

In this context it is interesting to note one of the results that Huang and Mishin [14] recently obtained in an experimental study of the ledges in $\Sigma = 3$ boundaries. They found that all the boundaries with ledges examined in their study had deviations of less than 2° from the exact CSL misorientation. A deviation of 2° corresponds to a value of $v/v_m = 0.33$ on the Palumbo-Aust criterion. The experimental threshold value for activity of $\Sigma = 3$ boundaries during diffusional creep is thus in quite good agreement with the value of v/v_m below which ledges are found. This supports the view that the threshold value for macroscopic activity of $\Sigma = 3$ boundaries during diffusional creep can be related to the presence of ledges on the boundaries.

The observation of dislocation tangles emanating from corners on the $\Sigma = 3$ boundaries also indicates that the lack of macroscopic activity during diffusional creep can be related to the presence of ledges. The tangles indicate that the boundaries have been active at the microscopic level during the deformation process. The dislocation tangles may arise from extrinsic grain boundary dislocations that are emitted from the boundary or they may be produced by sources in the neighbouring grain by stress concentrations from pile-ups of

GBDs. In both cases the appearance of dislocation tangles indicate that the boundary in principle has the ability to deform, but that the presence of a ledge impedes the deformation.

4. CONCLUSION

A number of $\Sigma = 3$ boundaries close to the exact CSL misorientation has been studied by transmission electron microscopy. It has been shown that these boundaries contain ledges and it is concluded that it is the presence of these ledges that make boundaries with $v/v_m < 0.14$ - 0.21 macroscopically inactive during diffusional creep. Dislocation tangles can be seen to emanate from the corners of some ledges, and this demonstrates that the boundaries are active at the microscopic level.

ACKNOWLEDGEMENT

We are grateful to Jan Larsen and Jørgen Lindbo for the experimental assistance. The present work was carried out within the Engineering Science Center for Structural Characterization and Modelling of Materials.

REFERENCES

1. Nabarro F. R. N., 1948, Report on a conference on the strength of solids, Bristol, 7-9 July 1947 (London: The Physical Society) pp. 75-90.
2. Coble, R. L., 1963, J. Appl. Phys., Vol. 34, pp. 1679-1682.
3. Hull, D., and Bacon, D. J., 1984, Introduction to Dislocations (Oxford: Pergamon Press) pp. 196-202.
4. Palumbo, G., and Aust, K. T., 1990, Acta metall. Vol. 38, pp. 2342-2352.
5. Farkas, D., 2000, J. Phys.: Condens. Matter. Vol. 12, pp. R497-R516.
6. King, A. H., and Smith, D. A., 1980, Philos. Mag., Vol. A42, pp. 495-512.
7. King, A. H., and Smith, D. A., 1980, Acta Cryst., Vol A36, pp. 335-343.
8. Thorsen, P. A., and Bilde-Sørensen, J. B., 1999, Mater. Sci. Eng., Vol A265, pp. 140-45
9. Bilde-Sørensen, J. B. and Thorsen, P. A., 1997, Boundaries and Interfaces in Materials; The David A. Smith Symposium (Warrendale: TMS), pp. 179-188.
10. Thorsen, P. A., and Bilde-Sørensen, J. B., 1999, Mater. Sci. Forum, Vol. 294-296, pp. 131-134.
11. Siegel, R.W., Chang, S. M., and Baluffi, R.W., 1980, Acta Metall., Vol. 28, pp. 249-257.
12. Wolf, U., Ernst, F., Muschik, T., Finnis, M., and Fischmeister, H. F., 1992, Philos. Mag., Vol A66, pp. 991-1016.
13. Huang, X., and Mishin, O., 2000, To be published in Acta Mater.

References

Apart from the articles directly noted in the text the following textbooks have been used for background reference, particularly for Chapter 1:

D. Hull & D.J. Bacon, *Introduction to Dislocations*, Pergamon Press (1984)
V. Randle, *The Measurement of Grain Boundary Geometry*, Institute of Physics Publishing Ltd. (1993)
M.F. Ashby & D.R.H. Jones, *Engineering Materials*, Pergamon Press (1980)
D.B. Williams & C.B. Carter, *Transmission Electron Microscopy*, Plenum Press (1996)
B. Burton, *Diffusional Creep of Polycrystalline Materials*, Trans Tech Publications (1977)
P.J. Goodhew & F.J. Humphreys, *Electron Microscopy and Analysis*, Taylor & Francis (1988)

---

[1] *Handbook of Chemistry and Physics,* 68 ed., Ed. by R.C. Weast, CRC Press Inc. (1987)

[2] M.F. Ashby, Acta Metal. **20** (1972), 887

[3] D. Wolf, Scripta Met. **23** (1989), 1913

[4] V. Randle, *The Measurement of Grain Boundary Geometry*, Institute of Physics Publishing Ltd. (1993)

[5] W. Rosenhain and J.C. Humfrey, J. Iron Steel Inst. **87** (1913) 219

[6] C. Goux, Can. Metall. Q. **13** (1974), 9

[7] D. Wolf, Phil. Mag. A. **62** (1990), 447

[8] V. Randle & B. Ralph, Text. Micro. **8&9** (1988), 531

[9] G. Palumbo, K.T. Aust, Acta Metall. **38** (1990), 2343

[10] H. Gleiter, J. de Phys. **46** (1985), C4-393

[11] A. Roy, U. Erb and H. Gleiter, Acta Metall. **30** (1982), 1847

[12] P.A. Thorsen and J.B. Bilde-Sørensen, Mat. Sc. Forum. **294-296** (1999),131

[13] D. Hull and D.J. Bacon, *Introduction to Dislocations*, Pergamon Press (1984)

[14] M. Winning, G. Gottstein and L.S. Shvindlerman, Acta Mater. **49** (2001), 211

[15] M.L. Kronberg and F.H. Wilson, Met. Trans. **185** (1949), 501

[16] D.G. Brandon, B. Ralph, S. Ranganathan and M.S. Wald, Acta Metall. **12** (1964), 813

[17] D.G. Brandon, Acta Metall. **14** (1966), 1479

[18] G. Palumbo, K.T. Aust, E.M. Lehockey, U. Erb and P. Lin, Scripta Mater. **38** (1998), 1685

[19] T. Watanabe, J. De Phys. **46** (1985), C4-555

[20] W. Bollmann, Phil. Mag. **16** (1967), 383

[21] W. Bollmann, *Crystal Defects and Crystalline Interfaces*, Berlin, Springer-Verlag (1970)

[22] W. Bollmann, Surface Sci. **31** (1972), 1

[23] W. Bollmann, Suppl. Adv. Appl. Prob. (1972), 151

[24] W. Bollmann, J. Microscopy **102** (1974), 233

[25] D.A. Smith and R.C. Pond, Int. Met. Reviews (1976), 61

[26] A.P. Sutton and R.W. Baluffi, *Interfaces in Crystalline Materials*, Oxford University Press (1995)

[27] R.I. Todd, Mat. Sci. and Techn. **16** (2000), 1287

[28] L. Priester, Rev. Phys. Appl. **24** (1989), 419

[29] A.P. Sutton, Phil. Mag. Let. **59** (1989), 53

[30] J. Harper and J.E. Dorn, Acta Metall. **5** (1957), 654

[31] W. Blum and W. Maier, Phys. Stat. Sol.(a) **171** (1999), 467

[32] F.R.N. Nabarro, Report of a Conference on the Strength of Solids, The Physical Society, London (1948), 75

[33] C. Herring, J. Appl. Phys. **21** (1950), 437

[34] R.L. Coble, J. Appl. Phys. **34** (1963), 1679

[35] B. Burton, *Diffusional Creep of Polycrystalline Materials*, Trans Tech Publications (1977), 46-47

[36] S.S. Sahay and G.S. Murty, Scripta. Mater. **44** (2001), 841

[37] A.H. King and D.A. Smith, Acta Cryst. **A36** (1980), 335

[38] R.S. Mishra, H. Jones and G.W. Greenwood, Scripta Met. **22** (1988), 323

[39] B. Burton, Mater. Sci. Eng. **18** (1975), 245

[40] H. Gleiter, Acta Metall. **27** (1979), 187

[41] J.B. Bilde-Sørensen and D.A. Smith, Proceedings of the 8th International Conference on the Strength of Metals and Alloys, Pergamon Press, Oxford (1988), 869

[42] J.B. Bilde-Sørensen and D.A. Smith, Scripta Metall. Mater. **30** (1994), 383

[43] J. Wolfenstine, O.A. Ruano, J. Wadsworth and O.D. Sherby, Scr. Metall. Mater. **29** (1993), 515

[44] K.E. Harris and A. King, Acta Mater. **46** (1998), 6195

[45] B. Cai, Q.P. Kong, L. Lu and K. Lu, Mat. Sci. Eng. **A286** (2000), 188

[46] R.L. Squires, R.T. Weiner and M. Phillips, J. Nucl. Mat. **8** (1963), 77

[47] W. Jaeger and H. Gleiter, Scripta Metall. **12** (1978), 675

[48] R. Timmins and E. Artz, Scripta Metall. **22** (1988), 1353

[49] U. Wolf, F. Ernst, T. Muschik, M.W. Finnis and H.F. Fischmeister, Phil Mag. A **66** (1992), 991

[50] K.R. Mcnee, H. Jones and G.W. Greenwood, *Creep Behaviour of Advanced Materials for the 21st Century*, (1999), 481

[51] J.B. Bilde-Sørensen and P.A. Thorsen, *Boundaries and Interfaces in Materials*, the David A. Smith Symposium, TMS (1997), 179

[52] P.A. Thorsen and J.B. Bilde-Sørensen, Mater. Sci. Eng. **A265** (1999), 140

[53] O.A. Ruano and O.D. Sherby, Mater. Sci. Eng. **56** (1982), 167

[54] J. Wadsworth, O.A. Ruano and O.D. Sherby*, Creep Behavior of Advanced Materials for the 21st Century*, (1999), 425

[55] I.G. Crossland, in *Physical Metallurgy of Reactor Fuel Elements*, Ed. By J.E. Harris and E.C. Sykes, Metals Society, London (1975), 66

[56] D.J Towle and H. Jones, Acta Metall. **21** (1976), 399

[57] I.G. Crossland and R.B. Jones, Met. Sci. **11** (1977), 504

[58] T. Sritharan and H. Jones, Acta Metall. **27** (1979), 1293

[59] T. Sritharan and H. Jones, Acta Metall. **28** (1980), 1633

[60] T. Sritharan and H. Jones, Mater. Sci. Eng. **61** (1983), 1

[61] O.A. Ruano and O.D. Sherby, Mater. Sci. Eng. **64** (1984), 61

[62] T. Yamane, N. Genma and Y. Takahashi, J. Mater. Sci. **19** (1984), 263

[63] O.A. Ruano, J. Wadsworth and O.D. Sherby, J. Mater. Sci. **20** (1985), 3735

[64] J. Fiala and J. Cadek, Mater. Sci. Eng. **75** (1985), 117

[65] I.M. Bernstein, Trans. AIME **236** (1967), 1518

[66] O.A. Ruano, J. Wadsworth and O.D. Sherby, Mater. Sci. Eng. **84** (1986), L1

[67] H. Udin, A.J. Shaler and J. Wulff, Trans AIME **185** (1949), 186

[68] E.R. Funk, H. Udin and J.Wulff, Trans AIME **191** (1951), 206

[69] A.T. Price, H.A. Holl and A.P. Greenough, Acta Metall. **12** (1964), 29

[70] B.C. Allen, Trans AIME **236** (1966), 903

[71] L.F. Bryant, R. Speiser and J.P. Hirth, Trans AIME **242** (1968), 1145

[72] G. Malakondaiah and P. Rama Rao, Mater. Sci. Eng. **52** (1982), 207

[73] E.R. Hayward and A.P. Greenough, Mater. Sci. Eng. **4** (1969), 106

[74] G. Malakondaiah and P. Rama Rao, Acta Metall. **29** (1981), 1263

[75] O.A. Ruano, J. Wadsworth and O.D. Sherby, Acta. Metall. **36** (1988), 1117

[76] C.H. Hamilton, C.C. Bampton and N.E. Paton, Superplastic Forming of Structural Alloys, Ed. by N.E. Paton and C.H. Hamilton, TMS-AIME, Warrendale (1982), 173

[77] H.E. Adabbo, G. González-Doncel, O.A. Ruano, J.M. Belzunce and O.D. Sherby, J. Mater. Res. **4** (1989), 587

[78] K.B. Knorr, R.M. Cannon and R.L. Coble, Acta Metall. **37** (1989), 2103

[79] O.A. Ruano, J. Wolfenstine, J. Wadsworth and O.D. Sherby, Acta Metall. **39** (1991), 661

[80] J.E. Harris and R.B. Jones, J. Nucl. Mater. **10** (1963), 360

[81] O.D. Sherby and P.M. Burke, Prog. Mater. Sci. **13** (1968), 333

[82] J.P. Poirier, *Creep of Crystals*, Cambridge Univ. Press, Cambridge (1985), 197

[83] J. Wolfenstine, O.A. Ruano, J. Wadsworth and O.D. Sherby, Scripta Metall. **29** (1993), 515

[84] O.A. Ruano, J. Wadsworth, J. Wolfenstine and O.D. Sherby, Mater. Sci. Eng. **A165** (1993), 133

[85] B. Pines and A.F. Sirenko, Fiz. Meta. Metalloved. **15** (1963), 584

[86] J. Fiala and T. Langdon, Mater. Sci. Eng. **A151** (1992), 147

[87] H. Jones, Mater. Sci. Eng. **4** (1969), 106

[88] B. Burton and G.W. Greenwood, Acta Metall. **18** (1970), 1237

[89] B. Burton and G. L. Reynolds, Mater. Sci. Eng. **A191** (1995), 135

[90] O.A. Ruano, O.D. Sherby, J. Wadsworth and J. Wolfenstine, Mater. Sci. Eng. **A211** (1996), 66

[91] G.W. Greenwood, Scripta Metall. Mater. **30** (1994), 1527

[92] B.W. Pickles, J. Inst. Met. **95** (1967), 333

[93] T. Langdon, Scripta Metall. Mater. **35** (1996), 733

[94] O.A. Ruano, O.D. Sherby, J. Wadsworth and J. Wolfenstine, Scripta Mater. **38** (1998), 1307

[95] J.B. Bilde-Sørensen and D.A. Smith, Scripta Metall. Mater. **30** (1994), 383

[96] J.B. Bilde-Sørensen and D.A. Smith, Proc. 8th Int.Conf. on the Strength of Metals and Alloys, Ed by P.O. Kettunen, T.K. Lepistö and M.E. Lehtonen, Pergamon Press (1988), 869

[97] A. Horsewell, Scripta Met. **13** (1979), 21

[98] P.B. Hirsch, A. Howie, R.B. Nicholson, D.W. Pashley and M.J. Whelan, *Electron Microscopy of Thin Crystals*, Butterworths, UK (1965)

[99] N.C. Krieger Lassen, Proc. 16th Risø Int. Symp. on Materials Science, Ed. by N. Hansen, D. Juul Jensen, Y.L. Liu and B. Ralph, Risø National Lab., Denmark (1995), 405

[100] N.C. Krieger Lassen, D. Juul Jensen and K. Conradsen, Scanning Microsc. **6** (1992), 115

[101] N.C. Krieger Lassen, *Automated determination of crystal orientations from electron backscattering patterns*, Ph.D. Thesis, The Technical University of Denmark (1994)

[102] B. Burton and B.D. Bastow, Acta Metall. **21** (1973), 13

[103] L. Ciupiński, B. Ralph and K.J. Kurzydlowski, Mater. Char. **38** (1997), 177

[104] P. Thorsen, *The Influence of the Grain Boundary Structure on Diffusional Creep*, Ph.D. Thesis, Risø National Laboratory, Denmark (1998)

[105] A. Ball and M.M. Hutchison, Met. Sci. J. **3** (1968), 1

[106] I.D. Prendergast, D.W. Budworth and N.H. Brett, Trans. Britt. Ceram. Soc. **71** (1971), 31

[107] S. Kishimoto, N. Shinya and M.D. Mathew, J. Mater. Sci. **32** (1997), 3411

[108] T. Malis, D.J. Lloyd and K. Tangri, Phys. Stat. Sol.(a) **11** (1972), 275

[109] T. Malis, D.J. Lloyd and K. Tangri, Phil. Mag. **26** (1972), 1081

[110] S. Poulat, J.P. Morniroli and L. Priester, Phil. Mag. **80** (2000), 453

[111] T. Leffers and P. Barlow, Phil Mag. **32** (1975) 491

[112] T. Leffers, J.B. Bilde-Sørensen and P. Barlow, Scand. J. Met. **6** (1977), 29

[113] J.B. Bilde-Sørensen and T. Leffers, Phil Mag. **36** (1977), 585

[114] K.E. Harris and A.H. King, Mat. Res. Soc. Symp. Proc. **317** (1994), 425

[115] K.E. Harris, V.V. Singh and A.H. King, Acta Mater. **46** (1998), 2623

[116] M.Y. Wu and O.D. Sherby, Acta Met. **32** (1984), 1561

[117] R.W. Siegel, S.M. Chang and R.W. Baluffi, Acta Metall. **28** (1980), 249

[118] O.V. Mishin and X. Huang, Mat. Sci. Forum **294-2** (1999), 401

[119] X. Huang, Private communication

Bibliographic Data Sheet **Risø-R-1379(EN)**

Title and authors

Studies of Grain Boundaries in Materials subjected to Diffusional Creep

Thomas Nørbygaard

ISBN	ISSN
87-550-3147-1 87-550-3149-8 (Internet version)	0106-2840

Department or group	Date
Materials Research Department	August 2002

Pages	Tables	Illustrations	References
107	9	51	119

Abstract (max. 2000 characters)

Grain boundaries in crystalline Cu(2%Ni) creep specimens have been studied by use of scanning and transmission electron microscopy in order to establish the mechanism of deformation. Creep rate measurements and dependencies were found to fit reasonably well with the model for diffusional creep (Nabarro-Herring) and this impression was strengthened considerably by the microstructural finds. Manual and automated EBSD surface scans have been performed on a specimen supplied with an inert reference grid in order to correlate individual grain boundary structure (in terms of deviation from CSL) with the activity displayed during diffusional creep testing. It was found that boundaries with low deviation from perfect Σ did not contribute macroscopically to the creep strain. A resist deposition procedure was examined to improve the reference surface grid so as to allow determination of the grain boundary plane by use of simple stereomicroscopy directly on the surface. The etched pattern deteriorated heavily during creep testing, supposedly because of dislocation creep, due to excessive creep stress. Grain boundaries have been studied and characterised by TEM providing an insight into the diversity of twin boundary structures. Ledges on low deviation Σ3 and Σ9 were observed repeatedly and the presence of these is proposed to relate to the inactivity of such boundaries. A handful of examples showed ledged boundaries emitting dislocations into the lattice, presumably because of stress accumulation due to restrictions on GBD movement from the ledge structure.

Descriptors

COPPER, CREEP DEFORMATION, DIFFUSION, DIFFUSIONAL CREEP, MICROSTRUCTURE, GRAIN BOUNDARIES, BOUNDARY STRUCTURE, CSL, BOUNDARY LEDGES, DISLOCATIONS, SURFACE GRID, SCANNING ELECTRON MICROSCOPY, TRANSMISSION ELECTRON MICROSCOPY